VNiVERSiDAD D SALAMANCA

CAMPUS DE EXCELENCIA INTERNACIONAL

FACULTAD DE CIENCIAS AGRARIAS Y AMBIENTALES

CIALE-INSTITUTO DE INVESTIGACIÓN EN AGROBIOTECNOLOGÍA

TESIS DOCTORAL

Nuevas estrategias basadas en geotecnologías de aplicación a la agricultura y ganadería de precisión

Programa de Doctorado: Agrobiotecnología

Javier Plaza Martín

Salamanca, mayo 2022

Facultad de Ciencias Agrarias y Ambientales

CIALE-Instituto de Investigación en Agrobiotecnología

Universidad de Salamanca

AUTOR:

D. Javier Plaza Martín

DIRECTORES

Dra. María Nilda Sánchez Martín

Dr. Rodrigo Pérez Sánchez

2022

Dña. María Nilda Sánchez Martín, Profesora Titular del Área de Ingeniería Cartográfica, Geodésica y Fotogrametría del Departamento de Ingeniería Cartográfica y del Terreno de la Universidad de Salamanca.

D. Rodrigo Pérez Sánchez, Profesor Contratado Doctor del Área de Producción Vegetal del Departamento de Construcción y Agronomía de la Universidad de Salamanca.

CERTIFICAN:

Que la memoria de tesis **"Nuevas estrategias basadas en geotecnologías de aplicación a la agricultura y ganadería de precisión"**, ha sido realizada por **D. Javier Plaza Martín** bajo nuestra dirección y es favorable para obtener el grado de Doctor por la Universidad de Salamanca en el programa de doctorado en Agrobiotecnología.

Para que así conste, firmamos el presente certificado en Salamanca, a 23 de marzo de 2022.

Dña. María Nilda Sánchez Martín D. Rodrigo Pérez Sánchez

Dr. Carlos Nicolás Rodríguez, Coordinador del Programa de Doctorado en Agrobiotecnología de la Universidad de Salamanca.

CERTIFICO:

Que la presente memoria de tesis titulada **"Nuevas estrategias basadas en geotecnologías de aplicación a la agricultura y ganadería de precisión"**, ha sido realizada en el Programa de Doctorado en Agrobiotecnología de la Universidad de Salamanca por **D. Javier Plaza Martín**, bajo la dirección y supervisión de la Prof. Dra. María Nilda Sánchez Martín y el Prof. Dr. Rodrigo Pérez Sánchez y cumple los requisitos exigidos para optar al grado de Doctor por la Universidad de Salamanca.

NICOLAS RODRIGUEZ CARLOS - 07874196P

Firmado digitalmente por NICOLAS RODRIGUEZ CARLOS - 07874196P
Fecha: 2022.03.24 10:36:50 +01'00'

Para que así conste, firmo el presente certificado en Salamanca a 24 de marzo de 2022.

Fdo: Dr. C. Nicolás Rodríguez

A mis padres, M.ª del Carmen y Toribio,

a mis hermanas, Helena y María,

y a mi compañera de viaje, Andrea

Índice General

Listado de contribuciones científicas

En virtud del Reglamento de Doctorado de la Universidad de Salamanca, la presente Tesis Doctoral está constituida como un compendio de tres **ARTÍCULOS CIENTÍFICOS**, en los que el doctorando Javier Plaza Martín es el primer autor de todos ellos. Estos artículos han sido publicados en sendas revistas internacionales de alto impacto con revisión por pares e indexadas en el *Journal Citation Report* (JCR) de la *Web of Science.* Se enumeran a continuación dichas publicaciones.

1. UAV multispectral imaging potential to monitor and predict agronomic characteristics of different forage associations.

Javier Plaza[1], Marco Criado[2], Nilda Sánchez[3], Rodrigo Pérez-Sánchez[1], Carlos Palacios[4], Francisco Charfolé[3]

[1] Plant Production Group, Faculty of Environmental and Agricultural Sciences, University of Salamanca, 37007 Salamanca, Spain.

[2] Edaphology Group, Faculty of Environmental and Agricultural Sciences, University of Salamanca, 37007 Salamanca, Spain.

[3] Department of Cartographic and Land Engineering, University of Salamanca, 05003 Ávila, Spain.

[4] Animal Production Group, Faculty of Environmental and Agricultural Sciences, University of Salamanca, 37007 Salamanca, Spain.

Agronomy (MDPI), Agosto 2021

DOI: https://doi.org/10.3390/agronomy11091697

Referencia: Plaza, J., Criado, M., Sánchez, N., Pérez-Sánchez, R., Palacios, C., & Charfolé, F. (2021). UAV Multispectral Imaging Potential to Monitor and Predict Agronomic Characteristics of Different Forage Associations. *Agronomy*, 11(9), 1697. https://doi.org/10.3390/AGRONOMY11091697.

Indicadores de calidad de la revista:

Agronomy	
Editorial	MDPI
ISSN	N/A
eISSN	2073-4395
Journal Impact Factor (JIF) (2020)	3.417
Journal Citation Indicator (JCI) (2020)	0.94
Category (ies) Web of Science and Rank by JIF	- Agronomy: JIF Rank: 16/91; JIF Quartile: Q1 - Plant Sciences: JIF Rank: 57/235; JIF Quartile: Q1

2. Classification of airborne multispectral imagery to quantify common vole impacts on an agricultural field.

Javier Plaza[1], Nilda Sánchez[2], Carmen García-Ariza[3], Rodrigo Pérez-Sánchez[1], Francisco Charfolé[2], Constantino Caminero-Saldaña[3]

[1] Plant Production Group. Faculty of Environmental and Agricultural Sciences. University of Salamanca, 37007 Salamanca, Spain.

[2] Department of Cartographic and Land Engineering. University of Salamanca, 05003 Ávila, Spain.

[3] Pest Area. Technological Agricultural Institute of Castilla y León (ITACyL). Zamadueñas, km 119, Avenida Burgos, 47071 Valladolid, Spain.

Pest Management Science (Wiley Online Library), Marzo 2022

DOI: https://doi.org/10.1002/PS.6857

Referencia: Plaza, J., Sánchez, N., García-Ariza, C., Pérez-Sánchez, R., Charfolé, F., & Caminero-Saldaña, C. (2022). Classification of airborne multispectral imagery to quantify common vole impacts on an agricultural field. Pest Management Science, Early view. https://doi.org/10.1002/PS.6857

Indicadores de calidad de la revista:

Pest Management Science	
Editorial	Wiley Online Library
ISSN	1526-498X
eISSN	1526-4998
Journal Impact Factor (JIF) (2020)	4.845
Journal Citation Indicator (JCI) (2020)	2.04
Category (ies) Web of Science and Rank by JIF	- Agronomy: JIF Rank: 9/91; JIF Quartile: Q1 - Entomology: JIF Rank: 5/102; JIF Quartile: Q1

3. GPS, LiDAR and VNIR data to monitor the spatial behavior of grazing sheep.

Javier Plaza[1], Nilda Sánchez[1,2], Carlos Palacios[1], Mario Sánchez-García[1], José-Alfonso Abecia[3], Marco Criado[1], Jaime Nieto[1]

[1] Faculty of Environmental and Agricultural Sciences. University of Salamanca, 37007 Salamanca, Spain.

[2] Department of Cartographic and Land Engineering, University of Salamanca, 05003 Ávila, Spain.

[3] Institute of Research in Environmental Sciences of Aragón, University of Zaragoza, 50009 Zaragoza, Spain.

Journal of Animal Behaviour and Biometeorology (Malque Pub.), Enero 2022

DOI: https://doi.org/10.31893/JABB.22014

Referencia: Plaza, J., Sánchez, N., Palacios, C., Sánchez-García, M., Abecia, J. A., Criado, M., & Nieto, J. (2022). GPS, LiDAR and VNIR data to monitor the spatial behavior of grazing sheep. *Journal of Animal Behaviour and Biometeorology*, 10(2), 2214. https://doi.org/10.31893/JABB.22014.

Indicadores de calidad de la revista:

Journal of Animal Behaviour and Biometeorology	
Editorial	Malque Publishing
ISSN	N/A
eISSN	2318-1265
Journal Citation Indicator (JCI) (2020)	0.39
Category (ies) Web of Science and Rank by JCI	- Agriculture, Dairy and Animal Science: JCI Rank: 56/80; JCI Quartile: Q3

La investigación objeto de esta tesis doctoral ha generado, además de las publicaciones anteriormente citadas, otras contribuciones científicas en forma de **COMUNICACIONES A CONGRESOS**, que se exponen a continuación.

1. Incidence assessment of common vole (*Microtus arvalis* Pallas) in an alfalfa field through multispectral imaging captured by drone.

Javier Plaza[1], Nilda Sánchez[1,2], Carmen García-Ariza[3], Rodrigo Pérez-Sánchez[1], Francisco Charfolé[2], Constantino Caminero-Saldaña[3]

[1] Faculty of Environmental and Agricultural Sciences, University of Salamanca, Avenida Filiberto Villalobos 119, 37007 Salamanca, Spain.

[2] Cartographic and Land Engineering Department. University of Salamanca, C/ Hornos Caleros 50, 05003 Ávila, Spain.

[3] Pest Area. Agriculture Technology Institute of Castilla y León (ITACyL). Zamadueñas, km 119, Avenida Burgos, 47071 Valladolid, Spain.

Mediterranean Geosciences Union Annual Meeting (MedGU-21).

Mediterranean Geosciences Union

25/112021 – 28/11/2021, Istanbul (Turkey).

2. Imágenes multiespectrales aerotransportadas en dron para la evaluación de impactos del topillo campesino (*Microtus arvalis* Pallas)

Javier Plaza[1], Nilda Sánchez[1], Carmen García-Ariza[3], Rodrigo Pérez-Sánchez[1], Francisco Charfolé[1], Constantino Caminero-Saldaña[3]

[1] Facultad de Ciencias Agrarias y Ambientales. Universidad de Salamanca, Avenida Filiberto Villalobos 119, 37007 Salamanca, España.

[2] Área de Plagas. Instituto Tecnológico Agrario de Castilla y León. Zamadueñas, km 119, Avenida Burgos, 47071 Valladolid, España.

XI Congreso Ibérico de Agroingeniería

Sociedad Española de Agroingeniería y Secção Especializada de Engenharia Rural de la Sociedade de Ciências Agrárias de Portugal

11/11/2021 – 12/11/2021, Congreso Virtual

3. L ´activité des moutons dans un pâturage libre suit un modèle stationnaire circadien calculé a l ´aide de registres de leur propre vitesse par technologie GPS.

Carlos Palacios[1], Javier Plaza[2], José Alfonso Abecia[2]

[1] Département de production animale de la Faculté des sciences Agraires et environnementales.

[2] Institut de Recherches en sciences environnementales de la région d ´ Aragon. Zaragosse (Espagne).

47eme Congrès de la Société Francophone de chronobiologie

Societé Francophone de Chronobiologie

13/10/2021 – 14/10/2021, Congrès Virtual

Proceedings publicados en la revista Médecine du Sommeil

ISSN 1769-4493

Reference: Palacios, C., Plaza, J., & Abecia, J. (2021). L'activité des moutons dans un pâturage libre suit un modèle stationnaire circadien calculé à l'aide de registres de leur

propre vitesse par technologie GPS. Médecine Du Sommeil, 18(4), 196. https://doi.org/10.1016/J.MSOM.2021.10.028

4. Análisis espacial y temporal del comportamiento en pastoreo de un rebaño de ovejas mediante el uso de GPS y técnicas de teledetección.

Javier Plaza[1], Mario Sánchez-García[1], Marco Criado[1], Jaime Nieto[1], Nilda Sánchez[1], José-Alfonso Abecia[2], Carlos Palacios[1]

[1] Facultad de Ciencias Agrarias y Ambientales, Universidad de Salamanca, 37007, Salamanca, España.

[2] Instituto de Investigaciones en Ciencias Ambientales de Aragón (IUCA), Miguel Servet, 177, 50013 Zaragoza, España.

XIX Jornadas AIDA sobre producción animal

Asociación Interprofesional para el Desarrollo Agrario (AIDA)

01/06/2021 – 02/06/2021, Congreso Virtual

Referencia: Plaza, J., Sánchez-García, M., Criado, M., Nieto, J., Sánchez, N., Abecia, J. A., & Palacios, C. (2021). Análisis espacial y temporal del comportamiento en pastoreo de un rebaño de ovejas mediante el uso de GPS y técnicas de teledetección. In Asociación Interprofesional para el Desarrollo Agrario (Ed.), Libro de Actas XIX Jornadas sobre Producción Animal (p. 258), ISBN: 978-84-09-30674-9

5. Monitoring spatial behaviour of pastoralist sheep through GPS, LiDAR data and VNIR image.

Javier Plaza[1], Carlos Palacios[1], Mario Sánchez-García[2], Marco Criado[1], Jaime Nieto[1], Nilda Sánchez[1,3]

[1] Faculty of Environmental and Agrarian Sciences. University of Salamanca, 37007 Salamanca, Spain.

[2] IIVV, University of León, 24071 León, Spain.

[3] Department of Cartographic and Land Engineering. University of Salamanca, 05003 Ávila, Spain.

ISPRS Congress 2020

International Society of Photogrammetry and Remote Sensing

21/08/2020 – 27/08/2020, Nice (France)

Referencia: Plaza, J., Palacios, C., Sánchez-García, M., Criado, M., Nieto, J., & Sánchez, N. (2020). Monitoring spatial behaviour of pastoralist sheep through GPS, LiDAR data and VNIR image. ISPRS - International Archives of the Photogrammetry, Remote Sensing and Spatial Information Sciences, XLIII-B4-2, 169–175. https://doi.org/10.5194/isprs-archives-XLIII-B4-2020-169-2020

Por último, es necesario mencionar que, durante el desarrollo de la tesis, el doctorando ha participado en **OTRAS PUBLICACIONES** en revistas JCR muy cercanas en contenido con la línea de investigación que sustenta la presente tesis doctoral, pero que no se incluyen como cuerpo de la misma, ya que el doctorando no ha liderado la investigación.

1. Fusion of multi-temporal PAZ and sentinel-1 data for crop classification.

Mario Busquier[1], Rubén Valcarce-Diñeiro[2], Juan M. López-Sánchez[1], Javier Plaza[3], Nilda Sánchez[3,4], Benjamín Arias-Pérez[4]

[1] Institute for Computer Research (IUII), University of Alicante, 03080 Alicante, Spain.

[2] School of Natural and Environmental Sciences, Newcastle University, Newcastle upon Tyne NE1 7RU, UK.

[3] Faculty of Agrarian and Environmental Sciences, University of Salamanca, 37007 Salamanca, Spain.

[4] Department of Cartographic and Land Engineering, University of Salamanca, 05003 Ávila, Spain.

Remote Sensing (MDPI), Septiembre 2021

DOI: https://doi.org/10.3390/rs13193915

Referencia: Busquier, M., Valcarce-Diñeiro, R., Lopez-Sanchez, J. M., Plaza, J., Sánchez, N., & Arias-Pérez, B. (2021). Fusion of multi-temporal paz and sentinel-1 data for crop classification. Remote Sensing, 13(19). https://doi.org/10.3390/rs13193915.

Indicadores de calidad de la revista:

Remote Sensing	
Editorial	MDPI
ISSN	N/A
eISSN	2072-4292
Journal Impact Factor (JIF) (2020)	4.848
Journal Citation Indicator (JCI) (2020)	1.15
Category (ies) Web of Science and Rank by JIF	- Remote Sensing: JIF Rank: 10/32; JIF Quartile: Q2 - Geosciences, Multidisciplinary: JIF Rank: 27/200; JIF Quartile: Q1 - Environmental Sciences: JIF Rank: 76/274; JIF Quartile: Q2 - Imaging Science and Photographic Technology: JIF Rank: 8/29; JIF Quartile: Q2

2. Spatial averages of *in situ* measurements versus remote sensing observations: a soil moisture analysis.

Nilda Sánchez[1,2], Laura Almendra[1], Javier Plaza[2], Ángel González-Zamora[1], José Martínez-Fernández[1]

[1] Instituto Hispano Luso de Investigaciones Agrarias (CIALE), University of Salamanca, Salamanca, Villamayor, Spain.

[2] Faculty of Environmental and Agrarian Sciences, University of Salamanca, Salamanca, Spain.

Journal of Spatial Science, Octubre 2020

DOI: https://doi.org/10.1080/14498596.2020.1833769

Referencia: Sánchez, N., Almendra, L., Plaza, J., González-Zamora, Á., & Martínez-Fernández, J. (2020). Spatial averages of in situ measurements versus remote sensing observations: a soil moisture analysis. *Journal of Spatial Science*, 1–16. https://doi.org/10.1080/14498596.2020.1833769.

Indicadores de calidad de la revista:

Journal of Spatial Science	
Editorial	Taylor & Francis
ISSN	1449-8596
eISSN	1836-5655
Journal Impact Factor (JIF) (2020)	1.981
Journal Citation Indicator (JCI) (2020)	0.32
Category (ies) Web of Science and Rank by JIF	- Remote Sensing: JIF Rank: 25/32; JIF Quartile: Q4 - Geography, Physical: JIF Rank: 38/50; JIF Quartile: Q4

Agradecimientos

Es difícil resumir en unas pocas líneas lo eternamente agradecido que me siento hacia toda la gente que me ha apoyado y ayudado a llevar la gran carga que supone la realización de una tesis doctoral. Personas que sin duda ya ocupaban un lugar importante en mi vida, pero que ahora ya pasan a formar parte de mi historia y de mi futuro.

No puedo por menos que agradecer especialmente la actitud y el trabajo realizado por mis directores de tesis, la Prof. Dra. Nilda Sánchez Martín y el Prof. Dr. Rodrigo Pérez Sánchez, quienes me abrieron la puerta a un contrato de investigación que posibilitó no sólo la realización de esta tesis, sino el poder sustentarme mientras lo hacía. En este sentido, el hecho de que me hayan descubierto que es posible vivir de aquello que se ha convertido en tu pasión y en tu vocación, algo que sencillamente no puedes llamar "trabajo" en el sentido estricto de la palabra, es una enseñanza que jamás les podré agradecer lo suficiente. Además, gracias a ellos, nació la conceptualización de esta tesis, enseñándome que a veces tenemos que mirar al cielo y desde él para saber lo que ocurre en la Tierra. Siguiendo su estela, me he subido en un tren del que nunca espero bajarme.

No obstante, siendo sincero conmigo mismo, y a pesar de que no figurase administrativamente como tal, en realidad he tenido la suerte de contar con tres directores de tesis. Infinitas gracias al Prof. Dr. Carlos Palacios Riocerezo, por estar siempre conmigo al pie del cañón, por su apoyo desinteresado, por ese incansable (y a veces loco) afán por seguir atravesando los horizontes del conocimiento de nuestro pequeño pero especial ámbito científico. Junto con el Prof. Dr. José Alfonso Abecia de la Universidad de Zaragoza, por quién profeso casi tanta admiración como gratitud, hemos conseguido abrir un pequeño "Ministerio" que espero que no cierre nunca. Por todo ello y por mucho más en la faceta emocional -él lo sabe bien- le estaré siempre agradecido.

Me gustaría agradecer también de todo corazón al gran grupo humano de profesores de la Facultad de Ciencias Agrarias y Ambientales de la Universidad de Salamanca, quienes han roto una lanza por mí en numerosas ocasiones y me han ofrecido y brindado su ayuda siempre que lo he necesitado. Mención especial a mis contemporáneos compañeros y amigos, el Dr. Marco Criado Nicolás y el doctorando y Prof. Asociado Jaime Nieto de la Losa, quienes se han batido el cobre conmigo en innumerables batallas y siguen peleando por lo que considero que es nuestro sueño en común. En definitiva, gente que responde.

A mis viejos compañeros del equipo de rugby universitario, pero eternos amigos, que siempre han estado ahí para ahogar mis puntuales agobios y algún que otro mal rato en una buena cerveza, acompañada de palabras reparadoras y con un toque de cariño, aunque siempre me lo nieguen para hacerme rabiar. Y al resto de amigos que también habéis estado siempre ahí, mil gracias.

Y, por último, gracias a mi pilar de carga fundamental, a mis cimientos, a mis raíces, a mi familia. Mis padres, mis hermanitas, Andrea, y mis catalanes favoritos, todo cuanto haya podido conseguir y todo lo que esté por venir, es gracias a vosotros. Permitidme que antes de agradeceros todo vuestro apoyo, os agradezca vuestra paciencia conmigo, que no ha tenido límite nunca. Quizá tú, mi querida Andrea, has podido sufrir más aún mi día a día, mis cambios de humor y mi escasez de tiempo para vivir, y aún con todo, nunca te he sentido lejos. Espero que en el tiempo que nos conceda la vida, sea capaz de agradecértelo lo suficiente. Todos habéis mirado siempre por mí, vigilantes por si necesitaba cualquier apoyo, y creedme que siempre lo he recibido, tanto de los que estáis hoy aquí conmigo, como de aquellas personitas especiales que un día se marcharon, pero cuyo apoyo he sentido tan cercano y cálido como el vuestro. Por esto y por muchísimo más que ya todos conocéis, esta tesis doctoral está dedicada especialmente a vosotros. Como siempre me ha dicho mi padre, “hoy soy lo que he hecho, mañana seré lo que haga”.

Resumen

Las geotecnologías han emergido como la piedra angular del nuevo paradigma digital en el que están actualmente inmersas la agricultura y la ganadería contemporáneas, es decir, la nueva revolución agrícola, conocida como Agricultura 4.0, en la que se enmarcan las denominadas agricultura y ganadería de precisión. La obligada modernización a la que se ven sometidas las prácticas agroganaderas tradicionales viene desencadenada por el incipiente crecimiento demográfico y la consecuente demanda de productos agroalimentarios. Esta drástica transformación del mundo rural se torna imprescindible no solo para conseguir abastecer las necesidades de una población creciente, sino para rescatar a un sector primario cada vez más castigado por los elevados precios de los insumos y los escasos beneficios que se perciben. Como avales también de esta necesaria reconversión de los sistemas de manejo agropecuarios, entran también en juego pilares fundamentales de la productividad agrícola y ganadera como son la sostenibilidad medioambiental y el bienestar animal, ambos muy demandados en los productos de primera necesidad por una sociedad cada vez más concienciada con la producción respetuosa con el medio y con los animales.

En este contexto, las geotecnologías no deben ser tomadas como herramientas que amenacen con sustituir los conocimientos agroganaderos tradicionales o que promuevan su desaparición. El enfoque es categóricamente opuesto, ya que tratan de perfeccionar la toma de decisiones de los agricultores y ganaderos, fundada en dicha sabiduría tradicional. Esta complementariedad resultará en nuevos modelos de gestión de los sistemas agropecuarios, que serán ostensiblemente más respetuosos con el medio que los sustenta, a la par que se maximizará el respeto hacia los principios básicos de sostenibilidad y bienestar animal. Por lo tanto, en este trabajo se plantea la siguiente hipótesis: la implementación de nuevas estrategias metodológicas basadas en geotecnologías en el sector agroganadero contribuirán a reducir los costes de producción, el tiempo empleado por agricultores y ganaderos en sus labores y el impacto medioambiental que dichas labores pudieran ocasionar, generando beneficios de corte económico, social y medioambiental.

Considerando la hipótesis anteriormente expuesta, el objetivo de la presente tesis doctoral se centró en demostrar el potencial de las geotecnologías como herramientas

alternativas y complementarias destinadas a la mejora de la gestión de los sistemas de manejo agroganaderos en el ámbito económico, medioambiental y desde el punto de vista del bienestar animal. Así mismo, se planteó que dichas estrategias geotecnológicas sirvan también para ahondar en el aprendizaje de nuevos conocimientos agrícolas y ganaderos. Para lograr este objetivo, se plantearon una serie de aportaciones que permitieran dilucidar la idoneidad de dichas geotecnologías en la gestión agroganadera.

La primera de dichas experiencias consistió en utilizar imágenes multiespectrales aerotransportadas captadas con drones para la monitorización de varios parámetros agronómicos de cultivos mixtos de aptitud forrajera. El agricultor, tradicionalmente, observa y mide *in situ* los parámetros o variables que le permiten tomar decisiones (regar, fertilizar, cosechar, etc.). Sin embargo, carece de una visión global de la distribución de esos parámetros en sus parcelas. Con este trabajo se pretendió demostrar que se pueden monitorizar algunos de los parámetros de los cultivos de forrajeras desde las mediciones del dron y, además, obtener los mapas de distribución de los mismos para optimizar el manejo actual y futuro de los cultivos en la zona. Particularmente, los índices espectrales de vegetación derivados del procesamiento de dichas imágenes, en conjunción con un modelo estadístico predictivo, arrojaron resultados muy satisfactorios en la modelización temporal y espacial de las características de las asociaciones forrajeras, puesto que se obtuvo una alta fiabilidad de predicción de dichos parámetros en cualquier momento del ciclo de crecimiento de los cultivos.

La segunda aportación manejaba un hardware similar al de la experiencia anterior, en definitiva, drones e imágenes multiespectrales, pero en este caso utilizados como metodología alternativa para la evaluación de impactos sobre la cobertura vegetal producidos por la plaga del topillo campesino (*Microtus arvalis* Pallas). Los procedimientos de clasificación multiespectral desarrollados aportaron resultados considerablemente precisos acerca del nivel de afectación del alfalfar estudiado, siendo la segmentación del conocido NDVI el que reflejó la situación real con mayor fidelidad. De nuevo, las geotecnologías demostraron ser una forma alternativa de evaluar el estado del cultivo, en este caso de afectación de la plaga, con una precisión muy alta. Estos resultados pueden ser de gran utilidad tanto para agricultores como para los organismos competentes en la gestión integrada de plagas, quienes no cuentan hasta la fecha con metodologías objetivas y precisas para este fin.

En la tercera de las investigaciones se trató de poner de manifiesto la capacidad de los dispositivos de geoposicionamiento global GPS, combinados con herramientas y recursos de teledetección (fundamentalmente LiDAR y ortofotografías del espectro VNIR), para revelar los patrones de comportamiento espacial de pequeños rumiantes durante el pastoreo. Además de la obvia utilidad de conocer la posición de los animales en todo momento, se pudo demostrar la gran utilidad de esta metodología para determinar que el comportamiento de las ovejas en pastoreo no se basa en la arbitrariedad, sino que los animales desarrollan patrones habituales de conducta relacionados con la morfología del terreno y la vegetación. Concretamente, las ovejas eligieron deliberadamente las zonas donde se encontraban los pastos más frescos y con mayor calidad nutricional, coincidiendo con áreas despejadas con pendientes suaves orientadas al norte, en las que predominaba el estrato herbáceo formado por especies pratenses. Esta información puede ayudar a los ganaderos a realizar una mejor gestión de las zonas destinadas al pastoreo y la distribución espacial de los rebaños.

Abstract

Geotechnologies have emerged as the cornerstone of the new digital paradigm in which contemporary agriculture and livestock farming are currently immersed, i. e., the new agricultural revolution, known as Agriculture 4.0, which includes the so-called precision agriculture and precision livestock farming. The forced modernization to which traditional agricultural and livestock farming practices are subjected is triggered by the incipient demographic growth and the consequent demand for agri-food products. This drastic transformation of the rural world is essential not only to meet the needs of a growing population, but also to rescue a primary sector that is increasingly punished by high input prices and low profits. Environmental sustainability and animal welfare are also fundamental pillars of agricultural and livestock productivity, both of which are in high demand for staple products in a society that is becoming increasingly aware of the need for environmentally and animal-friendly production.

In this context, geotechnologies should not be taken as tools that threaten to replace traditional farming knowledge or promote its disappearance. The approach is categorically the opposite, as they seek to improve the decision-making of farmers and livestock breeders, based on this traditional knowledge. This complementarity will result in new management models for agricultural systems, which will be ostensibly more respectful with the environment that sustains them, while maximizing respect for the basic principles of sustainability and animal welfare. Therefore, this work proposes the following hypothesis: the implementation of new methodological strategies based on geotechnologies in the agricultural and livestock sector will contribute to reduce production costs, the time spent by farmers and stockbreeders in their work and the environmental impact that such work could cause, thus generating economic, social and environmental benefits.

Considering the above hypothesis, the objective of this PhD thesis focused on demonstrating the potential of geotechnologies as alternative and complementary tools to improve the management of agricultural and livestock management systems in the economic, environmental and animal welfare spheres. It was also proposed that these geotechnological strategies could also be used to deepen the learning of new agricultural and livestock knowledge. To achieve this objective, a series of contributions were

proposed to elucidate the suitability of these geotechnologies in agricultural and livestock management.

The first of these experiments consisted of using airborne multispectral images captured with drones to monitor several agronomic parameters of mixed forage crops. Traditionally, the farmer observes and measures *in situ* the parameters or variables that allow him to make decisions (irrigation, fertilization, harvesting, etc.). But he lacks a global vision of the distribution of these parameters in his plots. The aim of this work was to demonstrate that some of the parameters of forage crops can be monitored from drone measurements and, in addition, to obtain their distribution maps to optimize current and future crop management in the area. Particularly, the spectral vegetation indices derived from the processing of these images, in conjunction with a predictive statistical model, provided very satisfactory results in the temporal and spatial modeling of the characteristics of the forage associations, since a high predictive reliability of these parameters was obtained at any time during the growth cycle of the crops.

The second contribution used similar hardware to the previous experience, namely drones and multispectral images, but in this case used as an alternative methodology for the evaluation of impacts on vegetation cover caused by the pest of the common vole (*Microtus arvalis* Pallas). The multispectral classification procedures developed provided considerably accurate results about the level of damage to the alfalfa studied, being the segmentation of the known NDVI the one that most accurately portrayed the real situation. Again, geotechnologies proved to be an alternative way to assess the crop status, in this case of pest damage, with a very high accuracy. These results can be very useful both for farmers and for the competent agencies in integrated pest management, which to date do not have objective and accurate methodologies for this purpose.

The third of the investigations sought to demonstrate the ability of GPS global geopositioning devices, combined with remote sensing tools and resources (mainly LiDAR and VNIR orthophotographs), to reveal the spatial behavioral patterns of small ruminants during grazing. In addition to the obvious usefulness of knowing the position of the animals at all times, it was possible to demonstrate the great utility of this methodology to determine that sheep grazing behavior is not random, but that the animals develop common behavioral patterns related to the morphology of the terrain and vegetation. Specifically, the sheep deliberately chose the areas where the freshest pastures with the highest nutritional quality were found, coinciding with cleared areas with gentle

north-facing slopes, where the herbaceous stratum formed by grassland species predominated. This information can help farmers to better manage grazing areas and the spatial distribution of herds.

Acrónimos

AEMet	*Agencia Española de Meteorología*
ASPRS	*Sociedad Americana de Fotogrametría y Teledetección*
C/A	*Coarse/Acquisition*
CHM	*Canopy Height Model*
CS	*Cold Spot*
DB	*Dry biomass*
DEM	*Digital Elevation Model*
DSM	*Digital Surface Model*
DTM	*Digital Terrain Model*
EBK	*Empirical Bayesian Kriging*
ESA	*European Spatial Agency*
FB	*Fresh biomass*
FVC	*Fractional Vegetation Cover*
GIS	*Geographical Information System*
GLONASS	*Global'naya Navigatsionnaya Sputnikovaya Sistema*
GNSS	*Global Navigation Satellite System*
GPS	*Global Positioning System*
GPS-GPRS	*Global Positioning System-General Packet Radio Service*
GRVI	*Green-Red Vegetation Index*
GSM	*Groupe Special mobile*
GVI	*Greenness Vegetation Index*
HS	*Hot Spot*
INS	*Inertial Navigation System*
ISODATA	*Iterative Self-Organization Data Analysis*
LAI	*Leaf Area Index*
LiDAR	*Light Detection And Ranging*
LOOCV	*Leave-One-Out Cross Validation*
LU/LC	*Land Use/Land Cover*
MODIS	*Moderate-Resolution Imaging Spectroradiometer*
MS	*Multispectral*
NAVSTAR	*Navigation Signal Timing and Ranging*
NDVI	*Normalized Difference Vegetation Index*
NIR	*Near Infrared*
OORF	*Object-Oriented Random Forest*
P	*Protected*
PBT	*Pea-Barley-Triticale*
PLS	*Partial Least Squares*
PO	*Pea-Oats*
PT	*Pea-Triticale*
PR	*Pea-Rye*

PRESS	*Predicted Residual Sum of Squares*
PRN	*Pseudo-Random Noise*
PWC	*Percentage of water content*
RF	*Random Forest*
RGB	*Red-Green-Blue*
RTK	*Real-Time Kinematic*
SAR	*Synthetic Aperture Radar*
SIG	*Sistemas de Información Geográfica*
SVM	*Support Vector Machine*
UAS	*Unmanned Aerial Systems*
UAV	*Unmanned Aerial Vehicle*
UE	*Unión Europea*
UTC	*Universal Time Coordinated*
VBT	*Vetch-Barley-Triticale*
VNIR	*Visible and Near Infrared*
VO	*Vetch-Oats*
VR	*Vetch-Rye*
VT	*Vetch-Triticale*
VWC	*Vegetation water content*

Lista de Figuras

Lista de Tablas

Capítulo 1. Introducción

Capítulo 1. Introducción

1.1. Motivación

El crecimiento exponencial que la población mundial ha experimentado desde la Revolución Industrial hasta la actualidad ha supuesto y supone un más que considerable aumento en el consumo global de todo tipo de recursos, fundamentalmente agua y alimentos. Dado el aumento de la longevidad del ser humano, de los procesos de urbanización del territorio y de la actividad económica, la población continuará creciendo a un ritmo sin precedentes, y con ella el consumo de recursos procedentes del sector primario. De hecho, las estimaciones de las Naciones Unidas prevén que las producciones agrícolas y ganaderas deberán verse incrementadas entre un 60% y un 100% para conseguir abastecer las necesidades nutricionales de una población que superará los once mil millones de habitantes en torno al año 2100. Por lo tanto, la presión ejercida sobre la agricultura y la ganadería es más grande que nunca, puesto que esta pronta e inexorable realidad poblacional amenaza con una grave crisis alimentaria a nivel global. Prueba de la fragilidad del mercado agropecuario, incluso en sistemas estrictamente regulados como el europeo, es la actual y preocupante desestabilización del abastecimiento de materias primas y alimentos que está generando el conflicto bélico entre Rusia y Ucrania. Para tratar de evitarlo, agricultores y ganaderos se verán obligados a modificar y adaptar sus sistemas productivos tradicionales a la nueva era tecnológica, puesto que la intensificación del sector ya se ha postulado como un problema añadido más que como una solución, dada la nula sostenibilidad medioambiental que le procede.

El sector agroganadero se ve abocado a aceptar la premisa de “producir más con menos”, premisa que es a su vez el estandarte de la nueva revolución agrícola que está atravesando el sector y que se conoce como “Agricultura 4.0”. Es en este contexto revolucionario en el que se enmarca el nacimiento de la agricultura y de la ganadería de precisión, estrategias de gestión que recogen, procesan y analizan datos temporales, espaciales e individuales a una escala de detalle que permite respaldar las decisiones de manejo de agricultores y ganaderos, optimizando así la gestión agronómica, económica y medioambiental. Este es, sin duda, el nuevo paradigma tecnológico digital de la

agricultura y de la ganadería: el surgimiento de tecnologías y procedimientos capaces de extraer con celeridad información precisa y relevante de las producciones agroganaderas en cada momento y necesidad. Dicha monitorización puede convertirse en la piedra angular en el proceso de toma de decisiones de los agricultores y ganaderos, quienes podrán incrementar sus rendimientos productivos a la vez que lo hacen de un modo sostenible con el medio ambiente que los sustenta.

Como complemento a los conocimientos agronómicos tradicionales, las geotecnologías son el pilar fundamental sobre el que se sustentan las metodologías de la agricultura y ganadería de precisión. Gracias a ellas, es posible romper con la limitación de ceñirse a un único tipo de cultivo o ganado, región o productor en concreto, ampliando la aplicabilidad y posibilidades de la monitorización agroganadera. Entre otros beneficios, permiten una zonificación precisa del territorio agrícola y ganadero para ajustar los insumos, la distribución de cargas y la minimización de residuos a la diversidad espacial. Además, permitirían abandonar modelos hiperproductivistas e insostenibles, a la par que actuarían como un salvavidas de un mundo rural que agoniza.

En la actualidad existe un amplio elenco de estrategias geotecnológicas que podrían llegar a ser trascendentales para el desarrollo de la agricultura y de la ganadería en este contexto de crecimiento poblacional y de crisis agroalimentaria. Entre otras, la teledetección, permite la caracterización de un objeto o superficie de manera remota a través de su respuesta emitida o reflejada en una banda de frecuencias del espectro electromagnético. El uso de imágenes de satélites procedentes de las misiones Sentinel o Landsat está ampliamente constatado para la monitorización de extensas zonas de cultivos agrícolas. Por el contrario, en aquellas situaciones en las que se requiere una mayor definición espacial, las imágenes de sensores miniaturizados a bordo de drones ofrecen la mejor alternativa. En este preciso contexto, se exponen en la presente tesis doctoral dos aportaciones metodológicas que combinan imágenes multiespectrales captadas con drones, también denominados *unmanned aerial systems* (UAS), con distintas técnicas de teledetección. Por un lado, se plantea la construcción de índices espectrales que sirvan para caracterizar diversas asociaciones de cultivos y estimar distintos parámetros agronómicos a lo largo de su ciclo. Por otro lado, se proponen diferentes metodologías de clasificación de imágenes multiespectrales que revelen con la

mayor exactitud posible el impacto sobre la cubierta vegetal provocado por la plaga de topillo campesino.

Otra prueba de la generalización de las geotecnologías en el ámbito de la agricultura y la ganadería es el creciente control de animales mediante collares portadores de dispositivos GPS-GPRS (*Global Positioning System-General Packet Radio Service*), los cuales transmiten a un receptor de forma periódica la posición del animal que lo lleva colocado. Sin embargo, esta es tan solo una aportación entre las muchas que ofrecen los dispositivos GPS-GPRS, dado su gran potencial en el ámbito ganadero. Combinadas con otras geotecnologías, las geolocalizaciones derivadas de la monitorización pueden ser utilizadas simultáneamente para investigar los patrones de comportamiento que desarrollan los animales en situaciones de pastoreo libre. Entre dichas geotecnologías, destaca el LiDAR (*Light Detection and Ranging*) sobre las demás, puesto que posibilita el estudio de los principales atributos topográficos del terreno a partir de una nube densa de puntos. Del mismo modo, merecen ser mencionadas también las ortofotografías en la franja del visible e infrarrojo cercano (*Visible and Near Infrared*, VNIR), ya que, a partir de ellas, se puede establecer una clasificación precisa de las distintas coberturas y usos del suelo. Por lo tanto, la monitorización animal con dispositivos GPS-GPRS en conjunción con las dos geotecnologías mencionadas posibilitó el estudio del comportamiento de las ovejas durante el libre pastoreo, siendo ésta la tercera aportación metodológica expuesta en esta memoria de tesis.

Estas razones constituyen la motivación de la presente tesis doctoral, en la que se plantean nuevas estrategias metodológicas basadas en geotecnologías emergentes que permitan no solo ampliar los conocimientos técnicos agroganaderos con lo que se cuenta hasta la fecha sino también facilitar las labores de agricultores y ganaderos. La aplicación de estas geotecnologías pretende contribuir a una reducción de los costes y del tiempo empleado en dichas labores y a un aumento, a su vez, de los rendimientos productivos de las explotaciones agropecuarias, implementando simultáneamente sistemas de manejo sostenibles con el medio natural.

1.2. Objetivos

El objetivo principal de la presente tesis doctoral es demostrar el potencial que tienen las geotecnologías como herramientas alternativas, y a la vez complementarias, para la mejora de la gestión de los actuales sistemas agroganaderos en cualquier ámbito, ya sea económico, medioambiental o desde el punto de vista del bienestar animal. Se pretende demostrar que estas geotecnologías permiten profundizar en el aprendizaje de los conocimientos agrícolas y ganaderos tradicionales y descubrir otros nuevos.

Para la consecución del objetivo principal anteriormente descrito, se plantean los siguientes objetivos específicos:

- Demostrar el potencial de las imágenes multiespectrales aerotransportadas captadas con drones para la monitorización de diversos parámetros agronómicos medidos a pie de campo de diferentes asociaciones forrajeras, así como para la predicción de dichos parámetros en cualquier momento de su ciclo de crecimiento. Se trata de revelar la idoneidad de determinados índices espectrales para sustituir las costosas mediciones de campo.

- Evaluar el uso de los drones como metodología alternativa para la evaluación de los impactos que el topillo campesino (*Microtus arvalis* Pallas) causa en las parcelas agrícolas, con el fin de poder asistir tanto a agricultores como a los organismos responsables de la gestión de plagas, quienes a día de hoy no cuentan con medios precisos para la estimación de dichos impactos. Para la consecución de este objetivo se comparan la metodología remota con las observaciones realizadas en campo.

- Poner de manifiesto la capacidad de los dispositivos GPS y de los recursos y herramientas de la teledetección, concretamente los datos LiDAR y ortofotografías en el espectro VNIR, para exhibir los patrones de comportamiento espacial de las ovejas en pastoreo libre en relación a los atributos del terreno y a las condiciones medioambientales a las que están expuestas.

1.3. Organización de la memoria

Esta memoria de tesis está organizada en siete capítulos. Tras el índice general, previo al presente capítulo, se listan las publicaciones y comunicaciones a congresos que han servido para la redacción de la memoria de tesis, así como otras publicaciones que no se han incluido en esta tesis doctoral pero que, sin embargo, han sido aportaciones relevantes en su relación con uso de geotecnologías en el ámbito agroganadero. En el capítulo 2 se presenta brevemente la fundamentación teórica de las metodologías utilizadas. Los capítulos 3, 4 y 5 recogen las diferentes metodologías geotecnológicas desarrolladas. Concretamente, en el capítulo 3 se expone una primera aproximación metodológica del potencial que presentan las imágenes multiespectrales aerotransportadas captadas con UAS para la monitorización y predicción de diversos parámetros agronómicos de distintas asociaciones forrajeras. El capítulo 4 muestra una segunda aplicación de imágenes multiespectrales captadas con UAS, pero en este caso como metodología alternativa para evaluar con mayor precisión el impacto del topillo campesino sobre una parcela agrícola. El capítulo 5 refleja cómo, mediante la combinación de dispositivos GPS-GPRS, imágenes del espectro VNIR y datos LiDAR, es posible identificar los patrones de comportamiento de ovejas que se encuentran bajo un sistema de libre pastoreo. La discusión y conclusiones extraídas de manera conjunta de las estrategias anteriores se presentan en el capítulo 6. Finalmente, el capítulo 7 recoge varias potenciales líneas futuras de investigación que se han podido plantear gracias a los resultados obtenidos durante la investigación.

La agricultura fomenta la sensatez: una sensatez de excelente índole.

Joseph Antoine René Joubert, 1804

Capítulo 2. Antecedentes

Capítulo 2. Antecedentes

2.1. Las geotecnologías

Las tecnologías de la información geográfica, comúnmente conocidas como geotecnologías, pueden describirse como el conjunto de métodos, técnicas, herramientas y procedimientos que posibilitan la recolección, tratamiento y análisis de la información geográfica digital, es decir, de aquella información digital que cuenta con una referencia geográfica (Bolfe, 2019). Las geotecnologías abarcan los sistemas de información geográfica (SIG), que permiten la organización, el análisis y la visualización de la información geográfica, junto con la cartografía digital, la teledetección, los sistemas globales de navegación por satélite, la fotogrametría o la topografía y la geodesia, entre otras. Todas estas herramientas y metodologías se han tornado imprescindibles en el desarrollo de estudios espaciales y temporales en ámbitos terrestres de diversa índole, ya sea a nivel global, regional o local. La característica común de las geotecnologías es el uso de diferentes técnicas y herramientas que permiten el tratamiento de información georreferenciada en la que el atributo de la localización geográfica es esencial para la comprensión coherente de la información con la que se trabaja (Zanardo et al., 2016).

El surgimiento de la Revolución Verde en la década de los 60, considerada como la tercera gran revolución agrícola de la historia, fue el detonante de la aparición de nuevas tecnologías que proporcionaron a agricultores y ganaderos métodos y herramientas con los que producir a gran escala, con medios de producción vanguardistas y permitiendo un mayor control de sus insumos (Alves et al., 2021). Este proceso de modernización técnica de la agricultura y de la ganadería trajo consigo la integración de la industria, materializada por la presencia cada vez mayor de insumos industriales como fertilizantes, productos fitosanitarios, combustibles líquidos, etc., y de máquinas industriales como tractores, equipamientos agrícolas o sistemas de regadío, entre los más importantes. Sin embargo, no fue hasta finales del siglo XX cuando las tecnologías de la información geográfica se popularizaron en el sector primario, dando lugar al inicio de la cuarta y última gran revolución agrícola hasta la fecha denominada Agricultura 4.0, cuyo pilar fundamental es la información, y en la que se enmarcan la agricultura y la ganadería

de precisión (Martínez-Casanovas, 2021). Este cambio de paradigma trató de amortiguar los efectos nocivos derivados del uso indiscriminado de productos químicos y de la intensificación generada por la integración de la industria en la agricultura y en la ganadería. Se propuso así el uso de las tecnologías de la información geográfica como herramientas para aumentar la eficiencia de los sistemas de manejo agroganaderos tomando como baluartes la sostenibilidad medioambiental y el bienestar animal.

El uso de geotecnologías en la actividad agroganadera es recurrente en la sociedad contemporánea, ya sea en labores relacionadas con el conocimiento de los atributos del terreno, predicción de cosechas, control de plagas y enfermedades o monitorización de animales, entre otras. Imágenes aerotransportadas, ya sean satelitales o captadas por drones, mapas digitales y bases de datos geocodificadas se conjugan para gestionar, administrar y monitorizar la agricultura y la ganadería a diferentes escalas, cambiando el enfoque hasta ahora inmutable de una agricultura y una ganadería homogénea hacia un sector heterogéneo que requiere de un conocimiento y un tratamiento pormenorizado de sus especificidades.

2.2. Imágenes multiespectrales en teledetección

La teledetección podría definirse como una metodología de exploración e investigación que utiliza las tecnologías e instrumentación adecuadas para el estudio de la Tierra o de objetos o procesos sobre la misma sin establecer un contacto directo (Schowengerdt, 2007). Es decir, es la técnica que permite obtener información a distancia sin que exista un contacto material con la superficie terrestre. Para que ello sea posible es necesario que exista algún tipo de interacción entre los objetos observados (situados sobre la superficie terrestre, marina o en la atmósfera) y un sensor situado en una plataforma exterior a la superficie terrestre (satélite, avión, UAS, etc.).

El tipo de producto más común derivado de la teledetección es una imagen digital tipo raster, donde cada pixel tiene asignado uno o varios valores numéricos (niveles digitales) que hacen referencia a la energía media recibida dentro de una determinada banda espectral. Concretamente, una imagen multiespectral (Figura 2.1) es aquella que lleva asociados varios valores numéricos a cada pixel, tantos como bandas espectrales sea capaz de detectar el sensor. Los niveles digitales, una vez convertidos a niveles de energía,

proporcionan la llamada “firma espectral” de cada pixel, es decir, una curva de energía a lo largo del espectro electromagnético única y específica de cada elemento existente en la superficie estudiada (Price, 1994). Cuanto mayor sea el número de bandas que proporciona el sensor, más prolija será la firma espectral, y por tanto mayor será la capacidad de análisis de dichos elementos.

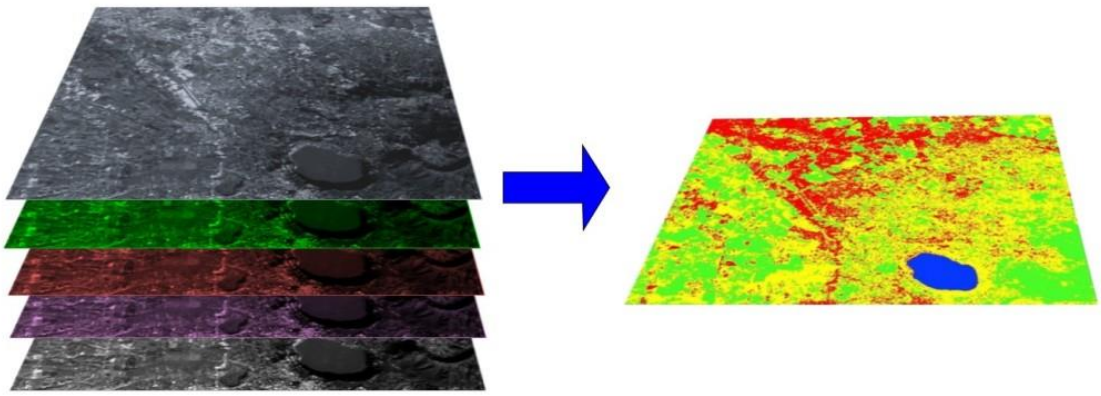

Figura 2.1. Imagen multiespectral de 5 bandas procesada para ser utilizada en una clasificación de la cobertura del suelo.

Fuente: https://semiautomaticclassificationmanual-v5.readthedocs.io/es/latest/remote_sensing.html

Existe una gran diversidad de sensores utilizados en el campo de la teledetección, si bien es cierto que, en líneas generales, se pueden clasificar en sensores activos y sensores pasivos. Mientras que los sensores activos son capaces de emitir un haz de energía que luego recogen tras su reflexión sobre la superficie, los sensores pasivos reciben la energía emitida de forma natural por una superficie (Fingas & Brown, 1997). Tanto los sensores activos como los pasivos pueden ser a su vez sensores con apertura real (el tamaño efectivo de la antena es el de la propia antena) o sensores con apertura sintética (el tamaño efectivo de la antena es virtualmente creado por la combinación de varias antenas reales). Es necesario señalar que, aunque se ha trabajado durante el período de la elaboración de esta tesis doctoral con sensores activos (imágenes radar del satélite PAZ), la investigación que se recoge en las publicaciones se ha centrado en el uso de sensores de teledetección pasivos en el espectro VNIR.

2.2.1. Firma e índices espectrales

La radiación solar domina aquellas regiones del espectro electromagnético que corresponden a la radiación visible y al infrarrojo reflejado. En cambio, la radiación terrestre domina el infrarrojo térmico, mientras que las radiaciones que corresponden a las microondas (radar) no aparecen en la naturaleza, deben ser por tanto de origen artificial, generadas por el propio sensor que las recibe posteriormente reflejadas.

Cada tipo de material, suelo, vegetación, agua, etc. refleja la radiación incidente de forma distinta, lo que permite distinguirlo de los demás al medir la radiación reflejada. A partir de ensayos de laboratorio en condiciones controladas se puede obtener la reflectividad para las distintas cubiertas en diferentes longitudes de onda y consecuentemente se han creado bibliotecas espectrales específicas para materiales, minerales, plantas, etc. El gráfico que, para cada longitud de onda, muestra la reflectividad en tanto por ciento a lo largo de las diferentes longitudes de onda se conoce, como se ha dicho anteriormente, como firma o signatura espectral (Price, 1994) (Figura 2.2), y constituye una marca de identidad de los objetos.

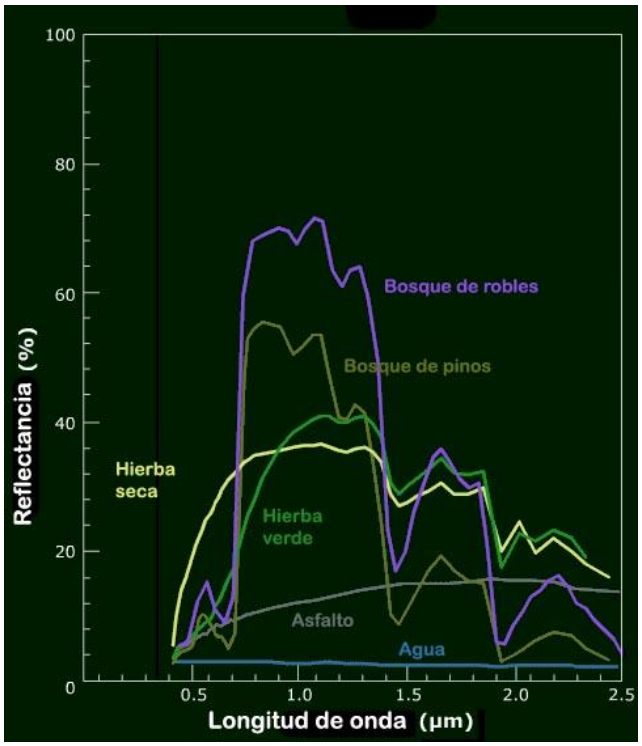

Figura 2.2. Firmas espectrales de diferentes materiales.

Fuente: http://concurso.cnice.mec.es/cnice2006/material121/unidad1/firma_es.htm

El agua clara tiene unas excelentes propiedades en cuanto a transmisión de la radiación electromagnética en el espectro visible y de absorción en el infrarrojo. En cuanto a la reflectividad, aparece un pico en el verde que va reduciéndose hasta el infrarrojo. Esta falta de reflectividad en el infrarrojo va a ser la clave para distinguir entre áreas de tierra y agua tanto en costas o lagos como en ríos, incluso en ríos pequeños. Sin embargo, cuando el agua contiene turbidez, las consecuencias sobre la respuesta espectral van a depender del tipo de turbidez. Por ejemplo, si se trata de fitoplancton, aparecerán importantes alteraciones en el verde (aumenta) y en el azul (disminuye), mientras que si se trata de sedimentos inorgánicos la reflectividad aumenta, especialmente en el rojo.

La vegetación sana tiene una reflectividad baja en el visible, aunque con un pico en el color verde debido a la clorofila. La reflectividad es muy alta en el infrarrojo reflejado o cercano debido a la escasa absorción de energía por parte de las plantas en esta banda. En el infrarrojo medio hay una disminución especialmente importante en aquellas longitudes de onda en las que el agua de la planta absorbe la energía. Durante el otoño, las hojas pierden los cloroplastos (órganos que contienen la clorofila) ya que dejan de ser necesarios, por tanto, deja de ser la clorofila el pigmento principal y las plantas adquieren un color pardo-amarillento debido a la cada vez mayor importancia relativa de carotenos y otros pigmentos. Esta curva tan contrastada se debilita en el caso de la vegetación enferma, en la que disminuye el infrarrojo y aumenta la reflectividad en el rojo y azul.

Las propiedades espectrales del suelo son relativamente simples, la transmisión es nula, por tanto, toda la energía se absorbe o se refleja. La reflectividad es relativamente baja para todas las bandas, aunque aumentando hacia el infrarrojo. Hay una cierta dependencia entre reflectividad y contenido de agua del suelo, cuanto mayor es el segundo, mayor es la primera (de ahí que un suelo mojado se vea más oscuro). Este aumento se ve interrumpido en aquellas regiones en las que el agua absorbe energía (infrarrojo de onda corta), por tanto, cuanto mayor sea el contenido de agua en el suelo, mayor va a ser la disminución en reflectividad de estas regiones. Otro factor que afecta la respuesta espectral del suelo es la textura, con una mayor reflectividad al aumentar el tamaño medio de las partículas de suelo (los suelos arenosos se ven más claros que los arcillosos). El problema es que la textura afecta también al contenido de humedad, por lo que no resulta fácil diferenciar con imágenes de satélite entre ambos factores, a no ser

que se recurra a imágenes en el espectro de las microondas. El contenido en materia orgánica también afecta a la reflectividad, cuanto mayor sea su contenido y cuanto menos descompuesta se encuentre, más oscuro resulta el suelo.

Una imagen multiespectral, ya sea obtenida mediante satélites o vehículos aerotransportados, en su estado bruto es realmente un conjunto de imágenes (una por banda) o de matrices (una por cada canal del sensor), cada una de las cuales lleva asignado un determinado valor numérico conocido como nivel digital. Con el fin de hacerlos físicamente interpretables, dichos niveles digitales deben ser transformados en energía emitida por algún tipo de variable física (vegetación, suelo, agua, nieve, etc.). Para ello es necesario llevar a cabo un procedimiento de calibración y corrección radiométrica para así poder evitar los sesgos e interferencias que pueden generar tanto la iluminación recibida por el objeto en un momento específico del día como los fenómenos atmosféricos que puedan darse en dicho momento (Pons & Solé-Sugrañes, 1994; Teillet, 2007). Una vez convertidos a valores de reflectividad, se pueden combinar algorítmicamente en forma de índices espectrales (Jackson, 1983).

En agronomía, los índices espectrales más utilizados son los índices de vegetación, ya que consiguen realzar la vegetación en función de su respuesta espectral y atenuar los detalles de otros elementos como el suelo, la iluminación, el agua, etc. Es decir, destacan los píxeles relacionados con parámetros de las coberturas vegetales, fundamentalmente con la densidad, el índice de área foliar y la actividad clorofílica (Bannari et al., 1995). Existe un elevado número de índices de vegetación, sin embargo, se citarán aquí los más relacionados con la investigación de la tesis. Destaca sobre los demás por su popularidad y versatilidad el índice de vegetación de diferencia normalizada (*Normalized Difference Vegetation Index*, NDVI) (Rouse et al., 1974), que está altamente asociado con la cantidad, calidad y desarrollo de la vegetación, permitiendo caracterizar su presencia y su distribución espacial. Utiliza la diferencia normalizada entre las reflectividades de las bandas espectrales infrarroja cercana (*Near Infrared*, NIR), ρ_{NIR}, y roja, ρ_{Red}, (Ecuación 2.1), de manera que los valores altos de NDVI corresponden a áreas que reflejan más en el espectro del infrarrojo cercano y, por tanto, refieren una vegetación más densa y más saludable. El hecho de dividir entre la suma de ambas reflectividades compensa tanto el efecto de mayor o menor luminosidad como el efecto de la atmósfera.

No obstante, su interpretación debe realizarse con cierta cautela puesto que es un índice sensible a la reflectividad del suelo.

$$NDVI = \frac{\rho_{NIR} - \rho_{Red}}{\rho_{NIR} + \rho_{Red}} \tag{2.1}$$

Por este motivo, es necesario considerar otros índices de vegetación que podrían aportar información relevante sobre la cobertura vegetal, y complementar así los resultados obtenidos con el NDVI. En este contexto, es muy común utilizar índices basados en el espectro RGB (*Red-Green-Blue*). Entre ellos, el índice de vegetación verde-rojo (*Green-Red Vegetation Index*, GRVI) (Tucker, 1979) utiliza las reflectividades de las bandas roja (ρ_{Red}) y verde (ρ_{Green}) (Ecuación 2.2), ofreciendo una interpretación más simple ya que distingue entre vegetación ($\rho_{Green} > \rho_{Red}$), suelo ($\rho_{Green} < \rho_{Red}$) y agua/nieve ($\rho_{Green} \approx \rho_{Red}$).

$$GRVI = \frac{\rho_{Green} - \rho_{Red}}{\rho_{Green} + \rho_{Red}} \tag{2.2}$$

Del mismo modo, el índice de verdor de la cobertura vegetal (*Greenness Vegetation Index*, GVI) (Sánchez et al., 2015) (Ecuación 2.3) ofrece una proporción de la reflectividad de la banda verde sobre el total del espectro RGB.

$$GVI = \frac{\rho_{Green}}{\rho_{Red} + \rho_{Green} + \rho_{Blue}} \tag{2.3}$$

En definitiva, cada índice de vegetación está diseñado para una función en concreto y presenta sus ventajas y sus limitaciones. Por ello, es necesario adecuar la elección del índice de vegetación no solo a los resultados buscados sino a determinados factores inherentes a las condiciones de partida, como son el tipo de cultivo, el momento del ciclo en el que se encuentra, el escenario atmosférico, etc.

2.2.2. Métodos de clasificación multiespectral

En el contexto de la teledetección, la clasificación de imágenes multiespectrales se considera un procedimiento mediante el que se asigna a cada píxel de la imagen original una etiqueta que corresponde a una de las clases de partida, bien sean clases

definidas por el usuario previo al proceso de clasificación en sí, bien clases generadas automáticamente durante el proceso por agrupación en base a la semejanza de características de los píxeles de la imagen. La imagen resultante es en realidad un mapa raster en el que las variables continuas propias de la imagen de partida son agrupadas en variables discretas según clases.

Existen diferentes criterios para distinguir entre los distintos tipos de clasificación multiespectral existentes. Las denominadas clasificaciones supervisadas se construyen mediante áreas de entrenamiento o regiones de interés marcadas previamente por el usuario, de manera que los patrones espectrales que caracterizan las diferentes clases se obtienen de dichas áreas. Por el contrario, las clasificaciones no supervisadas se construyen de manera automática basándose en la semejanza de los valores espectrales de los píxeles (Quirós-Rosado, 2009).

Tradicionalmente, las clasificaciones de imágenes multiespectrales (supervisadas o no) se han realizado mediante técnicas orientadas a tomar el píxel como unidad de clasificación. Sin embargo, recientemente se han desarrollado técnicas muy robustas y precisas como alternativas a las orientadas a píxel que toman los objetos, también denominados segmentos, como unidades de clasificación, es decir, agrupaciones de píxeles en base a diversos criterios de homogeneidad, ya sean espectrales o espaciales (Walter, 2004; Quirós-Rosado, 2009). Una de las principales ventajas de utilizar clasificaciones orientadas a objetos es que, además de la información espectral, a los objetos se les atribuyen una serie de características geográficas/geométricas, como textura, forma y longitud y entidades topológicas, como la adyacencia (Weih & Riggan, 2010). Estos atributos crean una base de conocimientos para los objetos muestrales mucho más rica en información que la de los píxeles individuales, y a la que se puede recurrir para desarrollar un proceso de clasificación basado en reglas (Zerrouki & Bouchaffra, 2014). Además, este tipo de clasificaciones elimina el denominado efecto *salt-and-pepper* (moteado de píxeles aislados entre las diferentes clases) que en ocasiones aparece en las clasificaciones orientadas a píxel (Yan et al., 2006; Dronova et al., 2011). En contrapartida, las clasificaciones orientadas a objetos requieren un conocimiento *a priori* de la zona y de los tipos de clase que se investigan, que no siempre está disponible. Otra desventaja es que el proceso de segmentación y el posterior cálculo de las relaciones topológicas descritas entre los objetos pueden suponer un gran consumo computacional.

Entre los algoritmos más utilizados en las metodologías de clasificación no supervisada destacan el *iterative self-organization data analysis* (ISODATA) (Tou & González, 1974) y el *K-means*. Por otro lado, los algoritmos y procedimientos más destacables utilizados en las clasificaciones supervisadas, ya sean basadas en píxeles o en objetos, son el *support vector machine* (SVM) (Hearst et al., 1998), el *random forest*, (RF) (Breiman, 2001), método de la máxima verosimilitud o el método del vecino más próximo.

2.2.3. Imágenes satelitales *vs.* imágenes de dron en el espectro VNIR

En el campo de la agricultura y ganadería de precisión, escoger una tecnología basada en análisis de imagen u otra para la captación de datos no es una decisión baladí. Ante esta disyuntiva, normalmente se presentan dos alternativas: teledetección con drones o mediante satélite. La premisa de la que es necesario partir es que ambas ofrecen ventajas e inconvenientes, es decir, ambas aportan prestaciones que la otra no puede proporcionar, razón por la que deben ser consideradas como tecnologías complementarias en lugar de opuestas.

En la actualidad, existen decenas de misiones espaciales con sensores a bordo de satélites de los que es posible extraer datos e imágenes con distinta resolución espacial, como son el MODIS (*Moderate-Resolution Imaging Spectroradiometer*) (250 a 1.000 metros/pixel), Landsat (30 a 100 metros/pixel) o Sentinel (10 a 60 metros/pixel), entre otros. Estos satélites posibilitan la obtención de una gran cantidad de información instantánea sin necesidad de tener que desplazarse al campo y permiten abarcar grandes extensiones de terreno. Concretamente, la franja de la superficie terrestre que se visualiza en las imágenes captadas con sensores satelitales, también denominada *swath*, abarca entre decenas y cientos de kilómetros de ancho, como es el caso de las misiones Landsat-8 o Sentinel-2 con 185 km y 290 km de anchura, respectivamente.

No obstante, la visibilidad de las imágenes obtenidas está condicionada por dos factores: el tiempo de revisita al mismo punto (entre una y dos semanas en el caso de Landsat y Sentinel y un día en el caso de MODIS) y la meteorología en el momento de la captación (Inoue, 2020). Un satélite toma los datos en una posición situada a cientos de kilómetros de la superficie terrestre, captando las ondas electromagnéticas en función de

la radiación solar, lo que implica que son necesarias unas condiciones meteorológicas libres de nubes para que las imágenes sean útiles. Dada la gran incertidumbre que generan tanto el tiempo de revisita como el sometimiento a las condiciones climáticas, la obtención de imágenes en una fecha específica se torna considerablemente complicada, lo cual es una limitación importante, más si cabe en el mundo agrícola, donde disponer de información en momentos clave del ciclo de los cultivos es vital. Por el contrario, aunque el dron implica el desplazamiento hasta la zona de estudio, no presenta un tiempo de revisita. Además, vuela por debajo del nivel de las nubes y no se ve tan afectado por esas condiciones de radiación de luz y nubosidad (lo que hace innecesaria la corrección atmosférica), si bien es cierto que la lluvia y los vientos fuertes limitan su funcionamiento y que, para aplicaciones precisas, es necesaria una calibración radiométrica para tener en cuenta las condiciones de luminosidad.

Las imágenes capturadas por sensores embarcados en plataformas satelitales son calibradas mediante correcciones geométricas y atmosféricas. El hecho de que la concentración de aerosoles presentes en la atmósfera cambie, hace necesaria la corrección atmosférica para evitar distorsiones entre imágenes tomadas en tiempos distintos. Por el contrario, las imágenes captadas por sensores portados por drones requieren una calibración radiométrica mucho más sencilla puesto que no precisa de una corrección atmosférica (Inoue, 2020). Esta particularidad permite una comparación temporal de imágenes con una elevada precisión. Los sensores habituales que se embarcan en drones captan imágenes en un número de bandas menor que en el caso de las imágenes satelitales, sin embargo, dada la baja altura de vuelo, su resolución espacial es mucho mayor (Figura 2.4), en ocasiones centimétrica, aportando un análisis de la superficie terrestre mucho más preciso. No obstante, es necesario señalar que el coste operacional que conlleva el uso de drones es considerablemente mayor que el uso de imágenes satelitales, tanto por la adquisición y mantenimiento del equipo como por la menor autonomía que ofrece en términos de extensión de vuelo.

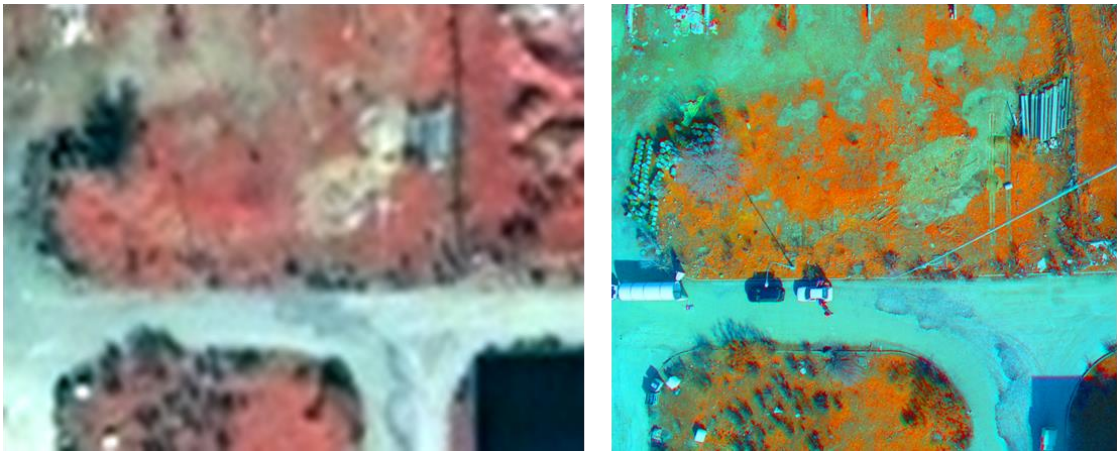

Figura 2.3. Comparación de la resolución espacial de una imagen multiespectral satelital procedente de la misión Sentinel-2 (Izquierda) y por un sensor portado por un dron (Derecha).

Fuente: http://www.comunidadism.es/blogs/los-drones-analisis-del-estado-del-arte-basado-en-la-experiencia

Como se ha mencionado anteriormente, esta comparativa no tiene como objetivo priorizar una tecnología sobre la otra sino poner en valor las principales aportaciones de cada una de ellas. La elección de una u otra debe basarse en los principales objetivos del estudio, que determinarán la resolución espacial que se necesita, la extensión de trabajo, la flexibilidad en cuanto a los sensores o al procedimiento de toma de imágenes y los costes, entre otros factores.

2.3. LiDAR

El LiDAR (*Light Detection And Ranging*) es una técnica de teledetección que utiliza la luz láser para obtener una muestra densa de la superficie de la tierra produciendo mediciones exactas de las coordenadas x, y, z. El LiDAR está surgiendo como una alternativa rentable para las técnicas de cartografía tradicionales como la fotogrametría. Produce datasets de nubes de puntos masivos que se pueden administrar, visualizar, analizar y compartir usando un software generalista de tipo SIG o bien aplicaciones específicas.

El LiDAR es en realidad un sensor activo en el espectro óptico que emite un pulso láser hacia un objetivo mientras se mueve a bordo de un avión, en el caso del LiDAR aerotransportado. Tras interceptar la superficie terrestre, el pulso es reflejado y detectado y almacenado en los receptores del sensor LiDAR. Estos receptores registran el preciso

momento desde que el pulso láser dejó el sistema hasta cuando regresó para calcular la distancia límite entre el sensor y el objetivo. Combinado con la información posicional (*Global Positioning System*, GPS, e *Inertial Navigation System*, INS), estas medidas de distancia se transforman en medidas de puntos tridimensionales reales del objetivo reflector en el espacio del objeto. Los datos de punto se procesan posteriormente después de que la recopilación de datos LiDAR se reconoce dentro de las coordenadas x, y, z georreferenciadas con alta precisión al analizar el rango de tiempo láser, ángulo de escaneo láser, posición del GPS e información del INS.

Los pulsos láser emitidos desde un sistema LiDAR se reflejan desde objetos sobre y por encima de la superficie del suelo: vegetación, edificios, puente, etc. Un pulso láser emitido puede regresar al sensor LiDAR como uno o muchas devoluciones o retornos (Figura 2.4). Cualquier pulso láser emitido que encuentre varias superficies de reflejo a medida que viaja hacia el suelo se divide en tantos retornos como superficies reflectoras existan.

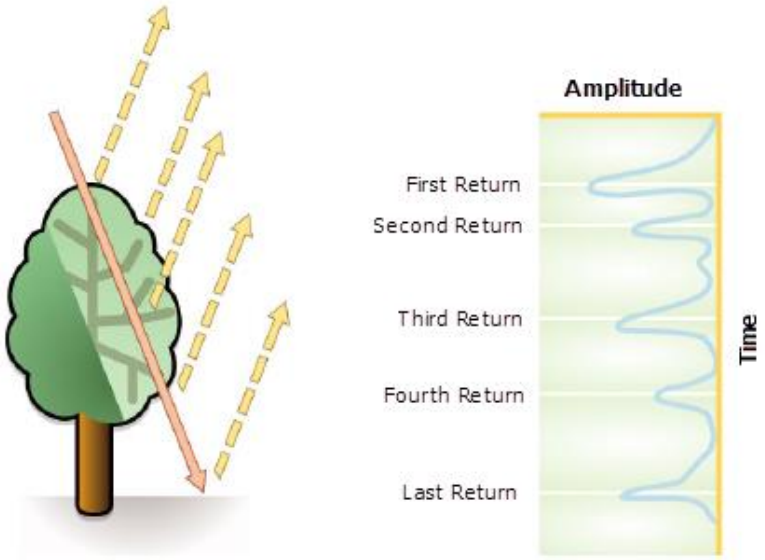

Figura 2.4. Diferentes retornos que podría registrar un sensor LiDAR.

Fuente: https://desktop.arcgis.com/es/arcmap/10.3/manage-data/las-dataset/what-is-lidar-data-.htm

El primer pulso láser devuelto es el más importante y se asociará con la entidad más grande en el terreno como una copa de árbol o la parte superior de un edificio. El primer retorno también puede representar el suelo, en cuyo caso el sistema LiDAR solo detectará una única devolución. Varios retornos pueden detectar las elevaciones de

diferentes objetos dentro de la huella láser de un pulso láser saliente. Los retornos intermedios, en general, se utilizan para la estructura de la vegetación, y el último retorno para los modelos de terreno de suelo desnudo.

Cada punto LiDAR puede tener una clasificación asignada que define el tipo de objeto que reflejó el pulso láser (terreno, vegetación, edificio, etc.). Los puntos LiDAR se pueden clasificar en varias categorías que incluyen suelo o terreno desnudo, parte superior de cubierta forestal y agua. Las diversas clases se definen mediante códigos numéricos de enteros en el archivo LAS. Los códigos de clasificación más habituales los definió la Sociedad Americana de fotogrametría y teledetección (ASPRS), aunque se pueden usar leyendas específicas. De hecho, aunque el dataset LiDAR incluye normalmente una clasificación, es conveniente revisarla y/o reclasificarla, ya que contienen errores (especialmente en los datos LiDAR de las primeras misiones cartográficas). De la misma manera, también es aconsejable filtrar la nube de puntos para evitar solapes, duplicidades y ruido.

2.4. GNSS

El término GNSS (*Global Navigation Satellite System*) hace referencia de forma genérica a los sistemas de navegación por satélite que proporcionan un posicionamiento geoespacial con cobertura global.

El GPS (*Global Position System*) fue el primer sistema GNSS operativo, el cual fue desarrollado por el Departamento de Defensa de Estados Unidos. Permite obtener la posición (sus coordenadas geográficas) en cualquier punto de la tierra mediante el uso de un aparato receptor que recoge la señal suministrada por un conjunto de satélites que orbitan entorno a la Tierra. El término GPS es un caso evidente de metonimia, pues está tan extendido en la cultura social que se confunde con el término GNSS, perdiéndose la verdadera perspectiva en la que el GPS es uno entre los diversos sistemas GNSS, tales como el GLONASS (*Global'naya Navigatsionnaya Sputnikovaya Sistema*), GALILEO, BEIDOU.

Cualquiera de los sistemas GNSS emplea una constelación de satélites que orbitan sobre la superficie terrestre. GALILEO es el sistema GNSS de creación, gestión y uso civil (a diferencia del GPS y GLONASS) desarrollado por la Unión Europea (UE) a través

de la Agencia Espacial Europea (ESA) y cuya constelación consta actualmente de 22 satélites operativos. En cambio, el sistema GLONASS cuenta con una constelación formada por 31 satélites, 24 de los cuales están en activo, 3 en repuesto y 4 en mantenimiento. El sistema BEIUDOU es un sistema de navegación por satélite chino cuya constelación consta a día de hoy de 35 satélites. La constelación de satélites que usa el sistema GPS consta de 24 satélites operativos (aunque en la actualidad tienen 31 satélites en órbita) situados a 20.200 km de distancia de la superficie terrestre, y se denomina NAVSTAR (*Navigation Signal Timing and Ranging*). El proyecto se puso en marcha en 1973 y se terminó de implementar en marzo de 1994. Como curiosidad, en 1983, dos aviones cazas soviéticos derribaron un Boeing de la Korean Airlines, que por un error de posicionamiento invadió espacio aéreo ruso y fue confundido con un avión espía estadounidense. En ese momento, con el fin de evitar otra tragedia similar, Estados Unidos liberó el sistema GPS para su uso libre por el resto del mundo, aunque sigue siendo gestionado por el Departamento de Defensa de los Estados Unidos.

Para entender el sistema GPS se hace necesario conocer los elementos que lo forman. Dentro del sistema GPS existen tres conjuntos de componentes denominados segmentos:

- Segmento Espacial: constituido por los satélites que soportan el sistema y las señales de radio que emiten. En el sistema NAVSTAR GPS se utilizan satélites no geoestacionarios, los cuales recorren órbitas elípticas respecto al centro de la Tierra, que forman un ángulo de 55º con el plano ecuatorial y recorren todos los puntos de la superficie terrestre. Sin embargo, sus órbitas deben ajustarse para obtener una cobertura global, es decir, que en cualquier punto se vean un número mínimo de tres satélites con una duración y periodicidad aceptable para permitir en recepción el cálculo de su posición con una precisión determinada.
- Segmento control: está constituido por todas las infraestructuras en tierra necesarias para el control de la constelación de satélites, mantenidas por la fuerza aérea estadounidense. Dichas infraestructuras tienen coordenadas terrestres de muy alta precisión y consisten en cinco grupos de

instalaciones repartidas por todo el planeta (Figura 2.5), para tener un control homogéneo de toda la constelación de satélites.

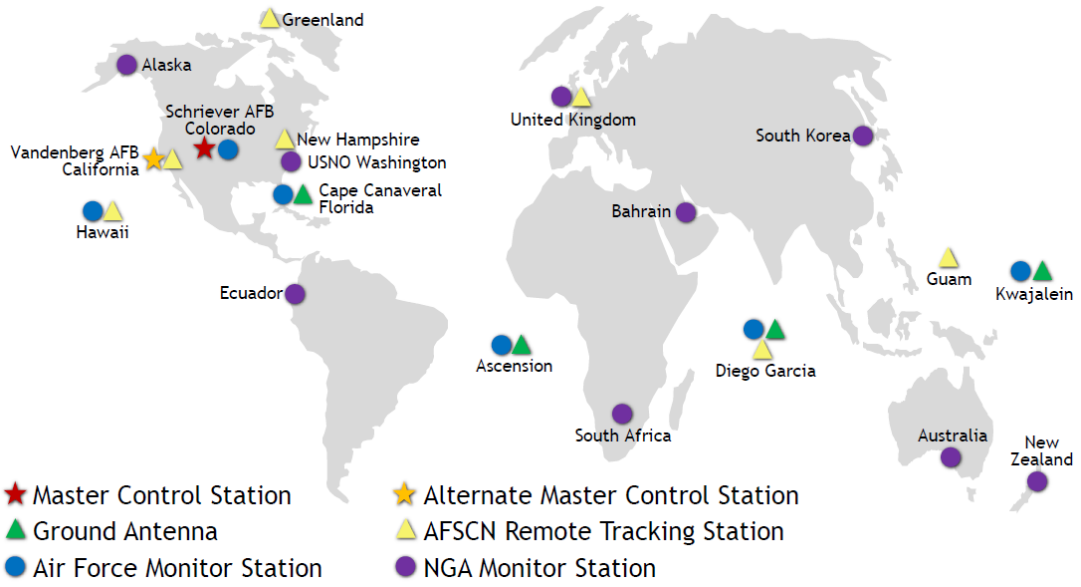

Figura 2.5. Situación de las estaciones de control.

Fuente: https://www.proteccioncivil.es/catalogo/carpeta02/carpeta24/vademecum19/vdm02560.htm.

Estas infraestructuras realizan un seguimiento continuo de los satélites que pasan por su región del cielo, acumulando los datos necesarios para el cálculo preciso de sus órbitas. Dichas órbitas son muy predecibles, dado que no existe fricción atmosférica en el entorno donde se mueven los satélites. Sin embargo, también tienen una degradación debido a una serie de factores: desigual densidad de la gravedad terrestre, mareas gravitatorias provocadas por el alineamiento de la luna y los planteas, viento solar, etc. Todos estos factores han de tenerse en cuenta para que el sistema GPS siga siendo preciso.

- Segmento del usuario: constituido por el hardware (equipos de recepción) y el software que se utilizan para captar y procesar las señales de los satélites. Para los usuarios del sistema GPS es quizá la parte más interesante, puesto que la precisión alcanzada depende del tipo de instrumental y métodos utilizados.

La señal GPS tiene un ancho de banda superior al necesario para poder asegurar las comunicaciones, y poder combatir las interferencias entre el transmisor (satélite) y el receptor (usuario). La fuente de frecuencia la general el oscilador o reloj, y a partir de la frecuencia nominal de 10,23 MHz instalada en GPS se generan el conjunto de portadoras y códigos que conforman la señal GPS.

Los satélites van a emitir tres tipos de señales: portadora, código y mensaje. Las ondas portadoras L por sí solas no sirven para resolver el problema de posicionamiento y deben someterse a unas operaciones de procesado de señal GPS. La más importante es la modulación orientada al acoplamiento de la señal a transmitir, para llevar los códigos llamados C/A (*Coarse/Acquisition*) y P (*Protected*). Cada satélite tiene un código C/A diferente, lo que genera un ruido pseudoaleatorio distinto (PRN, *Pseudo-Random Noise*) y esto es fundamental para que el receptor identifique cada satélite. El receptor que tiene almacenada las réplicas de todos los PRN, identifica al satélite, y a la vez genera una réplica del código recibido, desfasado, porque el recibido ha tenido que recorrer el trayecto. El receptor correlaciona los códigos generado y recibido, lo que permite medir el tiempo y la distancia recorrida.

Cuando los receptores GPS se colocan en collares en los animales, es necesaria la transmisión de las sucesivas posiciones que se generan a una plataforma de descarga. La tecnología GPRS (*Global Packet Radio Service*) se creó con objeto de transmitir datos más eficientemente mediante conmutación de paquetes desde terminales móviles. Es una evolución de la conocida red GSM (*Groupe Special mobile*), contando por tanto con su misma cobertura, pero subsanando claras deficiencias que presentaba en su infraestructura y arquitectura. Esto ha permitido la transmisión de datos de geolocalización aportados por dispositivos GPS situados en un collar que es portado por animales domésticos, ya sean animales de compañía o animales de granja.

2.4.1. Cálculo de parámetros derivados de las geolocalizaciones GPS

En el contexto de la utilización de dispositivos GPS en animales domésticos de granja, la información geográfica emitida periódicamente por un dispositivo GPS puede ser tratada de manera que se puedan calcular de una serie de parámetros o variables que puedan aportar información relevante para el ganadero acerca del comportamiento de sus

animales durante dicho periodo. A partir de las coordenadas geométricas, se puede obtener la distancia reducida que ha recorrido el animal entre un punto (X1,Y1) y el punto inmediatamente posterior a él (X2,Y2) (Ec. 2.4).

$$d = \sqrt{(X_2 - X_1)^2 + (Y_2 - Y_1)^2} \tag{2.4}$$

El tiempo invertido en recorrer esa distancia es el fijado en el protocolo de registro de datos. Por lo tanto, contando con la distancia y con el tiempo, se puede calcular la velocidad a la que se ha desplazado el animal. Llegado a este punto, es necesario considerar con cierta cautela el nivel de incertidumbre en la interpretación de la actividad del animal en base a los resultados de velocidad obtenidos, puesto que cuanto mayor sea el intervalo de tiempo entre registros, mayor será dicha incertidumbre.

Más allá de los parámetros mencionados, es posible obtener información acerca de la dirección que ha tomado el animal para desplazarse, a partir del denominado acimut. El acimut se define como el ángulo horizontal comprendido entre el punto Norte del horizonte y la dirección entre dos posicionamientos consecutivos, medido siempre en sentido horario (Figura 2.6). Su cálculo se basa en la función arco tangente de dos posiciones consecutivas, teniendo en cuenta el cuadrante de la posición 2 con respecto a la posición 1.

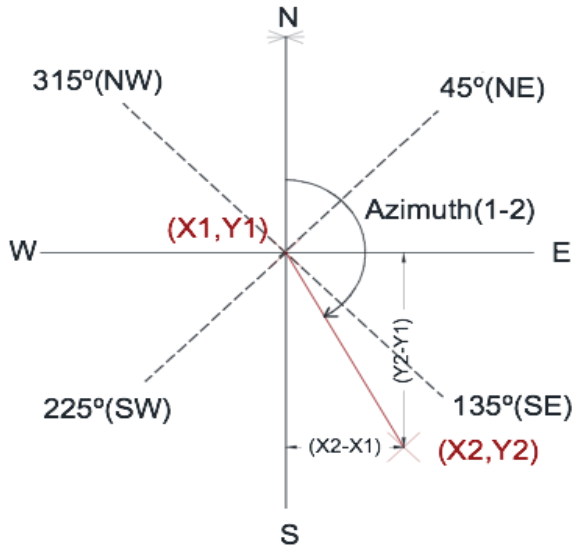

Figura 2.6. Cuadrantes de rumbo y esquema de acimut entre dos posiciones GPS consecutivas.

Fuente: Plaza et al. (2022b).

Capítulo 3. UAV multispectral imaging potential to monitor and predict agronomic characteristics of different forage associations

Plaza, J., Criado, M., Sánchez, N., Pérez-Sánchez, R., Palacios, C., & Charfolé, F. (2021). UAV Multispectral Imaging Potential to Monitor and Predict Agronomic Characteristics of Different Forage Associations. *Agronomy*, 11(9), 1697. https://doi.org/10.3390/AGRONOMY11091697

Capítulo 3. UAV multispectral imaging potential to monitor and predict agronomic characteristics of different forage associations

Resumen

Los forrajes son una de las principales fuentes de alimento para el ganado, especialmente para los rumiantes, que son capaces de transformar alimentos pobres en proteínas en productos de consumo humano con alto contenido proteico, como son la carne y la leche. Teniendo en cuenta, por tanto, la importancia de los forrajes en los sistemas agroganaderos, se hace necesario realizar evaluaciones periódicas del estado nutricional, fisiológico y sanitario de los forrajes a lo largo de su ciclo de crecimiento, labores que, hasta el día de hoy, se han realizado *in situ* con un gran consumo de tiempo y mano de obra. Estos hechos motivaron el objeto de este trabajo, en el que se evaluó la capacidad de las imágenes captadas mediante vehículos aéreos no tripulados (UAVs) para monitorizar y predecir la evolución de varias asociaciones forrajeras durante todo el ciclo de cultivo 2019-20. Para ello, se utilizaron ocho asociaciones forrajeras diferentes cultivadas por triplicado: veza-cebada-triticale (VCbT), veza-triticale (VT), veza-centeno (VC), veza-avena (VA), guisante-cebada-triticale (GCbT), guisante-triticale (GT), guisante-centeno (GC) y guisante-avena (GA). Se monitorizaron seis parámetros biofísicos mediante seis índices de vegetación en siete fechas de medición distribuidas a lo largo del ciclo de cultivo. El experimento se desarrolló en la finca de producción ecológica "Gallegos de Crespes", situada en el municipio de Larrodrigo (Salamanca, España). Los resultados obtenidos en el análisis exploratorio y de correlación mostraron una relación muy considerablemente fuerte entre los índices espectrales y las estimaciones de campo, sugiriendo consecuentemente la realización de un modelo predictivo (basado en la regresión de mínimos cuadrados parciales, PLS). En general, las asociaciones que contenían veza como leguminosa mostraron valores ligeramente superiores, tanto para los parámetros de campo como para los índices de vegetación, que las que contenían guisante. Las correlaciones fueron muy fuertes y significativas para

cada asociación a lo largo de su ciclo de crecimiento, lo que sugiere que la evolución de las asociaciones podría ser monitorizada a partir de los índices espectrales. Integrando estas observaciones multiespectrales en el modelo PLS, se predijeron los parámetros agronómicos de las asociaciones forrajeras con una fiabilidad superior al 50%. Una sola combinación de bandas del espectro visible e infrarrojo cercano -VNIR- (o incluso sólo visibles) fue capaz de alimentar el modelo de regresión, conduciendo a una predicción exitosa de los parámetros agronómicos.

Abstract

The capability of unmanned aerial vehicles (UAVs) imagery to monitor and predict the evolution of several forage associations was assessed during the whole growing cycle of 2019–20. For this purpose, eight different forage associations grown in triplicate were used: vetch-barley-triticale (VBT), vetch-triticale (VT), vetch-rye (VR), vetch-oats (VO), pea-barley-triticale (PBT), pea-triticale (PT), pea-rye (PR) and pea-oats (PO). Six biophysical parameters were monitored through six vegetation indices on seven measurements dates distributed along the growing cycle. The experiments were carried out on the organic farm "Gallegos de Crespes" located in the municipality of Larrodrigo (Salamanca, Spain). The results obtained in the exploratory and the correlation analysis suggested that a predictive model (PLS regression) could be performed. Overall, vetch-based associations showed slightly higher values for both the field parameters and the vegetation indices than pea-based ones. Correlations were very strong and significant for each association throughout their growing cycle, suggesting that the evolution of the associations would be monitored from the spectral indices. Integrating these multispectral observations in the PLS model, the agronomic parameters of forage associations were predicted with a reliability of more than 50%. A single combination of VNIR (or even only visible) bands was able to feed the regression model, leading to a successful prediction of the agronomic parameters.

Keywords: crop biophysical variables, drone, forage association, PLS, vegetation indices.

3.1. Introduction

Forages are one of the main feed sources for livestock, especially for ruminants, which are able to transform protein-poor feed into high-protein human consumption products such as meat and milk (Ghanbari-Bonjar & Lee, 2003). Generally, such forages are based exclusively on cereals such as barley, oats or wheat, among others, due to the high dry matter yield they produce at very low cost. These cereal-based forages provide large amounts of energy to the animals, but lack other vital elements such as protein, thus reducing their nutritional quality (Nadeem et al., 2010). The separate purchase of protein supplements results in high feed cost, and considering that high quality forage optimizes animal productivity, increasing the quality of such forages is a much more effective method of improving overall feed efficiency (Eskandari et al., 2009). One of the most cost-effective ways of increasing forage quality is by mixing cereal crops with others species capable of increasing the protein content of the overall ration, such as legumes. Crop associations or intercropping systems are defined as the simultaneous growing of two or more species on the same area during a significant period of their growing season (Willey, 1979). These crop mixtures show several potential advantages over sole crops, as they have higher yields and greater yield's stability from season to season, are more resistant to pests and diseases, improve forage production quality, maintain soil fertility due to legume's biological fixation of nitrogen and increase microbiota biodiversity (Staniak et al., 2014).

Considering the importance of forages in agriculture, it is necessary to carry out periodical assessments of the nutritional, physiological and sanitary status of forages throughout their growing cycle. This will allow to characterize the different crop associations and aid in estimating both the quality and potential yields of these crops (Chandel et al., 2021). Nowadays, the limited available methodologies to carry out this monitoring consist of painstaking field works (Hollinger, 1997), usually divided into two stages. The first one is a non-invasive stage based on visual observations to check the phenological and sanitary state of the crop (Undersander et al., 2011) and on parameter measurements that do not involve sample extraction, such as chlorophyll level (Puangbut et al., 2017), crop height or fractional vegetation cover (FVC) estimation (Pereira et al., 2020), among others. On the other hand, the second stage is an invasive one and consists

of collecting a sample over a known surface area in order to estimate leaf area index (LAI) (Guan & Nutter, 2003), productive yield and forage quality (Orloff, 1996; Salama, 2020).

Remote sensing, particularly piloted aircraft and satellite imagery (RGB, multispectral or hyperspectral), has emerged in the last twenty years as a widespread non-invasive methodology for crop monitoring (Mulla, 2013). However, their images lack high enough spatial resolution to perform accurate time series analysis (Chang et al., 2017). In this context, drones or unmanned aerial systems (UAVs) and the miniaturized sensors they carry have emerged as a useful technology. These sensors offer very high-resolution images, low operational and maintenance costs and instantaneous data transmission (Pádua et al., 2017). Among them, multispectral (MS) sensors stand out as one of the best options for assessing crop growth, biomass quantity and several biochemical indicators (X. Li et al., 2012; Verger et al., 2014; X. Zhou et al., 2017), specifically from forages (W. Castro et al., 2020). The more common MS sensors are able to register five or six bands in the visible-near infrared spectra region. Using different algebraic combinations of these bands, a wide range of vegetation indices can be calculated. The most widespread due to its great versatility is the normalized difference vegetation index (NDVI) (Rouse et al., 1974) as it not only provides information on the quality and development of vegetation, but has also been used to estimate productive yields in certain crops (Becker-Reshef et al., 2010; Maresma et al., 2020; Shafiee et al., 2021).

The hypothesis of the work is that it is possible, on the basis of a range of vegetation indices taken along the growing cycle, to predict several agronomic characteristics of crops at any moment of their growth cycle. If so, these indices could replace the laborious field work that must be carried out for *in situ* crop monitoring. Since the single indices may be insufficient to model the crop evolution, a wide range of regression models emerge as a way of integrate the information of all of them, such as the support vector machine (SVM) (Drucker et al., 2003), based on the machine learning theory, or the regression model based on partial least squares (PLS) (H. Wold, 1982; S. Wold et al., 2001), which is a multivariate statistical tool with applications in many academic disciplines, including precision agriculture (Osborne et al., 2002; Montes et al., 2011; Z. Zhou et al., 2019; Ma et al., 2020). PLS is the most successful multivariate

calibration method in the application of the combination of chemometrics with spectral data (Helfer et al., 2020). This technique addresses the problem of finding a linear regression model by mapping the explanatory variables and the observed variables into a new space. Besides, it is an easy and intuitive method that analyzes associations between two sets of data and highly recommended when the explanatory variables are correlated. It is a non-parametric technique which makes no distributional assumptions that works with small sample sizes (Abdi, 2010). The PLS transformations of the explanatory variables try to explain the covariance between the explanatory and observed variables as far as possible (Krishnan et al., 2011).

Considering the above, the present work shows a first screening of the potential of airborne multispectral images captured with UAVs for the monitoring and prediction of several *in situ* agronomic parameters of different forage associations. The research explored the relationships between a few spectral indices UAV-based and simultaneous field measurements over several fields of forage associations during a 2019–20 campaign. The indices suitability was first assessed after a descriptive analysis and a correlation analysis, whose promising results suggested the suitability of a robust mathematical method (PLS) to build a prediction model of the growing cycle parameters. Other contribution to the UAVs community is the assessment of the use of indices on the visible spectra as an alternative of the more costly infrared-based cameras. The paper was organized as follows: Section 2 explains the experimental layout, the data acquisition and the statistical analysis. Section 3 is devoted to the results and their discussion, and the Conclusions close the text.

3.2. Material and methods

3.2.1. Experimental design

This study was carried out from October 2019 to June 2020 on the organic production farm “Gallegos de Crespes” (40°42′13″ N–5°25′43″ W; 906 m above sea level) located in the municipality of Larrodrigo, in the southeast of the province of Salamanca in Castilla y León, Spain (Figure 3.1).

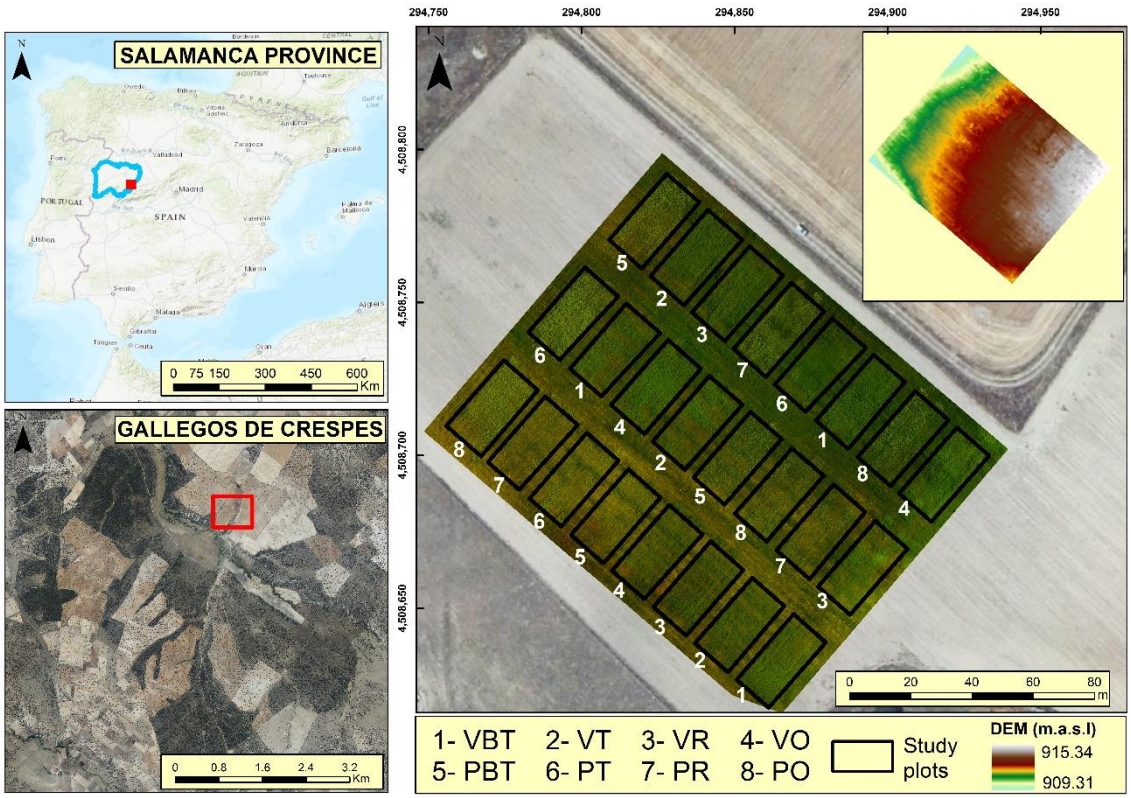

Figure 3.1. Farm location, experimental design and digital elevation model (DEM) of the study area. VBT: vetch-barley-triticale, VT: vetch-triticale, VR: vetch-rye VO: vetch-oats, PBT: pea-barley-triticale, PT: pea-triticale, PR: pea-rye and PO: pea-oats.

The climate in the area is Mediterranean with continental influence, characterized by a high thermal range and a frost period from October to April. According to the Spanish Meteorological Agency (AEMET), during the study period an average temperature of 9.50 °C, an accumulated rainfall of 380.34 mm and an accumulated radiation of 3,893.05 MJ/m^2 were recorded. The crops were grown on a plain terrain on sandy, gravelly and pebbly soils over arcosic sandstones (pH 5.5–6 and sandy-clay-loam texture).

Six different forage crops were selected to form the subsequent crop mixtures: vetch (*Vicia sativa* cv. "Rada"), pea (*Pisum sativum* cv. "Cabestrón"), triticale (*Triticum*×*Secale* cv. "Elleac"), six-row barley (*Hordeum vulgare* ssp. *Hexastichum* cv. "Yuriko"), rye (*Secale cereale* cv. "Serafín") and oats (*Avena sativa* cv. RGT "Chapela"). These crops were combined in eight different forage associations: vetch-barley-triticale (VBT), vetch-triticale (VT), vetch-rye (VR), vetch-oats (VO), pea-barley-triticale (PBT), pea-triticale (PT), pea-rye (PR) and pea-oats (PO). The associations containing vetch

were sown at a rate of 140 kg/ha (70% legume – 30% cereal) while those containing pea were sown at 130 kg/ha (60% legume – 40% cereal). The sowing took place on 19 October 2019 and the harvesting on 10 June 2020. All the associations have a similar growing cycle under a rainfed regime.

Each association was grown in triplicate in a random block design of 24 experimental plots of 400 m^2 each, covering an area of approximately one hectare (Figure 3.1). The characterization of these associations was carried out over the first row of plots, numbered from 1 to 8 consecutively.

3.2.2. Field and laboratory estimations

Several biophysical parameters of the associations were monitored along the growing cycle of 2020 ($n = 7$ measurements on dates 02/04; 02/26; 03/26; 04/14; 05/02; 05/17; 05/29). To estimate them, both destructive (sample collection) and non-destructive methods were carried out in the field. Then, laboratory estimations were conducted to obtain final values. The following parameters were estimated at association level: the Leaf Area Index (LAI), the fresh and dry biomass (FB and DB), the vegetation water content (VWC) and the percentage of water content (PWC). On the other hand, using non-destructive field methods, the fraction of vegetation cover (FVC) was estimated. Other parameters were also estimated (e.g., plant height, chlorophyll) but were discarded here as they were collected at plant level. Table 3.1 listed the selected parameters, which aimed to describe both the state of the plant and their rate of activity (Barnsley et al., 2000), and have been largely used in remote sensing applications to agronomy (T. J. Jackson et al., 2004; Jiang et al., 2006; Valcarce-Diñeiro et al., 2018).

Table 3.1. List of the field and laboratory parameters used in the study.

Field/Laboratory parameters		Units
Fraction of Vegetation Cover	FVC	%
Leaf Area Index	LAI	m^2/m^2
Fresh biomass	FB	gr/m^2
Dry biomass	DB	gr/m^2
Vegetation Water Content	VWC	gr/m^2
Percentage of Water Content	PWC	%

Two replicates of plant samples were taken at association level over a circular fenced area of 0.125 m^2, together with zenithal photographs taken at a same height of 1.5 m, following the protocol of Sánchez et al. (2012). Each sample was geolocated with a GPS receiver. Regarding the laboratory estimates, dry and wet weights of the sample were obtained, given that the wet weight is assumed as the FB, and their difference as the VWC expressed both in g/m^2 and in percentage. Forage samples were dried in a forced air oven at 60 °C for 48 h, until constant weight. To obtain the green LAI, leaf samples were scanned and digitally processed in the Image J software (Abràmoff et al., 2004), which is a very common way to estimate the foliar area (Martin et al., 2013; García-Estévez et al., 2017; Abdelkader et al., 2019). Finally, the FVC was estimated from the zenithal photographs using a supervised classification performed in PCI Geomatics Banff software, which allowed the segmentation of green/dry covers, bare soil and shadows (Calera et al., 2001).

3.2.3. Multispectral imaging collection and vegetation indices

Seven drone missions were flown simultaneously to the field measurements (around midday to avoid shadows). The mission area was approximately one hectare wide, and the flying altitude was fixed to 43 m above the ground. The UAV model was a DJI (SZ DJI Technology Co., Ltd., Shenzhen, China) Inspire1, with a Micasense (AgEagle Sensor Systems Inc., d/b/a MicaSense, Wichita, KS, USA) Red Edge M camera on board. The camera was mounted in the aircraft together with the GPS receiver and the downwelling light sensor using an ad hoc structure (Figure 3.2). The equipment was completed with a calibrated reflectance panel to radiometrically calibrate the imagery and four permanent ground control points to georeference the images.

Figure 3.2. DJI Inspire 1 with a hitched Red Edge M camera. GPS receiver and the downwelling light sensor were mounted by using an ad hoc structure.

The Micasense sensor is a multispectral camera with five discrete bands in the visible-near infrared spectra, namely blue (475±20 nm), green (560±20 nm), red (668±10 nm), near infrared (840±40 nm) and red edge (717±10 nm). The imager resolution is 1280×960 pixels, that afforded a spatial resolution for the resulting maps of 3 cm for all the acquisitions. The treatment of images was performed in Pix4D Mapper (Pix4D P.A., Prilly, Switzerland) software using a customized template that included, in addition to the geometric corrections and orthomosaicking, the radiometric calibration and the retrieval of the corrected reflectance maps together with the vegetation indices.

Three indices were proposed, in the first place the aforementioned NDVI (Eq. 3.1), the forefront of vegetation indices. Also, the normalized ratio between red and green bands, the green-red vegetation index (GRVI) (Eq. 3.2) (Tucker, 1979), and the proportion of green reflectance in the whole RGB space, the so-called Greenness index (Eq. 3.3). A red-edge version of the three indices was also obtained, replacing the red band for the red-edge one (Eq. 3.4, 3.5 and 3.6). Table 3.2 summarizes the six resulting vegetation indices and their formulation.

Table 3.2. Vegetation indices used in this study. R_{NIR}, R_{redge}, R_{red}, R_{green} and R_{blue} are the reflectance in the respective bands.

Vegetation indices		Equation	
Greenness	Gr	$\frac{R_{green}}{R_{red}+R_{green}+R_{blue}}$	(3.1)
Greenness_red_edge	Gr_redge	$\frac{R_{green}}{R_{redge}+R_{green}+R_{blue}}$	(3.2)
Normalized difference vegetation index	NDVI	$\frac{R_{NIR}-R_{red}}{R_{NIR}+R_{red}}$	(3.3)
Normalized difference vegetation index_red_edge	NDVI_redge	$\frac{R_{NIR}-R_{redge}}{R_{NIR}+R_{redge}}$	(3.4)
Green-red vegetation index	GRVI	$\frac{R_{green}-R_{red}}{R_{green}+R_{red}}$	(3.5)
Green-red vegetation index_red_edge	GRVI_redge	$\frac{R_{green}-R_{redge}}{R_{green}+R_{redge}}$	(3.6)

GRVI and Greenness were selected to investigate the feasibility of visible bands of RGB cameras, typically on board the UAVs, as an alternative to the most expensive multispectral cameras. RGB-based indices have been widely used to monitor vegetation status (Hunt et al., 2013; Sánchez et al., 2015), particularly after the advent of UAVs applications in agronomy (Jannoura et al., 2015; Khan et al., 2018; Lussem et al., 2018; Barbosa et al., 2019; Sumesh et al., 2021). In this vein, GRVI was successfully applied to estimate biomass and yield (Bendig et al., 2015; Jannoura et al., 2015; Lussem et al., 2018), nitrogen (Sripada et al., 2006) or phenology (Motohka et al., 2010). Besides, the greenness index is a simple way to indicate the proportion of vegetation cover (Sánchez et al., 2015), so it is expected to be related with FVC and LAI.

An area similar in size to that of the field measurements was extracted over the indices at their locations, to be fairly compared with the vegetation estimations.

3.2.4. Statistical analysis

a) Exploratory analysis of data variability

In the first place, a comparative analysis at association level between the temporal evolution both of the field estimations and the indices was performed to examine their matching. Conversely, a comparison at each date of measurement was carried out to

explore similarities in the behavior of the height associations and possible spatial patterns.

b) Correlation analysis

In order to assess the relationships between field and remote variables, a bivariate correlation process was conducted using Pearson's linear correlation coefficient (Pearson, 1904) as correlation indicator. Two-tailed significance test was performed, flagging significant ($p \leq 0.05^{*}$) and highly significant ($p \leq 0.01^{**}$) correlations. As in the exploratory analysis, correlations ($n = 16$) for each association along time and correlations ($n = 14$) for each date at spatial basis were calculated. The former were obtained to prove the potential of multispectral images captured by drone-borne sensors to match the evolution of vegetation indices with the real evolution of the associations throughout their cycle. Conversely, the latter were calculated to test how well the spatial variability of the studied parameters at each association and location is captured by these vegetation indices. In addition, the spatial analysis makes it possible to investigate whether the performance and evolution of the crop depends on the association itself or on its spatial location, which could be useful for decision making on crop management by the farmer and is one of the premises of the precision agriculture. The results obtained in this correlation analysis may suggest (or not) a step forward in the application of the indices by integrating them in a predictive model.

c) Prediction model of in situ agronomic parameters along the growing cycle based on partial least squares (PLS) regression

As previously mentioned, the aim of this work is to monitor and predict the set of field-measured variables (matrix Y), which play the role of dependent, observed or explained variables, through the vegetation indices obtained by the drone (matrix X), which would act as explanatory variables. To this end, after the exploratory and correlation analysis, a PLS regression model with the following algorithm was proposed:

Step 1. It considers the X and Y matrices given by the explanatory and standardized response variables, respectively.

Step 2. It computes a linear combination of the columns of X and Y, denoted by t_1 and u_1, respectively, in order to maximize the covariance, cov (t_1, u_1).

Step 3. It computes a classical linear regression model for the explanatory and response variables based on the value of the component t_1 (Eq. 3.7), given by:

$$X = t_1 p_1^t + X_1 \text{ and } Y = t_1 r_1^t + Y_1 \quad (3.7)$$

Step 4. It repeats the first step by substituting X and Y by the residual matrices X_1 e Y_1. Analogously, we obtain two new components t_2 and u_2, as linear combinations of the columns of X_1 and Y_1, respectively, which maximize the covariance, cov (t_2, u_2). It computes again a linear regression model (Eq. 3.8):

$$X_1 = t_2 p_2^t + X_2 \text{ and } Y_1 = t_2 r_2^t + Y_2 \quad (3.8)$$

where X and Y can be expressed recursively by the components t_1 and t_2 (Eq. 3.9),

$$X = t_1 p_1^t + t_2 p_2^t + X_2 \text{ and } Y = t_1 r_1^t + t_2 r_2^t + Y_2 \quad (3.9)$$

Step 5. It repeats this process until no significant improvement is seen in the explanation of Y. The algorithm ensures orthogonal components –uncorrelated– which are linear combinations of X.

Step 6. From the expression of Y as a function of the selected h components, $t_1, \ldots, t_h$ it can be easily computed the PLS regression equations of any response variable based on the explanatory variables.

The criteria of selecting the number of components, h, is based in the so-called leave-one-out cross validation (LOOCV) scheme. A single sample is deleted from the calibration set, developing a model with the remaining ones and predicting for the single left-out sample. The process is repeated as many times as samples and the squared prediction errors are summed up. This leads to the computation of the predicted residual sum of squares (PRESS) for the kt_h response variable as a function of model dimensionality, PRESS (k,h). Based on PRESS (k,h) the predicted R-squared is

computed, $R^2(k,h)$. Finally, the mean predicted R-squared, $R^2\ (h)$, is computed as the average of $R^2(k,h)$ for all response variables. Also PRESS (h) can be computed as the sum of PRESS (k,h). In this model, a $R^2\ (h)$ plot is used to draw conclusions. The best number of components is the one that maximize the overall mean predicted R-squared. Using the parsimony principle, if the $R^2\ (h)$ plot does not exhibit abrupt changes it will be chosen the model having a fewer number of parameters.

Although all the crop associations are compositionally different, the fact that all of them are formed by leguminous species in combination with winter cereal species means that they all have very similar behaviors throughout their growth cycles. On this premise, from an analytical point of view, it seems more suitable to consider the eight associations as a whole sample of the same population ($n = 112$), rather than treating them individually ($n = 14$). Advantages of this consideration imply a simplification in the understanding of the results and a better predictive capacity of the PLS regression model. This assumption was assessed by the results drawn from the exploratory analysis.

All the statistical processing was conducted using IBM-SPSS Statistics 26 software (IBM, Chicago, IL, USA).

3.3. Results and discussion

3.3.1. Spatio-temporal patterns

In Appendix A, Figure A1 shows the field estimations and the vegetation indices for the associations on each date of study, whereas Figure A2 shows their temporal evolutions.

a) Field measurements

Figure 3.A1 suggested that, as the crop cycle progressed, the values of all field measurements increased progressively on the ordinate axis, until they begun to decrease again as far as the forages approached their maturity point for harvesting. Besides, the associations containing vetch as legume (left side of the figures) showed greater adaptability to edaphoclimatic conditions and, therefore, higher biomass production. Cereal production prevailed over legume production in both cases, which was consistent

with the results of other studies (Hauggaard-Nielsen & Jensen, 2001). These results are in agreement with those shown graphically in Figure 3.A1 and with those reported by Roberts (1992). On the contrary, the PWC resulted essentially similar for all associations. Therefore, it could be concluded that for an equal consume of water (PWC) in all associations, the vetch-based associations reached considerably higher amounts of plant biomass. This could be of interest to farmers, who seek the highest forage reap while meeting a minimum supply. This result was also supported by the FVC and LAI results, where the vetch associations showed higher canopy coverage and leaf area. This fact is due to the greater tolerance of vetch to the high shading conditions inherent to the cereal-legume polyculture system (R. Li et al., 2020). Furthermore, it is also relevant the greater susceptibility of pea to attack by bacterial pathogens (*Pseudomonas syringae* pv. *pisi*) in high humidity or waterlogged soils (Roberts, 1992), as occurred at some stages of the cycle in the PR and PO fields (f.1 in Figure 3.A1). Those fields are located in the lower area of the plot (DEM in Figure 3.1), prone to become waterlogged.

These results agree well with the analysis of the temporal curve of each association (Figure 3.A2), since higher values of plant biomass were observed in the vetch associations (Figure 3.A2a–d) than in the pea associations, with the greatest differences occurring on dates close to harvest. However, the water consuming remained equal in all associations, as detected in the previous analysis. Additionally, the temporal evolution of the different associations showed a similar growth pattern for all the field parameters studied (except PWC, and to a lesser extent, the FVC), with all the associations showing a plateau-shaped curve (Calera et al., 2004), typical of the cycle of rainfed crops.

The box plot of the *in situ* estimations for each association (Figure 3.3) confirmed the results of the descriptive analysis of Figures 3.A1 and 3.A2. Although the range of those parameters was mainly similar for the eight crop associations, it was detected that the mean values of VBT, VT, VR and VO were slightly higher than those of PBT, PT, PR and PO.

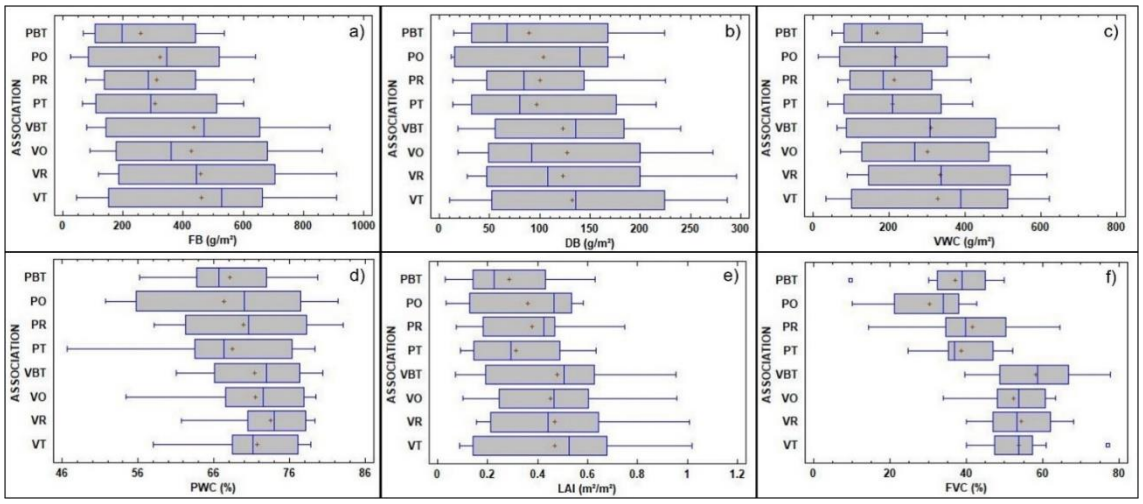

Figure 3.3. Box-Whisker plots of the *in situ* parameters for each association. (a) FB: fresh biomass, (b) DB: dry biomass, (c) VWC: vegetation water content, (d) PWT: percentage of water content, (e) LAI: leaf area index and (f) FVC: fraction of vegetation cover; PBT: pea-barley-triticale, PO: pea-oats, PR: pea-rye, PT: pea-triticale, VBT: vetch-barley-triticale, VO: vetch-oats, VR: vetch-rye and VT: vetch-triticale. Mean values are indicated by a red asterisk.

b) Spectral indices

The spectral indices followed a similar pattern, i.e., differences between vetch/pea associations were found in all dates, with higher index values for the first ones (Figure 3.A1). In addition, the temporal evolution of the indices (Figure 3.A2) corroborated the temporal behavior of the field estimations, with a similar plateau-shape, except for the case of the red edge versions.

Based on the analysis of the temporal evolution of each index for the eight associations (Figure 3.A2), it was found that the indices that better followed the different biomass production, VWC and LAI along time seemed to be Gr, NDVI and GRVI. The same abovementioned plateau-shape is evident in them (Figure 3.4). Hence, it can be expected a plausible way to monitor the associations behavior through the vegetation indices, as it was explored in next sections. Interestingly, the RGB-based indices showed a similar potential to follow the temporal evolution of plants than the NDVI, even though their dynamic range is smaller (Figure 3.4), as also found in other applications (Gutierrez et al., 2005), because the difference in reflectance between the green and red bands for vegetation and soil is small compared with that between near-infrared and red bands (Hunt et al., 2005). Particularly, the Gr maps (Figure 3.5) at the tillering (Figure 3.5a), heading (Figure 3.5b) and senescence (Figure 3.5c) followed the expected behavior of the

growing cycle. On the contrary, the three indices based in the red-edge region exhibited a plain temporal evolution (Figure 3.A2) and notably smaller differences between vetch/pea associations.

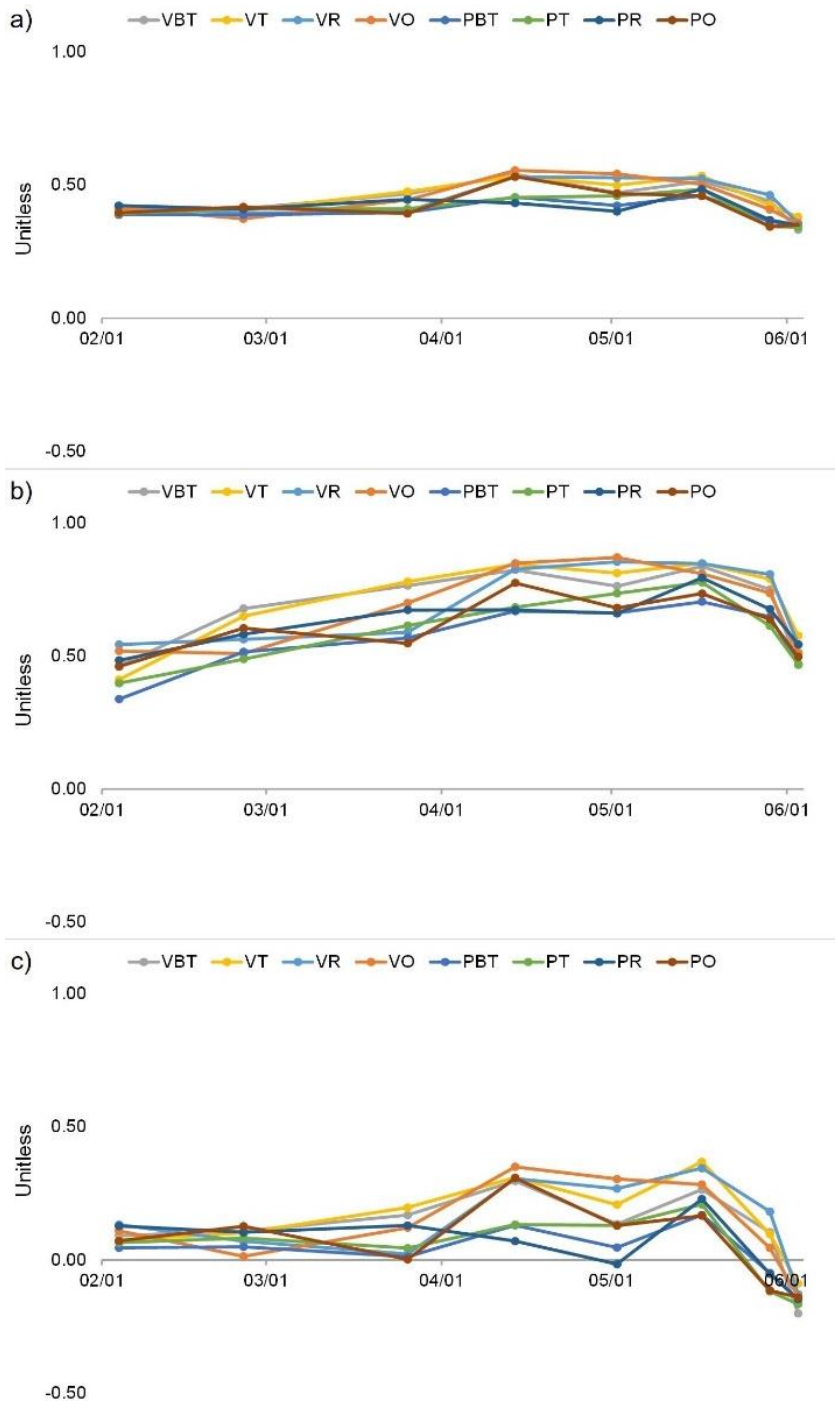

Figure 3.4. Temporal evolution of (a) Gr, (b) NDVI and (c) GRVI for the eight associations.

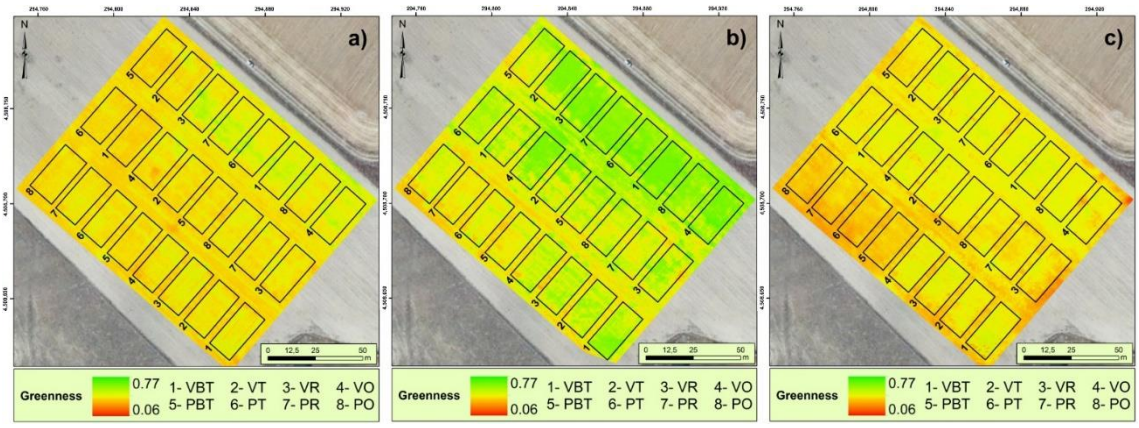

Figure 3.5. Temporal evolution of Gr index in three growing cycle points: (a) 26 February 2020, (b) 2 May 2020 and (c) 5 May 20. VBT: vetch-barley-triticale, VT: vetch-triticale, VR: vetch-rye, VO: vetch-oats, PBT: pea-barley-triticale, PT: pea-triticale, PR: pea-rye and PO: pea-oats.

To correctly interpret the proposed indices, it should be noted that low values of the vegetation-related indices such as GRVI (even negative, in this case), NDVI and Gr indicate limited vegetation activity. On the contrary, when the red-edge band replaces the red one in the GRVI_redge and Gr_redge versions, the lower the index, the greater the plant vigor, as it is expected a higher reflectance of the red-edge band than in the red one for healthy vegetation (Table 2).

3.3.2. Correlation analysis

When the dates were analyzed separately (Table 3.A1), the correlations were better on the central dates of the cycle (14 April and 2 May), coinciding with the maxima of the growing cycle. This suggested that the observations at the booting and the flowering stages were the best suited to better characterize the state of different associations or crops, as also found in (Fu et al., 2020). The best suited indices were NDVI, Gr and GRVI.

Although there seemed to be a clear pattern that distinguishes vetch from pea in the previous exploratory analysis, the correlations at association level did not produce such a difference (Table 3.A2), since no remarkable differences in the correlation values were found along associations. However, it should be noted that the Pearson coefficient seeks for a similar behavior, ignoring the absolute values. Thus, it would be inferred that the temporal behavior was similar between associations (as already seen in Figure 3.A2), even though the higher vetch yields.

Since the associations are a mix of different plants, all of them with different growing characteristics (e.g., different foliage, height and density), the vegetation indices did not reach saturation, which typically occurs for dense vegetation coverages of single canopies with the remotely sensed NDVI (Gamon et al., 1995; T. J. Jackson et al., 2004), and it was also observed for the UAV-based GRVI for biomass greater than 150 g/m^2 in corn and soybean (Hunt et al., 2005) and in wheat (Fu et al., 2020). In such scenarios, the correlation declines due to the saturation of the index at some point, which is not the case here. This fact may explain the higher correlation as regard of other similar works on drone vegetation indices for monitoring individual plant species (Jannoura et al., 2015; Lussem et al., 2018). In addition, removing the influence of lighting changes and solar reflection angle is particularly necessary for the RGB images (Bacsa et al., 2019; Barbosa et al., 2019), used here to calculate the indices. The sun-downlight correction and the reflectance calibration applied to the Micasense images could have been improved the results of correlation, as regards of other similar research in which RGB indices were correlated with biomass and LAI (Jannoura et al., 2015).

As regard of the associations, the worst characterized was PO, while the best was VO (Table 3.A2). The most difficult parameter to monitor was FVC. The indices that correlated best with the temporal evolution were NDVI, Gr and GRVI. On the contrary, the indices based in the red-edge band did not perform well and also had a negative correlation due to their inverse behavior, which makes their interpretation difficult. However, other studies have revealed the red-edge NDVI as a good indicator of nitrogen level over rice fields (Bacsa et al., 2019) as well as other chemical parameters of corn (Janoušek et al., 2021). The relationship of the red-edge indices with other different parameters as the chlorophyll content will be explored in further research in the same area. In this work, the bad results of the red edge-based indices to depict structural parameters such as LAI and biomass could be due to an inadequate replacement of the red band for the red edge one in the indices formulation, especially in the Gr_redge and GRVI_edge cases. The higher reflectance of the red edge band than that of the green one for vigorous plants led to unwanted results in their calculation (Table 3.2).

Correlations were very strong and significant for each association throughout their growing cycle (Table 3.A2), suggesting that the evolution of the associations would be

monitored from the spectral indices. These high correlations invited an attempt at more complex statistical modeling to predict plant behavior based on the indices, as done in the next section.

3.3.3. Modeling and prediction of the behavior of the associations. PLS regression

An attempt to model the associations time evolution was carried out by means of a PLS regression. The PLS-regression model is one of the least restrictive of all classical multivariate regression models. Due to this fact, it can be used to predict in situations where other models are limited. In particular, it is appropriated when there are fewer observations than predictor variables, which is a common situation in drone applications, where the image analysis affords a large set of predictor variables whereas the ground observations to fit the models are usually scarce. Several examples of these PLS regression predictive applications in precision agriculture can be found in Nguyen et al. (2006), Abdel-Rahman et al. (2014) and more recently in Kawamura et al. (2018), Erler et al. (2020) and Helfer et al. (2020).

In the same way, our final aim was to predict the field parameters at any time of the growing cycle with the sole input of the vegetation indices. To test this objective, and to account for the previous exploratory results, three variants of the PLS analysis were proposed, i.e., a global one considering all the associations as a whole, and another two PLS for the associations based in vetch (VBT, VT, VR and VO) and in pea (PBT, PT, PR and PO).

a) Global PLS analysis for all associations as a whole

The first PLS regression used data from all crop associations treated simultaneously. Table 3.3 shows X (vegetation indices of all associations) and Y (field measurements of all associations) capability to capture the relevant information, expressed as % of variance, with the subsequent mean predicted value R^2 depending on the number of extracted components by the PLS regression model. In view of these results, a regression model based solely on the first four components was constructed. Firstly, because the predictive value R^2 remains nearly stable from the fourth component

onwards. Besides, a greater number of components would lead to a model with more parameters and complexity while similar predictive capacity. With four components the model was able to explain 99.67% of the variability of the explanatory variables and 57.75% of the variability of the response variables. It was noteworthy that the first component explained a higher percentage of the variability of X and, with just two components, more than 90% of this variability was explained. The mean predictive capacity (R^2) after the LOOCV was 53.38%. In other words, the six explanatory variables provided by the multispectral images captured by the drone were sufficient to predict more than 50% of the field parameters. However, a model with a single component also provided significant levels of prediction ($R^2 = 42.50$). Hence, some redundancy between the vegetation indices (the explanatory variables) was detected. This is not surprising, since the vegetation indices formulation (Table 3.2) was based in a combination of the same bands in the VNIR spectra. Far for being a problem, this result afforded two main advantages of our hypothesis: (1) PLS regression was able to deal with multicollinearity in data and eliminate the less important or redundant variables, as also found in Zhou et al. (2019), and (2) a single combination of VNIR bands, or even visible bands solely, was able to feed the regression model, leading to a successful prediction of the agronomic parameters.

Table 3.3. Capability of explanatory (X) and response variables (Y) of VBT, VT, VR, VO, PBT, PT, PR and PO associations to capture % of variance depending on the number of components. Predictive potential expressed as R^2.

Component (h)	% Variance X	% Accumulated X	% Variance Y	% Accumulated Y	Mean predicted R^2
1	69.94	69.94	44.43	44.44	42.50
2	22.09	92.03	7.01	51.45	48.74
3	7.13	99.16	2.07	53.52	49.97
4	0.51	99.67	4.23	57.75	53.38
5	0.32	99.99	0.34	58.09	53.06
6	0.01	100.00	1.13	59.22	52.83

VBT: vetch-barley-triticale, VT: vetch-triticale, VR: vetch-rye, VO: vetch-oats, PBT: pea-barley-triticale, PT: pea-triticale, PR: pea-rye and PO: pea-oats.

Table 3.4 shows the predictive capacity of the global PLS analysis with four components for each of the response variables, and Figure 3.6 shows the plots of observed vs. predicted values for each of the six response variables of all associations considering

a four-component model. Overall, a strong dependency relationship was detected between the explanatory and observed variables, with a remarkable predictive capacity for LAI ($R^2 = 57.79$), FB ($R^2 = 62.63$), DB ($R^2 = 67.07$), VWC ($R^2 = 57.32$) and PWC ($R^2 = 47.34$). The relationship seemed to be linear in all cases (Figure 3.6) excepting for FVC, in which the prediction ($R^2 = 28.54$) was notably lower than for the rest of the variables and with no evident linear relationship (Figure 3.6f).

Table 3.4. Predictive capacity of the PLS analysis for each of the response variables of VBT, VT, VR, VO, PBT, PT, PR and PO associations for four components.

Explanatory Variable	R^2	Mean PRESS	Predicted R^2
FB (g/m^2)	65.75	22,520.30	62.23
DB (g/m^2)	70.40	2017.47	67.07
VWC (g/m^2)	61.12	12,493.50	57.32
PWC (%)	52.47	31.23	47.34
LAI (m^2/m^2)	62.02	0.02	57.79
FVC (%)	34.77	133.34	28.54

FB: fresh biomass, DB: dry biomass, VWC: vegetation water content, PWC: percentage of water content, LAI: leaf area index, FCV: fraction of vegetation cover, VBT: vetch-barley-triticale, VT: vetch-triticale, VR: vetch-rye, VO: vetch-oats, PBT: pea-barley-triticale, PT: pea-triticale, PR: pea-rye and PO: pea-oats.

In similar research (Z. Zhou et al., 2019) it was proven that the PLS performed better under linearity conditions and with a number of predictor variables equal or greater than the number of predicted variables, as it was the case here. For no linear relationships, the SVM was preferred (Yao et al., 2015; Du et al., 2016).

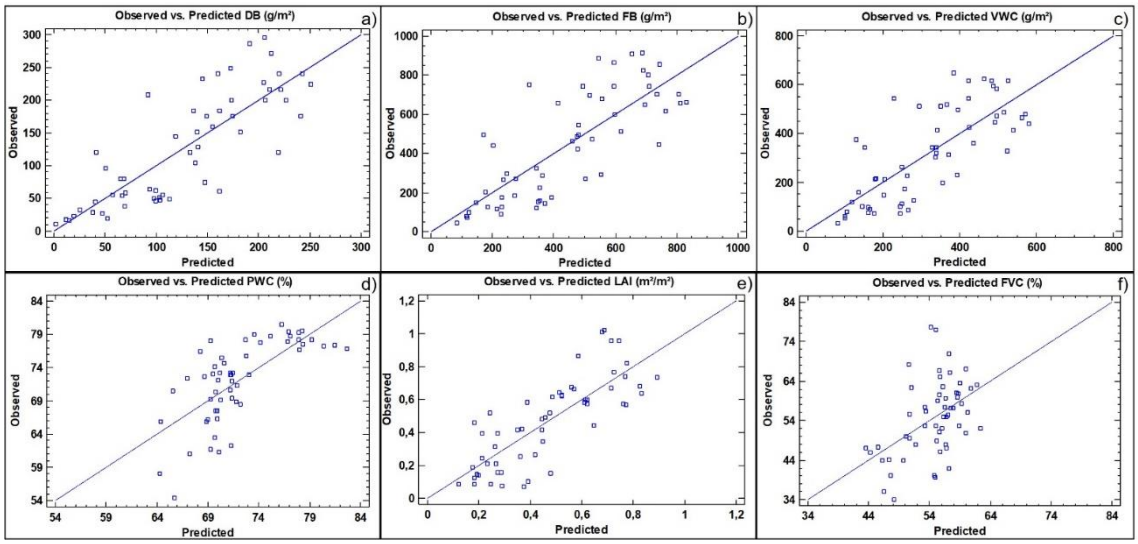

Figure 3.6. Observed *vs.* predicted values for the six response variables of VBT, VT, VR, VO, PBT, PT, PR and PO associations in a four-component model. (a) FB: fresh biomass, (b) DB: dry biomass, (c) VWC: vegetation water content, (d) PWC: percentage of water content, (e) LAI: leaf area index and (f) FCV: fraction of vegetation cover. VBT: vetch-barley-triticale, VT: vetch-triticale, VR: vetch-rye, VO: vetch-oats, PBT: pea-barley-triticale, PT: pea-triticale, PR: pea-rye and PO: pea-oats.

b) PLS analysis for the vetch-based associations (VBT, VT, VR and VO)

Table 3.5 shows the percentage of variance retained by the explanatory variables (X) and by the response variables (Y). In this case, the regression model was based on the first three components, and was able to explain 99.28% of the variability of the explanatory variables and 54.08% of the variability of the response variables. The mean predictive capacity (R^2) after the LOOCV was 46.42%. This R^2 value was slightly lower than that obtained in the global analysis (53.38%), probably due to its smaller amount of data.

Table 3.5. Capability of explanatory (X) and response variables (Y) of VBT, VT, VR and VO associations to capture % of variance depending on the number of components. Predictive potential expressed as R^2.

Component (h)	% Variance X	% Accumulated X	% Variance Y	% Accumulated Y	Mean predicted R^2
1	76.03	76.03	44.15	44.15	40.81
2	12.58	88.61	8.29	52.45	45.97
3	10.67	99.28	1.63	54.08	46.42
4	0.51	99.89	2.10	56.18	46.37
5	0.18	99.98	0.63	56.82	45.74
6	0.02	100.00	3.18	60.01	47.85

VBT: vetch-barley-triticale, VT: vetch-triticale, VR: vetch-rye and VO: vetch-oats.

The predictive capacity of the PLS analysis for each response variable for three components (Table 3.6) was lower than in the global analysis in terms of the predicted R^2. Again, FVC was the worst predicted, this time with a clearly worse R^2 of 9.50. This bad result is difficult to interpret, since LAI and FB, typically related with FVC (Sánchez et al., 2012), reached good performances both in the correlation analysis (Tables 3.A1 and 3.A2) and in their prediction capability (Tables 3.4, 3.6 and 3.8). Two explanations may arise. Firstly, the time-lag found between the FVC curve and the rest of parameters and indices (occurring at five out of the height associations, see Figure 3.A2), coinciding with the findings of Sánchez et al. (2012) for grass coverages. Second, the methodology to estimate the FVC from the classification of zenithal photographs may be questionable when the canopy is a mix of species with different coloration, as found by Calera et al. (2001).

Table 3.6. Predictive capacity of the PLS analysis for each of the response variables of VBT, VT, VR and VO associations for three components.

Explanatory Variable	R^2	Mean PRESS	Predicted R^2
FB (g/m^2)	62.65	31,210.60	56.77
DB (g/m^2)	67.90	2590.51	62.71
VWC (g/m^2)	58.26	17,213.00	51.74
PWC (%)	49.11	22.17	38.90
LAI (m^2/m^2)	64.09	0.03	58.86
FVC (%)	22.49	81.60	9.50

FB: fresh biomass, DB: dry biomass, VWC: vegetation water content, PWC: percentage of water content, LAI: leaf area index, FCV: fraction of vegetation cover, VBT: vetch-barley-triticale, VT: vetch-triticale, VR: vetch-rye and VO: vetch-oats.

c) PLS analysis for the pea-based associations (PBT, PT, PR and PO)

Although the results in Table 3.7 were similar to those obtained in the previous scenario with the vetch associations, two slight differences should be noted: on the one hand, the variability of X was better distributed between the first and second components (92.14% *vs.* 88.61%) and, on the other hand, a four-component model, just like in the global analysis, could be chosen in this case, because the mean predicted R^2 increased slightly between the third ($R^2 = 44.92$) and fourth ($R^2 = 48.62$) components.

Table 3.7. Capability of explanatory (X) and response variables (Y) of PBT, PT, PR and PO associations to capture % of variance depending on the number of components. Predictive potential expressed as R^2.

Component (h)	% Variance X	% Accumulated X	% Variance Y	% Accumulated Y	Mean predicted R^2
1	54.70	54.70	41.70	41.70	37.02
2	37.43	92.14	8.10	49.81	44.29
3	6.86	99.01	1.83	51.65	44.92
4	0.82	99.8	5.81	57.46	48.62
5	0.15	99.99	1.65	59.11	48.97
6	0.01	100.000	3.70	62.82	49.80

PBT: pea-barley-triticale, PT: pea-triticale, PR: pea-rye and PO: pea-oats.

As in the previous case, the prediction model for the FVC variable showed the lowest $R\text{^}2$ (Table 3.8). On the other hand, the PWC variable was now notably better explained ($R^2 = 59.36$ *vs.* $R^2 = 38.90$). As in the vetch model, the mean predictive R^2 value is slightly lower than that obtained in the global analyses (48.62% *vs*. 53.38%).

Table 3.8. Predictive capacity of the PLS analysis for each of the response variables of PBT, PT, PR and PO associations for four components.

Explanatory Variable	R^2	Mean PRESS	Predicted R^2
FB (g/m^2)	62.19	16,471.20	54.89
DB (g/m^2)	69.70	1802.05	63.16
VWC (g/m^2)	54.96	8598.87	46.65
PWC (%)	66.10	30.90	59.36
LAI (m^2/m^2)	58.21	0.02	48.68
FVC (%)	33.61	101.64	18.99

FB: fresh biomass, DB: dry biomass, VWC: vegetation water content, PWC: percentage of water content, LAI: leaf area index, FCV: fraction of vegetation cover, PBT: pea-barley-triticale, PT: pea-triticale, PR: pea-rye and PO: pea-oats.

3.4. Conclusions

Camera-based VNIR vegetation indices on board UAVs platforms could offer an effective and affordable alternative to field-consuming, destructive sampling to monitor crops. This methodology, together with the support of statistical modeling techniques have shown a high capability of monitoring and predicting the behavior of height forage associations.

The exploratory analysis, together with the correlation analysis, exhibited a strong relationship between the spectral indices and the field estimations, suggesting a further prediction model. Owing the linearity found in these relationships, a simple regressive prediction model (PLS) was proposed.

The vetch-based and the pea-based associations showed a different behavior both at the field and image estimations. While the water consuming was similar for both, biomass production was higher for the first, which may be a useful result for farmers seeking the highest forage production. Interestingly, the spectral indices were also able to detect this behavior, offering an alternative way to evaluate both the production and the use of water of their crops.

Using a reduced number of multispectral observations (in the form of vegetation indices) and applying the PLS model, we were able to predict agronomic parameters of forage crop associations at any time of their cycle with a reliability of more than 50%. In fact, six indices were integrated in the model, but it was sown that they provided redundant information. Therefore, they could have been reduced by half, since the red edge-based indices were not satisfactory in the exploratory and correlation analysis. An alternative use of the red edge indices should be explored in further research, both in their formulation and in their relationships with other observed parameters, such chlorophyll. On the contrary, the indices Gr and GVRI, based in the green and red bands, correlated well with the field parameters and revealed a similar capacity to predict the temporal behavior than the NDVI, with the advantage of being easier to acquire through the RGB cameras, typically onboard UAVs.

Overall, a strong, linear dependency relationship was detected between the explanatory and the observed variables, with a remarkable predictive capacity. This predictive capacity could be refined avoiding the redundant information while adding new explanatory variables such as other vegetation indices. In addition, other parameters such as yield and chlorophyll content will be explored in the future.

Appendix A

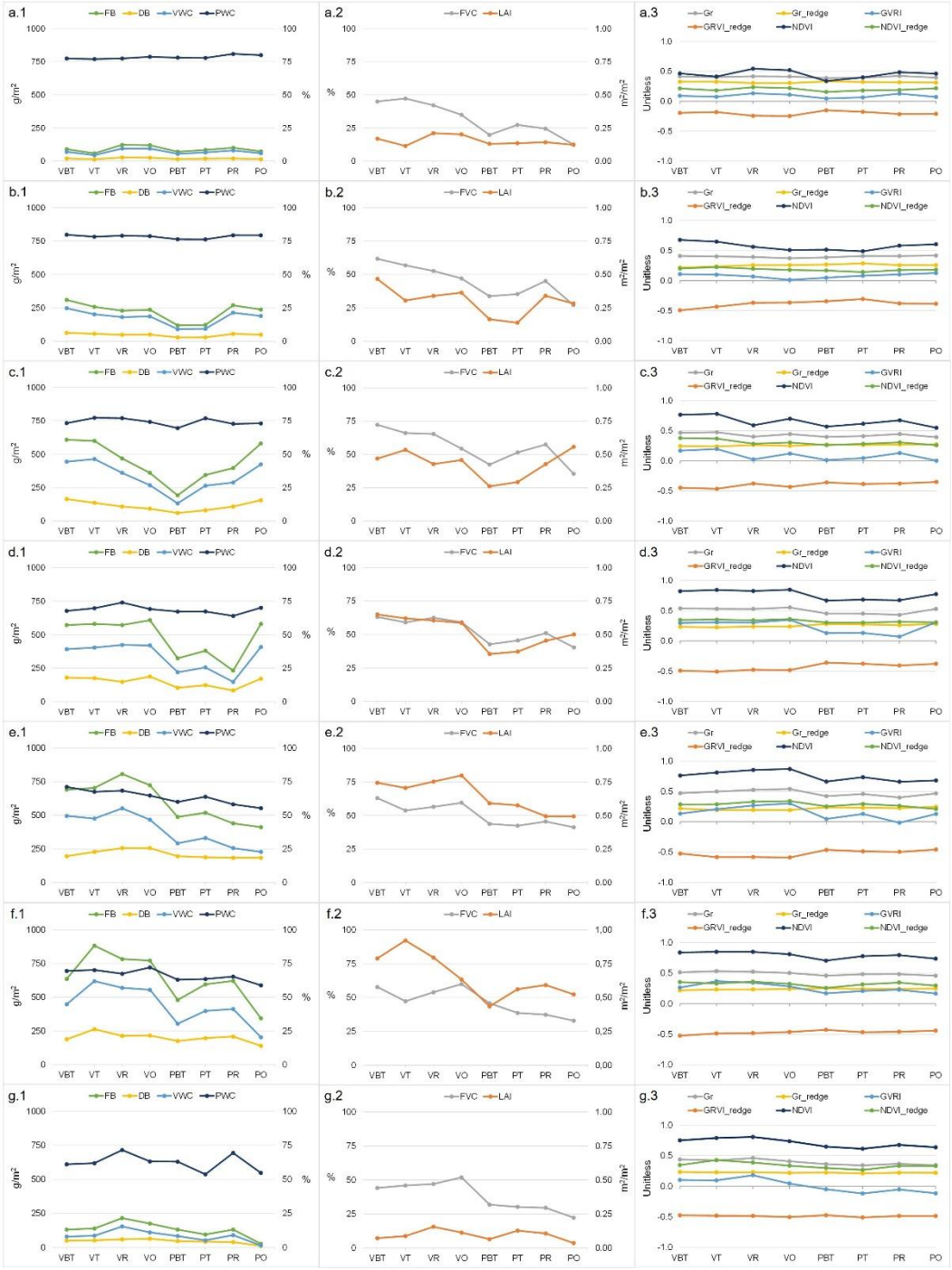

Figure 3A.1. Field estimations and spectral indices for the associations at each of the seven measurement dates. Letter (**a**) correspond to 4 February 2020, (**b**) to 26 February 2020, (**c**) to 26 March 2020, (**d**) to 14 April 2020, (**e**) to 2 May 2020, (**f**) to 17 May 2020 and (**g**) to 29 May 2020. FB: fresh biomass, DB: dry biomass, VWC: vegetation water content, PWC: percentage of water content, VBT: vetch-barley-triticale, VT: vetch-triticale, VR: vetch-rye, VO: vetch-oats, PBT: pea-barley-triticale, PT: pea-triticale, PR: pea-rye and PO: pea-oats. Subfigures 1 show, FB, DB, VWC and PWC, subfigures 2 show FVC and LAI and subfigures 3 show the vegetation indices.

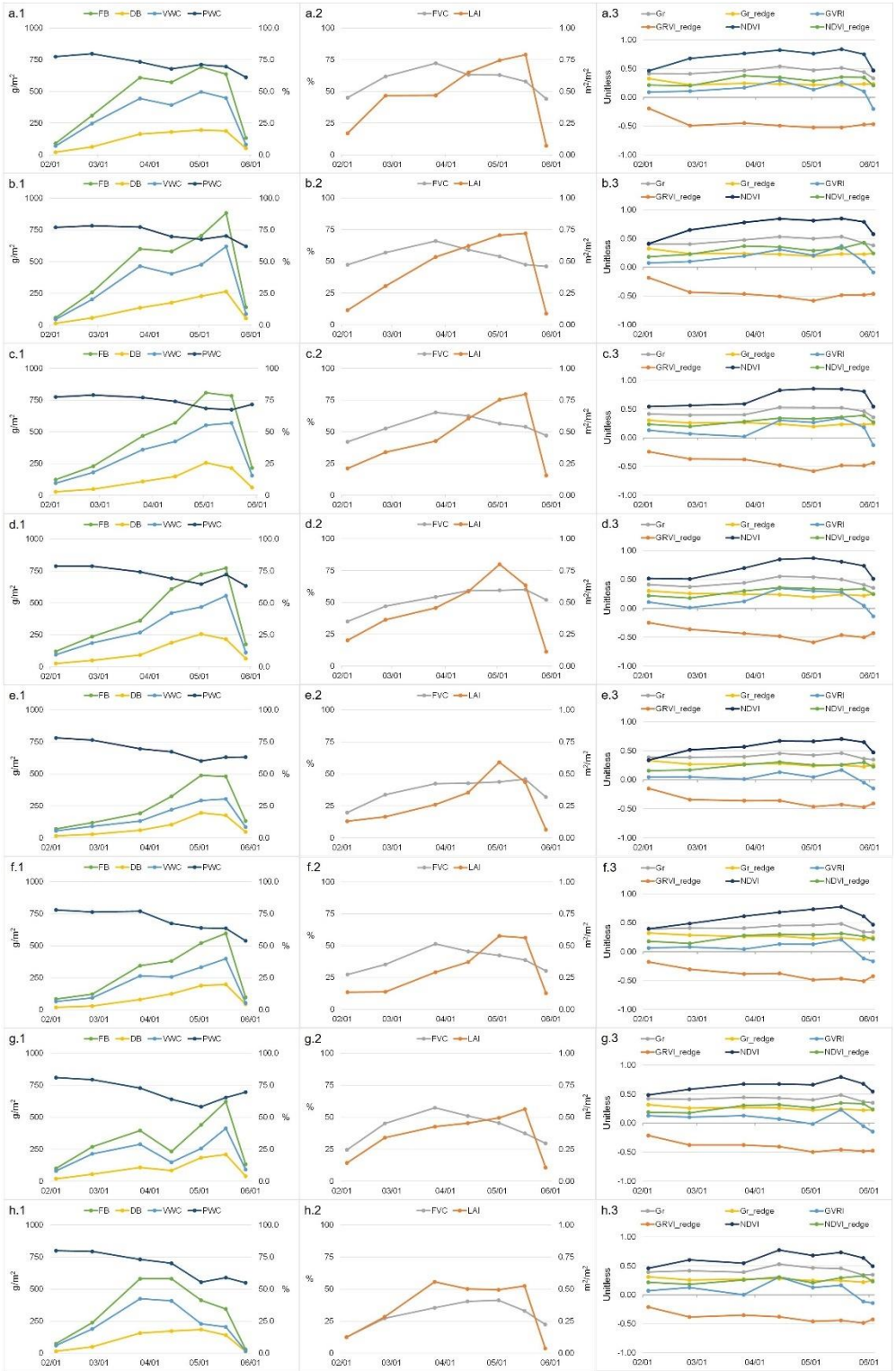

Figure 3A.2. Temporal evolution of field measurements and spectral indices for the eight associations. Letter (**a**) correspond to vetch-barley-triticale (VBT), (**b**) to vetch-triticale (VT), (**c**) to vetch-rye (VR), (**d**) to vetch-oats (VO), (**e**) to pea-barley-triticale (PBT), (**f**) to pea-triticale (PT), (**g**) to pea-rye (PR) and (**h**) to pea-oats (PO). FB: fresh biomass, DB: dry biomass, VWC: vegetation water content, PWC: percentage of water content. Subfigures 1 show, FB, DB, VWC and PWC, subfigures 2 show FVC and LAI and subfigures 3 show the vegetation indices

Appendix B

Table 3A.1. Correlations ($n = 16$) at each date between field measurements and spectral indices of the eight associations in a whole (Pearson Correlation Coefficient).

Meas. Date	Parameter	FB	DB	VWC	PWC	FCV	LAI	Meas. Date	Parameter	FB	DB	VWC	PWC	FCV	LAI
4 February 2020	Gr	0.244	0.275	0.232	−0.204	0.374	0.265	26 February 2020	Gr	0.173	0.190	0.168	0.036	0.039	0.010
	Gr_redge	−0.587 *	−0.533 *	−0.597 *	−0.111	−0.027	−0.594 *		Gr_redge	−0.618 *	−0.638 **	−0.0610 *	−0.360	−0.715 **	−0.642 **
	GRVI	0.383	0.402	0.373	−0.172	0.316	0.385		GRVI	0.288	0.311	0.281	0.104	0.133	0.108
	GRVI_redge	−0.566 *	−0.530 *	−0.570 *	−0.026	−0.174	−0.593 *		GRVI_redge	−0.641 **	−0.664 **	−0.633 **	−0.361	−0.716 **	−0.635 **
	NDVI	0.512 *	0.512 *	0.506 *	−0.118	0.294	0.555 *		NDVI	0.591 *	0.619 *	0.582 *	0.330	0.594 *	0.497
	NDVI_redge	0.475	0.498 *	0.463	−0.209	0.303	0.577 *		NDVI_redge	0.428	0.461	0.419	0.300	0.639 **	0.399
26 March 2020	Gr	0.399	0.330	0.415	0.231	0.587 *	0.309	14 April 2020	Gr	0.821 **	0.765 **	0.817 **	0.629 **	0.518 *	0.708 **
	Gr_redge	−0.400	−0.292	−0.430	−0.396	−0.597 *	−0.389		Gr_redge	−0.446	−0.426	−0.440	−0.296	−0.836 **	−0.811 **
	GRVI	0.401	0.334	0.417	0.226	0.578 *	0.308		GRVI	0.829 **	0.756 **	0.829 **	0.665 **	0.492	0.673 **
	GRVI_redge	−0.407	−0.307	−0.434	−0.366	−0.621 *	−0.377		GRVI_redge	−0.548 *	−0.530 *	−0.538 *	−0.358	−0.837 **	−0.871 **
	NDVI	0.459	0.390	0.475	0.253	0.655 **	0.340		NDVI	0.836 **	0.782 **	0.830 **	0.616 *	0.675 **	0.848 **
	NDVI_redge	0.627 **	0.573 *	0.634 **	0.239	0.743 **	0.402		NDVI_redge	0.594 *	0.560 *	0.588 *	0.376	0.809 **	0.749 **
2 May 2020	Gr	0.606 *	0.566 *	0.585 *	0.434	0.573 *	0.572 *	17 May 2020	Gr	0.635 **	0.528 *	0.662 **	0.610 *	0.518 *	0.651 **
	Gr_redge	−0.701 **	−0.584 *	−0.699 **	−0.631 **	−0.691 **	−0.638 **		Gr_redge	−0.302	−0.195	−0.336	−0.545 *	−0.483	−0.460
	GRVI	0.606 *	0.576 *	0.581 *	0.429	0.553 *	0.580 *		GRVI	0.742 **	0.639 **	0.766 **	0.643 **	0.504 *	0.698 **
	GRVI_redge	−0.710 **	−0.591 *	−0.708 **	−0.631 **	−0.712 **	−0.643 **		GRVI_redge	−0.297	−0.194	−0.329	−0.517 *	−0.463	−0.452
	NDVI	0.712 **	0.617 *	0.702 **	0.598 *	0.691 **	0.655 **		NDVI	0.597 *	0.499 *	0.622 *	0.628 **	0.459	0.608 *
	NDVI_redge	0.661 **	0.563 *	0.655 **	0.608 *	0.645 **	0.608 *		NDVI_redge	0.501 *	0.457	0.508 *	0.514 *	0.396	0.513 *
29 May 2020	Gr	0.699 **	0.524 *	0.723 **	0.553 *	0.790 **	0.314								
	Gr_redge	0.382	0.143	0.454	0.625 **	0.303	−0.075								
	GRVI	0.713 **	0.523 *	0.742 **	0.582 *	0.797 **	0.332								
	GRVI_redge	0.187	−0.032	0.263	0.521 *	0.021	−0.180								
	NDVI	0.582 *	0.478	0.584 *	0.400	0.812 **	0.342								
	NDVI_redge	0.266	0.221	0.267	0.234	0.585 *	0.172								

** Correlation is significant at the 0.01 level (2-tailed) (Light grey), * Correlation is significant at the 0.05 level (2-tailed) (Dark grey). FB: fresh biomass, DB: dry biomass, VWC: vegetation water content, PWC: percentage of water content, FCV: fraction of vegetation cover, LAI: leaf area index, VBT: vetch-barley-triticale, VT: vetch-triticale, VR: vetch-rye, VO: vetch-oats, PBT: pea-barley-triticale, PT: pea-triticale, PR: pea-rye and PO: pea-oats.

Table 3A.2. Correlations at each association ($n = 14$) between field measurements and spectral indices along the whole growing cycle (Pearson Correlation Coefficient).

Association	Parameter	FB	DB	VWC	PWC	FCV	LAI	Association	Parameter	FB	DB	VWC	PWC	FCV	LAI
VBT	Gr	0.661 **	0.693 **	0.637 *	−0.203	0.426	0.643 *	PBT	Gr	0.708 **	0.656 *	0.728 **	−0.320	0.474	0.652 *
	Gr_redge	−0.537 *	−0.530	−0.530	0.245	−0.481	−0.553 *		Gr_redge	−0.395	−0.448	−0.352	0.764 **	−0.491	−0.256
	GRVI	0.573 *	0.555 *	0.570 *	−0.003	0.456	0.587 *		GRVI	0.548 *	0.483	0.579 *	−0.075	0.297	0.481
	GRVI_redge	−0.590 *	−0.605 *	−0.573 *	0.325	−0.497	−0.587 *		GRVI_redge	−0.523	−0.562 *	−0.486	0.821 **	−0.604 *	−0.387
	NDVI	0.667 **	0.710 **	0.638 *	−0.423	0.560 *	0.593 *		NDVI	0.682 **	0.680 **	0.670 **	−0.799 **	0.718 **	0.522
	NDVI_redge	0.496	0.585 *	0.452	−0.585 *	0.392	0.254		NDVI_redge	0.427	0.425	0.419	−0.733 **	0.573 *	0.278
VT	Gr	0.700 **	0.741 **	0.678 **	−0.237	0.165	0.771 **	PT	Gr	0.773 **	0.744 **	0.772 **	0.027	0.520	0.713 **
	Gr_redge	−0.422	−0.479	−0.397	0.494	−0.216	−0.459		Gr_redge	−0.366	−0.460	−0.303	0.835 **	−0.191	−0.409
	GRVI	0.729 **	0.747 **	0.715 **	−0.104	0.112	0.790 **		GRVI	0.675 **	0.637 *	0.682 **	0.186	0.415	0.608 *
	GRVI_redge	−0.481	−0.535 *	−0.456	0.504	−0.231	−0.515		GRVI_redge	−0.504	−0.580 *	−0.448	0.814 **	−0.323	−0.526
	NDVI	0.584 *	0.621 *	0.565 *	−0.507	0.185	0.595 *		NDVI	0.846 **	0.872 **	0.812 **	−0.596 *	0.578 *	0.809 **
	NDVI_redge	0.213	0.234	0.203	−0.634 *	0.078	0.152		NDVI_redge	0.731 **	0.736 **	0.711 **	−0.570 *	0.569 *	0.697 **
VR	Gr	0.660 *	0.683 **	0.645 *	−0.792 **	0.209	0.676 **	PR	Gr	0.688 **	0.579 *	0.729 **	−0.064	0.331	0.614 *
	Gr_redge	−0.550 *	−0.580 *	−0.532	0.817 **	−0.328	−0.551 *		Gr_redge	−0.368	−0.452	−0.299	0.663 **	−0.195	−0.279
	GRVI	0.654 *	0.683 **	0.636 *	−0.725 **	0.061	0.658 *		GRVI	0.530	0.373	0.609 *	0.247	0.186	0.398
	GRVI_redge	−0.584 *	−0.606 *	−0.570 *	0.834 **	−0.359	−0.576 *		GRVI_redge	−0.452	−0.536 *	−0.380	0.733 **	−0.281	−0.390
	NDVI	0.631 *	0.658 *	0.615 *	−0.887 **	0.199	0.589 *		NDVI	0.721 **	0.723 **	0.689 **	−0.638 *	0.421	0.580 *
	NDVI_redge	0.499	0.519	0.486	−0.817 **	0.189	0.380		NDVI_redge	0.438	0.492	0.384	−0.644 *	0.275	0.323
VO	Gr	0.841 **	0.854 **	0.817 **	−0.319	0.735 **	0.732 **	PO	Gr	0.653 *	0.704 **	0.586 *	−0.028	0.613 *	0.641 *
	Gr_redge	−0.566 *	−0.679 **	−0.498	0.802 **	−0.771 **	−0.496		Gr_redge	0.156	−0.020	0.231	0.743 **	−0.214	0.065
	GRVI	0.823 **	0.807 **	0.814 **	−0.174	0.678 **	0.704 **		GRVI	0.548 *	0.537 *	0.518	0.193	0.435	0.537 *
	GRVI_redge	−0.653 *	−0.750 **	−0.591 *	0.793 **	−0.838 **	−0.557 *		GRVI_redge	−0.086	−0.279	0.012	0.794 **	−0.445	−0.164
	NDVI	0.797 **	0.845 **	0.756 **	−0.631 *	0.872 **	0.630 *		NDVI	0.413	0.532	0.329	−0.508	0.569 *	0.429
	NDVI_redge	0.603 *	0.673 **	0.555 *	−0.727 **	0.769 **	0.400		NDVI_redge	0.062	0.064	0.058	−0.454	0.077	−0.034

** Correlation is significant at the 0.01 level (2-tailed) (Light grey), * Correlation is significant at the 0.05 level (2-tailed) (Dark grey). FB: fresh biomass, DB: dry biomass, VWC: vegetation water content, PWC: percentage of water content, FCV: fraction of vegetation cover, LAI: leaf area index, VBT: vetch-barley-triticale, VT: vetch-triticale, VR: vetch-rye, VO: vetch-oats, PBT: pea-barley-triticale, PT: pea-triticale, PR: pea-rye and PO: pea-oats.

Capítulo 4. Classification of airborne multispectral imagery to quantify common vole impacts on an agricultural field

Plaza, J., Sánchez, N., García-Ariza, C., Pérez-Sánchez, R., Charfolé, F., & Caminero-Saldaña, C. (2022). Classification of airborne multispectral imagery to quantify common vole impacts on an agricultural field. Pest Management Science, Early view. https://doi.org/10.1002/PS.6857

Capítulo 4. Classification of airborne multispectral imagery to quantify common vole impacts on an agricultural field

Resumen

El topillo campesino (*Microtus arvalis*) es una plaga agrícola muy destructiva. Es un microtínido semifosorial que habita principalmente en paisajes agrícolas como prados, márgenes de campos y parcelas de alfalfa. Sin embargo, durante los periodos de explosión poblacional, los topillos se dispersan, invaden y colonizan otros hábitats subóptimos, incluyendo zonas cultivadas con una amplia gama de cultivos (por ejemplo, cereales, legumbres, colza, girasol, etc.). En algunas regiones mediterráneas, como las tierras de cultivo del centro-oeste de la Península Ibérica (España), los topillos causan importantes daños como consecuencia de su mayor prevalencia. Por este motivo, su seguimiento es esencial, no sólo para una adecuada gestión y previsión de explosiones poblacionales, sino también para determinar con precisión el impacto que tiene en los campos afectados. En la actualidad, el seguimiento de los topillos se realiza mediante laboriosos y prolongados trabajos de campo. Los métodos de trampeo son procedimientos de campo muy eficaces para estimar las poblaciones de topillos, aunque requieren importantes recursos humanos y materiales. Por este motivo, se suelen sustituir por métodos indirectos, basados en la detección de signos de actividad de los topillos (excrementos, huras activas o recortes de vegetación, entre otros), que son más fáciles y rápidos de desarrollar. En este contexto, la fotografía, las tecnologías de vídeo y las imágenes de teledetección han surgido como herramientas muy útiles para el seguimiento de las poblaciones de roedores. Bajo esta premisa, en este estudio se presentan varias alternativas para estimar los daños causados por el topillo campesino en un ambiente de alfalfar mediante la combinación de vehículos aéreos no tripulados (UAS) y cámaras multiespectrales. En la actualidad, tanto los agricultores como los organismos implicados en los programas de gestión integrada de esta plaga no disponen de métodos suficientemente precisos para evaluar con exactitud el impacto real que tiene en los cultivos.

En general, los cuatro métodos de clasificación multiespectral estudiados mostraron rendimientos similares. Sin embargo, la segmentación basada en el índice de vegetación de diferencia normalizada (NDVI) fue la que mostró una valoración más precisa y fiable de las zonas afectadas. No obstante, hay que señalar que el método más sencillo, basado en una clasificación automática, proporcionó resultados similares a los obtenidos por métodos más complejos. Además, se encontró una relación directa significativa entre el número de huras activas y los daños en la cubierta de alfalfa.

Los vehículos aéreos no tripulados, combinados con la clasificación de imágenes multiespectrales, son una metodología eficaz y fácilmente transferible para la evaluación y seguimiento de los daños causados por el topillo campesino en las parcelas agrícolas. Las fluctuaciones en la población de topillos, especialmente el agudo descenso registrado a principios del mes de marzo, fueron coincidentes con una fuerte anomalía meteorológica de bajas temperaturas ocurrida en enero de 2021. En definitiva, esta combinación de métodos facilita la toma de decisiones para las estrategias de control integrado contra esta plaga.

Abstract

BACKGROUND: The common vole (*Microtus arvalis*) is a very destructive agricultural pest. Particularly in Europe, its monitoring is essential not only for adequate management and outbreak forecasting but also for accurately determining the vole's impact on affected fields. In this study, several alternatives for estimating the damage to alfalfa fields by voles through unmanned vehicle systems (UASs) and multispectral cameras are presented. Currently, both the farmers and agencies involved in the integrated management programs of this pest do not have sufficiently precise methods for accurate assessments of the real impact to crops.

RESULTS: Overall, the four multispectral classification methods presented showed similar performances. However, the normalized difference vegetation index (NDVI)-based segmentation exhibited the most accurate and reliable appraisal of the affected areas. Nevertheless, it must be noted that the simplest method, which was based on an automatic classification, provided results similar to those obtained by more complex methods. In addition, a significant direct relationship was found between the number of active burrows and damage to the alfalfa canopy.

CONCLUSION: Unmanned vehicle systems, combined with multispectral imagery classification, are an effective and easily transferable methodology for the assessment and monitoring of common vole damage to agricultural plots. This combination of methods facilitates decision-making processes for integrated control strategies against this pest.

Key words: *Microtus arvalis* Pallas, alfalfa, UAS, multispectral, classification, NDVI

4.1. Introduction

European agricultural landscapes host numerous species of small mammals (mainly rodents), some of which are considered to be highly destructive agricultural pests (Heroldová & Tkadlec, 2011). A well-known and highly prevalent pest is the common vole (*Microtus arvalis* Pallas 1778), hereafter referred to as the vole. It is a semifossorial microtinid that primarily inhabits agricultural landscapes such as meadows, field margins and alfalfa plots (Rodríguez-Pastor et al., 2016). However, during periods of population outbreak, they disperse, invade and colonize other suboptimal habitats, including areas cultivated with a wide range of crops (cereals, legumes, rapeseed, sunflower, etc.) (Rodríguez-Pastor et al., 2016; Giraudoux et al., 2019). In some Mediterranean regions, such as the farming lands of the west-central part of the Iberian Peninsula (Spain), voles cause significant damage due to their increased prevalence (Luque-Larena et al., 2013).

However, the population and prevalence increase are caused not only by the inherent behavior of the voles but also by human modification of their natural environment (Jareño et al., 2015; Heroldová et al., 2021). An anthropogenic modification to a natural environment is often a precursor to the emergence and propagation of zoonotic diseases such as tularemia, caused by *Francisella tularensis* bacterium (Luque-Larena et al., 2015), and population explosions among pests that can wreak havoc on agricultural production. Specifically, voles undergo a recurring demographic phenomena every two to five years, during which they multiply very quickly and attain densities of more than two thousand individuals per hectare in extreme cases (Heroldová & Tkadlec, 2011; Heroldová et al., 2021). This phenomenon leads to the biological invasion and colonization of all spaces, including cultivated plots (Jacob & Tkadlec, 2010). Indeed, extraordinary explosions of vole populations have occurred in recent decades in the agricultural areas of the Castilla y León region (Spain). An instance occurred in 2007 (between three and four million hectares of agricultural landscapes were invaded), when overabundant vole populations caused the highest loss of cereals, potatoes and vineyards observed in over a decade in this region. Mitigation costs were estimated at 15 million € (Jacob & Tkadlec, 2010; Luque-Larena et al., 2013). This led to mandatory and systematic monitoring of vole populations and their incidences of damage. Monitoring is crucial to optimize the management and to predict an outbreak of voles, because

monitoring not only allows for assessments of the presence of voles and the resulting damage in a specific plot at a given time but also allows for the establishment of preventive actions to effectively reduce the spread of a plague.

Currently, vole monitoring is performed through laborious and time-consuming fieldwork. Trapping methods are very effective field procedures for estimating vole populations, although they require significant human and material resources. For this reason, they are usually replaced by indirect methods, based on detecting signs of vole activity (i.e., droppings, active burrows and vegetation clippings), which are easier and faster (Witmer, 2005). These estimations of activity are usually linked to reduced vegetation cover (Terraube et al., 2011). Quantification of the reduction in vegetation cover is based on a sampling hierarchy, which often involves subjective biases emanating from the criteria used by the technician performing the sampling procedure.

In this context, photography, video technologies, and remote sensing imagery have emerged as very useful tools for monitoring rodent populations (Juanes, 2018; Sun et al., 2018). For instance, satellite images have been used to monitor agricultural damage caused by rats (Addink et al., 2010; Li et al., 2016), large gerbil burrows (Wilschut et al., 2018), and to predict a microhabitat's suitability for endangered rodent species (Valerio et al., 2020). Unfortunately, satellite images have coarse spatial resolutions. However, other low-altitude remote sensing methods, such as unmanned aerial systems (UASs), commonly known as drones, are currently available to solve this resolution problem. Recently, drones have been widely used in landscape ecology studies because of their high spatial resolutions, low cost, and easy operability (Zhang & Wang, 2017). Presently, there is scientific literature related to the use of drones and red/green/blue (RGB)-based imagery for rodent infestation assessment and monitoring. In regards to rodent populations, two main areas have been explored in the literature: 1) survey and recognition of rodent infestation (Dammer et al., 2018; Juanes, 2018; Nar et al., 2020); and 2) automatic identification of rodent evidence, such as burrows, by following a feature-extraction schema (Sun et al., 2018; Ezzy et al., 2021). A third group of investigations explores objective assessments of the damaged areas caused by the rodents, but in this case, the research relies on remote sensing, mainly by the use of Moderate Resolution Imaging Spectroradiometer (MODIS) imagery (Xu et al., 2014). Currently, very little scientific research exists on the combined use of UAS and multispectral

imagery for assessments of rodents' impact on agricultural fields, and more specifically in relation to the common vole. However, identifying the crop damage resulting from rodent infestations is vital for agricultural managers. The fine scale of the crop canopy damage caused by the voles makes necessary an evaluation at plot level, typically with pixel resolution of few centimeters. This suggests the use of very high-resolution imagery, which can be gathered by close-range flights done by UAS. Unmanned aerial system imagery enables estimations of the proportion of affected vegetation cover, plant foliar area, or a segmentation of the soil or damaged areas, among other parameters (de Castro et al., 2021). Multispectral sensors are particularly useful in these estimations, owing to their inclusion of infrared bands, which are sensitive to plant vigor (Wahab et al., 2018). The most common method to assess the percentage of vegetation loss and damage to the canopy, regardless of the cause of the loss, is through classification methods applied to the imagery inputs. These methods include the "unsupervised" clustering initiated in the late 1970s, to the current "deep learning"-based classifications (X. Zhang et al., 2020). There is an extensive body of scientific literature regarding developing methods such as subpixel, knowledge-based, contextual-based, object-based classification analysis and hybrid approaches (Phiri & Morgenroth, 2017). However, little effort has been devoted to distinguishing pest-damaged areas from healthy vegetation at a fine scale. For example, classification methods can help differentiate fully vegetated areas from "bald" areas created by voles (Ezzy et al., 2021), and also identify intermediate stages of damage. In pest damage evaluations, different classification approaches have been used, such as vegetation index thresholds (Xu et al., 2014), automatic classification methods (Barnas et al., 2019), and supervised classifications based on machine learning, either pixel-oriented (each pixel is classified independently) (Pilaš et al., 2020), or object-oriented methods (all pixels within defined objects are included to define spectral behavior through an iterative classification process) (Yuan & Hu, 2016). Imagery segmentations of damaged areas from UASs have also been used in the diagnoses of precision applications of control measures by drones (Morley et al., 2017). Considering the above, through our research, we developed a UAS-based alternative to accurately evaluate the impact of the common vole in an agricultural field. Our principal motivation was to assist farmers and pest managers who currently do not have methods to accurately determine the vole's impact on their crop fields. The secondary objective was to test different image classification

methods as well as to compare them with traditional field observations of vole impacts. To do so, both the fine-scale and spectral capabilities of an airborne multispectral sensor to monitor the impact of a common vole plague on crop fields were explored. In particular, an alfalfa field in the center of the Iberian Peninsula was monitored during 2020-21 to assess the potential of this methodology.

4.2. Material and methods

4.2.1. Study area

This study was carried out in an irrigated alfalfa (*Medicago sativa* L.) field located in the province of Valladolid (41°38'01''N-4°12'14''W, 741 m above sea level), which belongs to the region of Castilla y León, in the northern center of the Iberian Peninsula (Figure 4.1). The study was conducted from December 2020 to May 2021 between two alfalfa harvests (14th September 2020 and May 21st 2021). Thus, during the entire study period, the alfalfa remained unharvested. This region has a Mediterranean-continental climate that is characterized by cold winters and hot summers, with a very short spring and autumn and a frost period from October to April. Temperatures are considered extreme, exceeding 35 °C in summer and -12 °C in winter (Spanish State Meteorological Agency, AEMET, http://www.aemet.es/en/). Annual rainfall in this region is remarkably scarce and irregular, ranging from 300 to 400 mm.

A monitoring and surveillance program carried out by the regional government detected vole population increases since the summer of 2020. Moreover, due to its location and management system, this specific zone is representative of the irrigated alfalfa plots in the area.

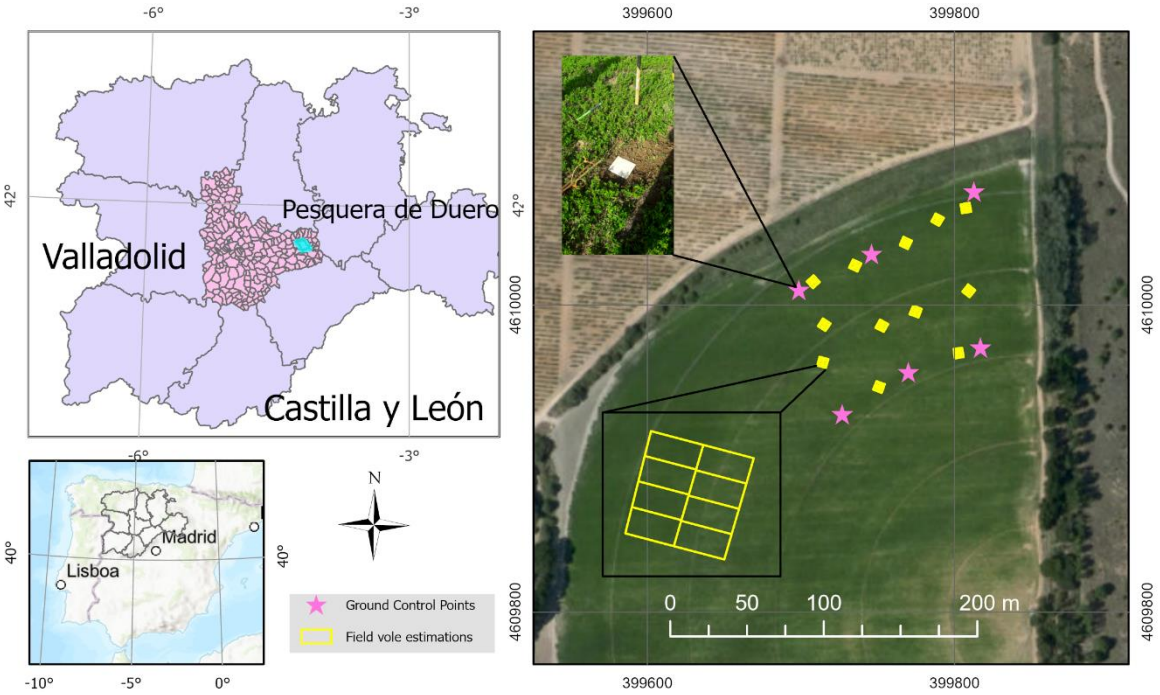

Figure 4.1. Map indicating the study area, including the squares where the field estimations took place (in yellow) and the GPS ground control points (in pink).

4.2.2. Data acquisition and pretreatment

a) Field data

Four drone flights were conducted during the study period (e.g., 12/18/20, 02/19/21, 03/10/21 and 05/04/21). Simultaneously, field estimations were taken as described in the following sections.

I. GPS collection

The GPS equipment was a 1200 Leica GPS receiver (Leica Geosystems, Heerbrugg, Switzerland) composed of a Leica Smartover ATX 1200 GNSS 1200 GG & GPRS dual-frequency modem (compatible with GPS and GLONASS signals), a Leica GX1220 GPS and GLONASS dual-frequency geodetic receiver for fixed or static observations, a standard antenna for a GX1220 receiver, a Satelline radio modem, and a mobile phone SIM card. Real-time kinematic (RTK) observations were recorded using the ITACyL network services, guaranteeing a final geolocation error of less than 2 cm. This system allowed for accurate geolocation and orthomosaiking of UAS images. To produce these images, six ground control points (GCPs) (i.e., target plates) were

strategically placed in the field (Figure 4.1) and were recorded with GPS. In addition, GPS measurements were recorded in the damaged areas to use them as ground truths to validate the results of the four classification methods ($n = 111$ locations throughout the flight area). The validation points were comprised of burrows, tracks and bare stands. These field measurements took place on dates 12/18/20 ($n = 58$ validation points), 02/19/21 ($n = 36$) and 03/10/21 ($n = 17$), excluding the last flight in May, since there were no visibly affected areas at that time. It should be noted that there were fewer validation points in May because there was less damaged surface at this date, as will be shown in the Results section.

II. Vole field monitoring

A total of 12 6 × 6 m^2 plots were field-designed and inspected in this work. Each of them was divided into eight sample units of 3 x 1.5 m^2 (Figure 4.2), which were established as experimental units for further analyses. The squares were selected after a careful inspection of the plot. They were regularly distributed within a maximum area of one hectare (fitting the flight extents) and separated by 20 meters from the nearest square and from the closest field margin.

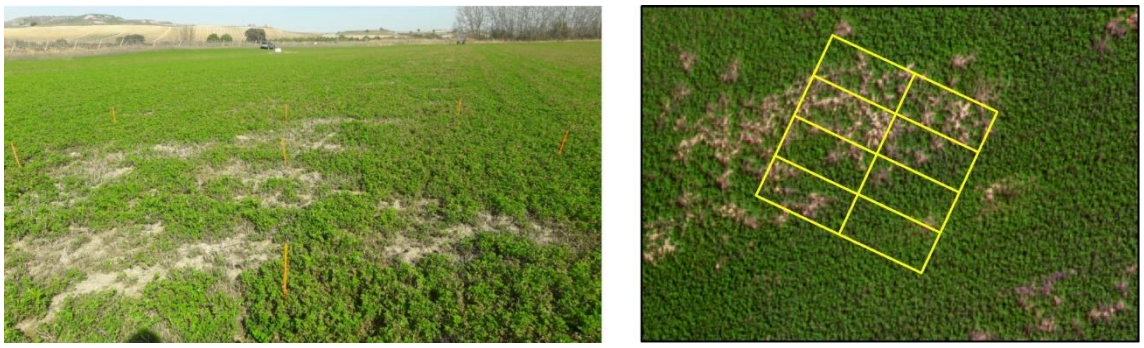

Figure 4.2. Squared plots of the vole field estimations at the field scale (left) and by drone image (right). Date acquisition 02/19/21.

In each sample unit, the degree of active vole colonization and canopy damage was assessed. To ensure that the selected colonies within the squares were active, two methods were used. The first method included the detection of the vole activity linked to the colonies (fresh droppings, recent digging and/or vegetation clipping) (Jareño et al., 2014). The second method included burrow renewal (Liro, 1974), in which all the burrow mouths were lightly covered with soil so that voles, if present, could easily reopen them.

After 24 hours, the number of reopened burrows was counted. Vole activity was estimated by counting the number of burrow entrances (hereafter "burrows"). In this study, all the observed colonies showed activity according to the two abovementioned methods.

To evaluate the magnitude of damage to vegetation cover caused by the voles found in each experimental plot, a visual scale from 0 (total affectation with absence of plants) to 6 (no affectation, no absence of plants) was used (Table 4.1). This visual assessment was always conducted by the same technician.

Table 4.1. Scale used to assess the effect of common vole infestation on the vegetation cover.

Code	Estimation of affected area (%)
0	100
1	80-100
2	60-80
3	40-80
4	20-40
5	0-20
6	0

These field estimations took place on the dates 02/19/21 and 03/10/21, on the same day, immediately after the flights of February and March.

b) Drone flights

Four flights were conducted between December 2020 and May 2021 at an altitude of 26 m, resulting in four maps at a spatial resolution of 2 cm. Each flight covered an area of approximately 1 ha within the alfalfa field.

A Micasense RedEdge-M camera (AgEagle Sensor Systems Inc., d/b/a MicaSense, Wichita, KS, USA) was mounted on a DJI-Inspire-1 drone (SZ DJI Technology Co., Ltd., Shenzhen, China). This camera has five-band images in the visible-near infrared (VNIR) space, namely, blue, green, red, red-edge and near-infrared wavelengths. The onboard Micasense equipment also included a GPS receiver and a downwelling light sensor (DLS) to account for the illumination conditions during each acquisition, which were taken around noon (11:00-13:00 UTC) to avoid shadows. In addition, to convert the raw values stored in each band into absolute reflectance, several images of a calibrated reflectance panel were taken before and after each flight. This

procedure is designed to obtain a fair comparison between the derived image products of each date that were used for the analysis.

The flight mission design and image processing were performed using Pix4D Capture and Pix4D Mapper (Pix4D P.A., Prilly, Switzerland), respectively. The latter allowed geometric correction, radiometric calibration and orthomosaicking of the absolute reflectance maps, following a standard workflow described in detail by Plaza et al. (2021).

4.2.3. Estimation of the affected area: clasiffications

Voles are able to invade irrigated crops year-round, especially pluriannual crops such as alfalfa, which provide them with continuous food and shelter (Rodríguez-Pastor et al., 2016). In fact, voles can consume between 1.6 and 45.8% of the annual alfalfa production; consumption can reach over 80% in outbreak events (Jacob & Tkadlec, 2010). In addition, given that alfalfa is harvested several times each year, the losses are cumulative. Voles remove and eat both the aerial parts of the plants and their roots, creating clearance areas without vegetation around the burrows (Figure 4.2). These bare soil stands account for crop-damaged areas, and are also comprised of burrows, paths and turned-over soil. In the absence of other biotic or abiotic causes, such as water or nutritional deficiencies or any other plague/disease, we considered vole activity to be the sole cause of alfalfa decay and loss.

All image analyses were performed in ArcGIS Pro 2.6 (Redlands, CA, USA: Environmental Systems Research Institute). Since the classification was intended to separate only two categories, i.e., “damaged” *vs*. “nondamaged” areas, three simple and conventional methods of image classification were proposed; all of them belong to the so-called “pixel-oriented” methods. The high spatial resolution of the UAS imagery (without mixed spectral characteristics) also indicated there was no need for subpixel classifications.

The simplest method was NDVI segmentation, a widely used method to partition the landscape into bare soil and vegetation (Glenn et al., 2008). The procedure of Wilschut et al. (2018) and Xu et al. (2014) was adapted for the task. First, 20 points of the damaged areas within the bare stands scattered throughout the image were visually selected and

used as training points. Second, buffers of a radius of 2 pixels (4 cm) were applied at each point, assuming that the minimum damaged area slightly exceeded the width of a burrow-mouth size, which ranged between 1.9 and 4.5 cm (Mougeot et al., 2020), due to the absence of plants and the soil accumulation around it. Therefore, an area of approximately 7-8 cm in diameter was considered the minimum affected unit.

The maximum, minimum, median and quartiles of the NDVI values at each buffer were extracted. After several tests, the criterion of the maximum NDVI (averaged for all buffers) was selected as the "damage" threshold. Therefore, all pixels with NDVI values below this threshold were considered damaged areas.

The second method is a supervised classification based on the Support Vector Machine (SVM) algorithm using the classification tool in the ArcGIS Pro 2.6 platform (Zhang & Milanova, 2013). The five multispectral bands of the camera were used as the input for the classification. To train the model, the same visual selection of damaged areas was used as in the previous methods.

The third method is a pixel-based automatic classification without training samples, using the ISO Cluster classifier available in ArcGIS Pro 2.6 (Iterative Self-Organization Data analysis, ISODATA) (Tou & González, 1974), which assigns pixels to both classes based on their spectral characteristics. Since it is an unsupervised method, there is no need to train the damaged areas. For the supervised method, the five bands of Micasense Red_edge M were computed.

Alternatively, a more complex "object-oriented" method of classification was applied. The object-based classification is similar to the pixel-based classification, with the difference that all the pixels are combined in the objects and are classified together (Walter, 2004). Therefore, this method requires a previous step of grouping neighboring pixels, the so-called segmentation, based on the integration of the spectral, shape and size characteristics of each group. In this case, we chose the values of 16, 15 and 10, respectively, to balance the importance of their spectral/geometric characteristics, as well as the superhigh spatial resolution of the image inputs. The second step consisted of creating training samples for the features resulting from the segmentation. Finally, the classification algorithm was applied. In this case, after several tests of the four available

algorithms in ArcGIS, the random trees classifier (Breiman, 2001; Breiman et al., 2017) was selected for its slightly better performance.

An accuracy assessment of the four methods consisted of testing the coincidence of the resulting damaged areas in the image with those taken in the field as ground truths, which was overlaid on each classification and date. Overall accuracy was defined as the percentage of correctly classified damaged areas. In contrast, the true-damaged areas observed in the field that were incorrectly assigned as healthy vegetation in the segmented maps were deemed as the percentage of "false negatives" (100% minus the percentage of correct). No "false-positives" were assessed since only damaged areas were gathered with the GPS as the ground truth.

A final accuracy assessment of the resulting maps consisted of comparing the ranking of severity of the field estimations (estimated at the sub-square level) with the percentages in the classified maps extracted for each sub-square.

4.2.4. Statistical analysis

The relationship between the percentage of damaged canopy resulting from the classifications and field observations (number of burrows/m^2) was assessed using a bivariate correlation process based on Pearson's linear correlation coefficient as the correlation indicator (Pearson, 1901). A two-tailed significance test was performed, flagging significant ($p \leq 0.05^{*}$) and highly significant ($p \leq 0.01^{**}$) correlations. These correlations were calculated using data collected from 96 sample units on days 02/19/21 and 03/10/21 ($n = 192$).

Significant differences among remote methodologies and field estimations were obtained using one-way analysis of variance (ANOVA). The means and standard errors (SEs) were calculated for all variables. The statistical significance was assessed at a 95% confidence level ($\alpha = 0.05$) using Snedecor's F as the contrast statistic. For differentiation of homogeneous subsets, Tukey's test was used (Tukey, 1949). For a better understanding of the results, and to avoid redundant information, the results of this analysis will be presented together with the graphical output of the comparison between the different methodologies.

Statistical processing was performed using the IBM-SPSS Statistics 26 software (IBM, Chicago, IL, USA).

4.3. Results

4.3.1. Accuracy assessment of the four classification methods

The overall accuracy, i.e., the percentage of field damaged areas correctly identified in the classified maps (Table 4.2), indicated that the NDVI segmentation was the most accurate method (overall accuracy greater than 80% for all dates and less than 20% of false negative identifications), closely followed by the object-oriented random forest classification (OORF) and then by the SVM supervised and ISODATA unsupervised classifications. In general, all the methodologies were similar in accuracy (more than 70% on average). Therefore, NDVI segmentation showed the best performance among the four methods. It is noteworthy, however, that the simplest method, the unsupervised ISODATA, performed quite similarly (overall accuracy 72.9%) to the more complex methods of supervised classification (72.4% for SVM and 80.2% for OORF) or NDVI segmentation (84.2%), both of which require training datasets and a higher level of knowledge.

Table 4.2. Accuracy assessment of the four classification methods.

Flight date	NDVI Segmentation	Supervised Pixel-based Classification (SVM)	Unsupervised Pixel-based Classification (ISODATA)	Supervised Object-based Classification (OORF)
12/18/2020	84.0	80.0	76.0	92.0
02/19/2021	82.9	65.7	57.1	71.4
03/10/2021	85.7	71.4	85.7	77.1
Average	84.2	72.4	72.9	80.2

NDVI: normalized difference vegetation index, SVM: support vector machine, ISODATA: iterative self-organizing data analysis and OORF: object oriented random forest.

4.3.2. Percentage of damage and accuracy assessment

Figure 4.3 shows the damaged canopy (%) using the four different methods, together with the field estimations. The total number of burrows/m^2 was also included.

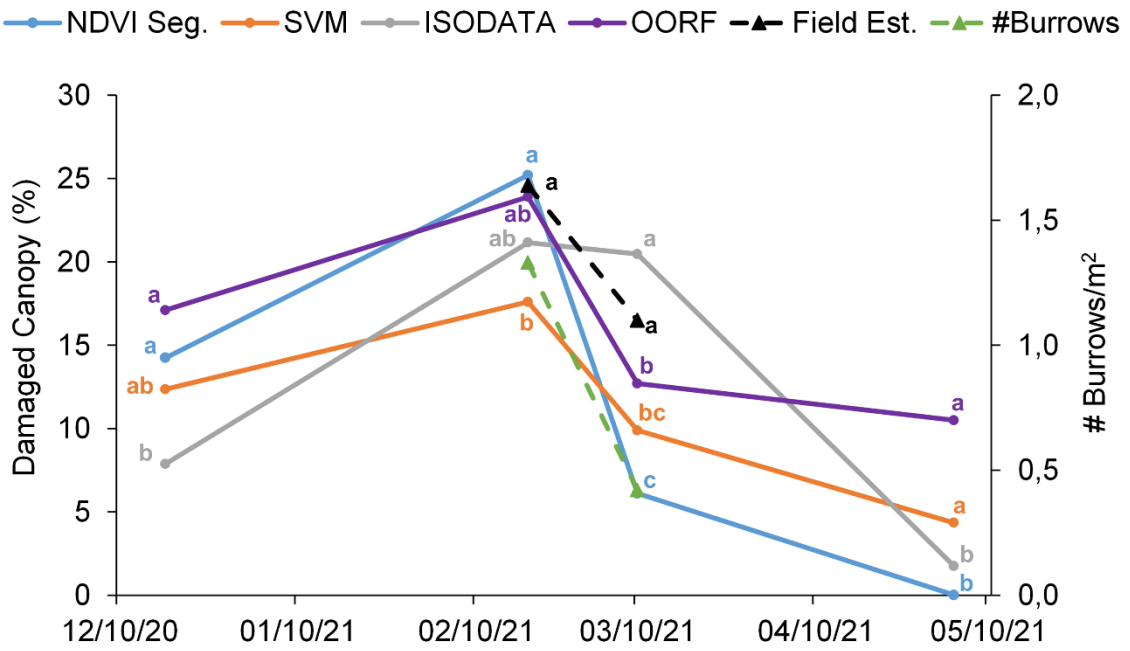

Figure 4.3. The damaged canopy and number of burrows simultaneously accounted for the field estimations. Lower case letters refer to the different homogeneous subsets resulting from the Tukey analysis. NDVI: normalized difference vegetation index, SVM: support vector machine, ISODATA: iterative self-organizing data analysis, OORF: object oriented random forest, Field Est.: field estimations of damaged areas and #Burrows/m^2: number of burrows per square meter.

The four classifications showed a similar trend, which was also corroborated by field estimations of the damaged areas and the number of burrows. In all cases, an increasingly damaged canopy was revealed from December to February, after which it drastically plummeted, albeit not as sharply as in the case of the ISODATA classification. This event was directly related to a lower presence and activity of voles in the study area, as evidenced by the reduction in the number of burrows/m^2 from February (1.33 burrows/m^2) to March (0.42 burrows/m^2). Immediately after that period, the alfalfa gradually recovered from the damage until the end of the study period, and the affection was negligible.

The NDVI segmentation indicated that the highest canopy damage occurred in December and February, finding no differences from the results obtained in the field measurements later on in the growing season. Conversely, it was the methodology that showed the lowest values for canopy damage to occur during March and May. Furthermore, the ISODATA classification registered the lowest percentage of damaged canopy in December but showed the highest percentage in March, which is statistically equal to the field estimations. The SVM classification accounted for the lowest value in

the February measurement but the highest value occurred during May. The OORF classification, compared to the other methods, recorded the highest values for canopy damage at the beginning and at the end of the study cycle. However, the most noticeable aspect is that this supervised classification methodology showed statistically equal results as those of the SVM, which followed an analogous supervised procedure throughout the complete study period.

According to the results exhibited in Figure 4.3, and given the same trend shown by the four implemented methods and the number of burrows, the correlation between the percentage of damage and the number of burrows/m^2 was explored (Table 4.3). The resulting correlations were all statistically significant ($p < 0.01$), with the SVM classification having the highest coefficient value, closely followed by the NDVI segmentation, with the OORF classification in third place. The ISODATA classification showed the lowest correlation with the number of burrows. Similarly, the correlation between the field estimates of the % damaged areas and the classified maps, all of them significant, showed the highest values for the SVM method and the lowest for ISODATA.

Table 4.3. Pearson linear correlation coefficients between the remote methodologies and the number of active burrows.

	NDVI Segmentation	**Supervised Pixel-based Classification (SVM)**	**Unsupervised Pixel-based Classification (ISODATA)**	**Supervised Object-based Classification (OORF)**
#Burrows	0.534**	0.577**	0.256**	0.439**
Field Est.	0.455**	0.513**	0.300**	0.376**

** Correlation is significant at the 0.01 level (2-tailed). #Burrows: number of burrows/m^2, NDVI: normalized difference vegetation index, SVM: support vector machine, ISODATA: iterative self-organizing data analysis, OORF: object oriented random forest and Field Est.: field estimations.

4.4. Discussion

Remotely sensed multispectral imagery is a common method for evaluating the status of the crop canopy by means of vegetation indices or multispectral classifications (Wiegand et al., 1991). In this situation, drones were the preferred tool for imagery acquisition because of the small size of the agricultural plots and the very high resolution needed to achieve an accurate estimation of the damage.

The four classification methods exhibited similar performances in terms of the percentage of overall accuracy and false negatives. Nevertheless, following the recommendations of Anderson et al. (1976) and Thomlinson et al. (1999) only the NDVI segmentation and the OORF classification maps had a low-enough degree of uncertainty, although the limits for the minimum level of overall accuracy are quite variable in the literature. Interestingly, if the accuracy is analyzed date by date, we found that the maps with the lowest accuracy corresponded to the February flight, coinciding with the highest canopy damage. Therefore, although the percentage of damaged areas should be analyzed carefully, the most accurate results belonged to the NDVI segmentation. Notably, simpler methods, such as the unsupervised classification provided acceptable results while avoiding subjectivity in the clustering algorithm. This is particularly interesting when trying to translate these geotechnologies into real-world field monitoring results. Indeed, the introduction of new geotechnologies holds the promise of increasing both agricultural productivity and the welfare of farmers (Adams et al., 2021). However, it is prudent to point out that unsupervised methods perform better when assigning broad or uncomplicated classes, such as "bare ground" *vs.* "vegetated cover" (Booth et al., 2005), as was done in this study with "damaged" *vs.* "nondamaged". Categories with less separability may benefit from a supervised approach. In addition, the OORF method achieved slightly better results than the pixel-based methods, indicating that object-oriented classifications are less influenced by the salt-and-pepper effect (Dronova et al., 2011), i.e., the distribution of speckled pixels between different classes (Benz et al., 2004), which could artefact the classification results. The OORF method's elevated cost in training and computing outweighs this modest improvement, especially in the context of moderately skilled users.

It seems that implementing simple methods that require little technical training but are useful for farmers to control their crop status should be compulsory. These results reveal a clear relationship between vole activity (number of burrows/m^2) and the observed damage to the alfalfa cover. Specifically, the greatest canopy damage, which was observed in February 2021, implied a larger damaged area than in March 2021 (Table 4.3). Hence, it could be assumed that there is a significant correlation between the vole damage to the alfalfa canopy and the number of burrows, albeit this relation should be verified with distributions other than a linear one. This significant relationship was in

agreement with the correlation found between the number of burrows and the field-observed damaged areas, with a Pearson linear coefficient of 0.591**.

In some agricultural areas of the Czech Republic, Truszkowski (1982) reported that with moderate populations of voles (129 voles/ha), approximately 198 kg of alfalfa dry mass/ha are consumed, but during population outbreaks (551 voles/ha), they can consume almost one ton of alfalfa dry mass/ha. Others suggest that a population density of 200 voles/ha can consume at least 5% of the alfalfa plants (Robert Eadie & Nelson, 1980), which is economically important. However, the problem is related not only to the aboveground consumed biomass but also to the total biomass eliminated (cut down) for further production. The latter is greater than the former by almost a factor of four (Truszkowski, 1982).

Active burrow counts would be useful if they varied consistently with the fluctuations in the rodent population density (Van Horne et al., 1997). In our work, a significant relationship between vole activity (and thus the vole population), expressed as the number of burrows/m^2, and the observed damage to the alfalfa canopy was found on the measurement dates when field estimations were available (February and March). However, it was even more evident in February, where all four classification methods and the field estimations reached their peak values, coinciding with a density of 1.33 burrows/m^2.

It is worth mentioning the relationship observed between the resulting population dynamics of the vole and meteorological conditions during the study period. A temperature anomaly took place in January 2021, with extremely low values (-11 °C), making it the coldest January since 1985 (Agencia Estatal de Meteorología (AEMET), 2021). Two difficult cold periods occurred in January 2021. The first occurred between the 5th and 8th, and the second cold period extended from the 11th to 18th. The latter was exceptionally intense and began after the passage of the Filomena storm and the establishment of an anticyclone over the peninsula. This phenomenon resulted in heavy snows covering large regions, which led to unusually low temperatures, reaching values below -20 °C in some areas (Agencia Estatal de Meteorología (AEMET), 2021).

There was a sharp decline in the vole population, which resulted in increased canopy coverage from February until the end of the studied period. We believe these cold

temperatures might have negatively affected the fecundity of voles and the ensuing canopy recovery. Related to this fact, Giraudoux et al. (2019) found a strong but complex relationship that proved that female vole reproduction was depressed after cold winters.

4.5. Conclusion

The change in agricultural practices in recent years, with the introduction of new cropping systems and new technologies, together with the influence of external factors such as climate change and natural resource conservation policies, makes it imperative to design new approaches to control troublesome species, like voles, that cause pests and diseases. Voles has drawn the attention of not only those involved in the agricultural sector but also of society as a whole due to the impact they have had on the economy, food safety, health and environmental protection. In this research, new UAS-based alternatives are used to monitor and estimate vole damage in an agricultural field. A multispectral camera onboard the drone provided aerial imagery to test four classification methods. All of them showed similar performances, although the NDVI segmentation exhibited the most accurate and reliable results. Moreover, a significant relationship between vole activity (measured by the number of burrows in active colonies) and observed damage to the alfalfa canopy was identified.

Unmanned aerial systems and multispectral imagery classification proved to be an effective and easily transferable methodology to help identify vole damage to the alfalfa field and to inform integrated management programs against this pest. The combination of these techniques with field measurements of vole activity, such as the number of active burrows, revealed the actual fluctuations of the common vole population. These variations, specifically the sharp decrease in vole activity and alfalfa damage up to the beginning of March, were coincidental with a strong negative temperature anomaly that occurred in January 2021.

In the foreseeable future, the applicability of this method can be further extended by expanding the automation of burrow counting by object detection algorithms from the deep learning domain.

Capítulo 5. GPS, LiDAR and VNIR data to monitor the spatial behavior of grazing sheep

Plaza, J., Sánchez, N., Palacios, C., Sánchez-García, M., Abecia, J. A., Criado, M., & Nieto, J. (2022). GPS, LiDAR and VNIR data to monitor the spatial behavior of grazing sheep. *Journal of Animal Behavior and Biometeorology*, 10(2), 2214. https://doi.org/10.31893/JABB.22014

Capítulo 5. GPS, LiDAR and VNIR data to monitor the spatial behavior of grazing sheep

Resumen

Tradicionalmente, en el sector ovino español, el control y la supervisión de los animales se han llevado a cabo en base a las prácticas tradicionales de pastoreo, que suelen implicar observaciones directas, continuas o periódicas por parte del pastor. Sin embargo, dado el gran tiempo necesario para adquirir esos conocimientos, junto con la influencia de los factores sociales y económicos del momento, dichos conocimientos tradicionales sobre el comportamiento del ganado en pastoreo están a punto de desaparecer. En este estudio se parte de la premisa de que los pastores son conocedores de que el comportamiento de las ovejas sigue patrones que no son aleatorios. Por lo tanto, como alternativa novedosa a la búsqueda de patrones de comportamiento, este estudio evaluó las actividades de pastoreo de dos rebaños de ovejas de raza churra (ambos en la misma zona, pero separados 10 años) mediante técnicas de monitorización basadas en los sistemas de posicionamiento global (GPS) y en la teledetección. En el primer periodo de seguimiento (2009-10) se registraron geolocalizaciones cada 5 min (4.240 registros), mientras que en el segundo (2018-20) se tomaron registros cada 30 min (7.636 registros). Los datos se agruparon en función de la franja horaria día/noche y de la actividad (descanso, desplazamiento o pastoreo), medida en función de la velocidad de desplazamiento del animal. Para estudiar los principales atributos topográficos del terreno (pendiente y su orientación) así como la altura de la vegetación, se utilizó un conjunto de datos LiDAR. Además, se realizaron mosaicos de cuatro ortofotografías en el infrarrojo visible y se clasificaron para obtener el mapa de uso y cobertura del suelo (LU/LC). A continuación, se superpusieron las localizaciones GPS a las características del terreno, y se evaluaron las relaciones entre las localizaciones y las características del terreno mediante un test Chi-cuadrado. Para obtener un mayor detalle de la distribución espacial de las geolocalizaciones, se calcularon también tres estadísticas geoespaciales (distribución direccional, densidad Kernel y análisis de puntos calientes). Los resultados obtenidos en ambos periodos de seguimiento sugieren que, de acuerdo con los

conocimientos tradicionales de los pastores, la distribución espacial de las ovejas en pastoreo libre no es aleatoria, sino que desarrollaron patrones habituales de conducta. Particularmente, la altura de la vegetación, los usos y coberturas del suelo, la pendiente y su orientación fueron las variables más influyentes en la localización de las ovejas en pastoreo. Los rebaños mostraron fuertes preferencias por las zonas de pastoreo con suaves pendientes orientadas al norte, donde predomina la capa herbácea formada por especies pratenses. Esta elección resultó ser deliberada, ya que se comprobó en dos periodos de estudio independientes de dos rebaños que fueron evaluados según diferentes enfoques estadísticos. En resumen, podría aseverarse que las ovejas eligen las zonas de pastoreo que ofrecen el alimento más fresco y de mayor calidad nutricional. Por tanto, se ha puesto de manifiesto que las geotecnologías son una potente herramienta para demostrar la influencia de los atributos ambientales y del terreno en el comportamiento espacial no aleatorio de las ovejas en pastoreo.

Abstract

Traditional knowledge about the behavior of grazing livestock is about to disappear. Shepherds well know that sheep behavior follows non-random patterns. As a novel alternative to seeking behavioral patterns, this study quantified the grazing activities of two sheep flocks of Churra breed (both in the same area but separated by 10 years) based on Global Position System (GPS) monitoring and remote monitoring sensing techniques. In the first monitoring period (2009-10), geolocations were recorded every 5 min (4,240 records), while in the second one (2018-20), records were taken every 30 min (7,636 records). The data were clustered based on the day/night and the activity (resting, moving, or grazing). An airborne LiDAR dataset was used to study the slope, aspect, and vegetation height. Four visible-infrared orthophotographs were mosaicked and classified to obtain the land use/land cover (LU/LC) map. Then, GPS locations were overlain on the terrain features, and a Chi-square test evaluated the relationships between locations and terrain features. Three spatial statistics (directional distribution, Kernel density, and Hot Spot analysis) were also calculated. Results in both monitoring periods suggested that the spatial distribution of free-grazing ewes was non-random. The flocks showed strong preferences for grazing areas with gentle north-facing slopes, where the herbaceous layer formed by pasture predominates. The geostatistical analyses of the sheep locations corroborated those preferences. Geotechnologies have emerged as a potent tool to demonstrate the influence of environmental and terrain attributes on the non-random spatial behavior of grazing sheep.

Keywords: behavioral patterns, geolocations, pastoralism, remote sensing, topographic attributes.

5.1. Introduction

Historically, in the Spanish sheep industry, the control and supervision of animals have been carried out based on traditional grazing practices, which usually involve direct, continuous, or periodic observations by the shepherd (Escribano et al., 2020; Bertolozzi-Caredio et al., 2021). In the process, the shepherd acquires profound knowledge about the daily and seasonal behavior of the ewes concerning grazing resources and environment features, among other factors; however, the time required to acquire that knowledge, along with social (the expanding rural exodus) and economic (the detriment of extensive practices due to the higher economic profitability of intensive production systems) factors has greatly diminished traditional grazing practices and, consequently, the loss of knowledge of these animals behavior.

Given the critical situation, it is essential to introduce new technologies that contribute to developing an objective method for understanding how grazing flocks behave and which factors have the most influence. Modern extensive systems, which strive to maximize economic profitability and sustainability, might benefit from an objective analysis of the suitability of habitat for grazing as a means of improving the organization and distribution of flocks and increasing support for decision-making in sheep management (Launchbaugh & Howery, 2005). Understanding the behavior of grazing flocks is a difficult challenge because the processes occur at multiple spatial and temporal scales (Senft et al., 1987; Hulbert et al., 2019). Nevertheless, abiotic factors (environmental, climatological, and topographical) affect the feeding behavior of ewes in free-range systems (Arnold & Dudzinski, 1978; Harris et al., 2002). Abiotic factors include the location of waterholes, the size, and geometry of rangelands, the topographic attributes, soils, and weather fluctuations (e.g., wind, temperature, atmospheric pressure). However, it is also important to evaluate the physiological state of the animals and the social conformation of the flock. Thus, when analyzing the distribution of grazing ewes, the environment, the flocks, and their interaction must be considered.

Technologies for monitoring flocks have proven effective and have become common among farmers. As geolocation and remote sensing technologies have become widespread, farmers have been implementing new practices at the expense of the more traditional ones, some of which have become almost obsolete. In the last decade,

numerous global navigation satellite system (GNSS) applications have been suggested as highly effective alternatives for tracking and monitoring cattle. Specifically, global positioning system (GPS) collars is a robust research method in science and have become a widely used technique in cattle (Turner et al., 2001; Ganskopp, 2001; Pandey et al., 2009). In several studies, cattle location data are integrated into a geographic information system (GIS) in which the point cloud is overlaid on a reference map, an orthophotograph, or a digital elevation model (DEM) (Turner et al., 2000, 2001; Putfarken et al., 2008; Schoenbaum et al., 2017; Schieltz et al., 2017). Other studies (Clark et al., 2009; Venter et al., 2019) integrated satellite images from Landsat and Sentinel-2 remote sensing missions to characterize vegetation cover. All this research demonstrated that ground-based sensors and remotely sensed satellite images could be jointly used to identify animal-landscape interactions (Handcock et al., 2009). However, although these methodologies have been widely used in cattle, very little has been done in sheep.

Furthermore, scarce research has been done on the complementary use of the most advanced remote sensing technologies such as light detection and ranging (LiDAR), probably because of the limited freely available data until recently. Yet, some studies (Lim et al., 2003; Sillero & Gonçalves-Seco, 2014), have suggested that LiDAR data are appropriate for the study of terrain and vegetation characteristics, particularly in mixed habitats such as open forests used as pasture (e.g., “dehesa”, the typical Spanish agroforestry system). LiDAR uses active laser sensors to obtain a dense point cloud of the Earth's surface; specifically, it emits laser light to the ground and measures the amount of energy reflected and the time for its return. As such, it can measure the height and density of vegetation on the ground. Due to its increasing availability, in recent years, LiDAR and other remote sensing technologies; e.g., aerial photographs (Chen et al., 2012; C. Zhang et al., 2013; Su et al., 2016; Shi et al., 2020), thermal (Baccini et al., 2012; Yandún-Narváez et al., 2016), and microwave imagery (Baccini et al., 2012; Ghosh et al., 2014) have been used extensively to map forests and vegetation characteristics.

“Dehesa” is an anthropogenic ecosystem that involves traditional forest exploitation of holm oak that creates open spaces between trees, which become over time grasslands and meadows dominated by herbaceous and shrub plant species that are consumed by livestock (Escribano, 2019). As in other natural grazing habitats, the spatial-temporal heterogeneity of the vegetation has a strong influence on the behavior of grazing

animals and their spatial distribution. The presence of over-or under-grazed areas caused by an uneven distribution of grazing can immediately affect the efficiency of forage resource use, which might affect the productivity and biodiversity of grasslands (Herrera, 2018).

The work hypothesizes that it is possible to identify behavioral patterns of pastoralist sheep related to terrain attributes and environmental conditions using innovative remote sensing techniques. GPS monitoring and remote sensing resources may offer a great potential to quantify the behavioral patterns of grazing sheep flocks. To do so, data recorded with GPS devices, together with airborne visible and near-infrared (VNIR) imagery and LiDAR data were exploited on two grazing sheep flocks.

5.2. Material and methods

5.2.1. Study area

The study was carried out in 800 ha of communal pastures (41º 24’ 23’’N – 6º 15’ 38’’W) of Fariza, a village in the Sayago region of the province of Zamora (Castile and Leon, Spain) (Figure 5.1). Fariza belongs to a natural area, part of the Natura 2000 Network; specifically, it is part of the “Arribes del Duero” Natural Reserve. The ecosystem known as the “dehesa”, predominates in the study area.

The semi-arid Mediterranean climate, the diverse topography, and the poor quality of siliceous soils are the main characteristics that have led to these areas being used for extensive livestock farming. Most of the study area was within a rangeland, where other types of vegetation were present: holm oak “dehesa”, pastures, shrubs (rockrose, heather, and thyme), and oaks of different heights and densities (Figure 5.1). In addition, some small areas were used to cultivate dry-land cereals. The area's diversity provided the sheep flocks with a wide variety of habitats for grazing.

The study area has a communal use; i.e., the land belongs to the municipality and all residents have the right to graze their livestock in the area. Apart from fences and one road (Figure 5.1, in black), there were no other physical barriers to impede the free movement of the animals.

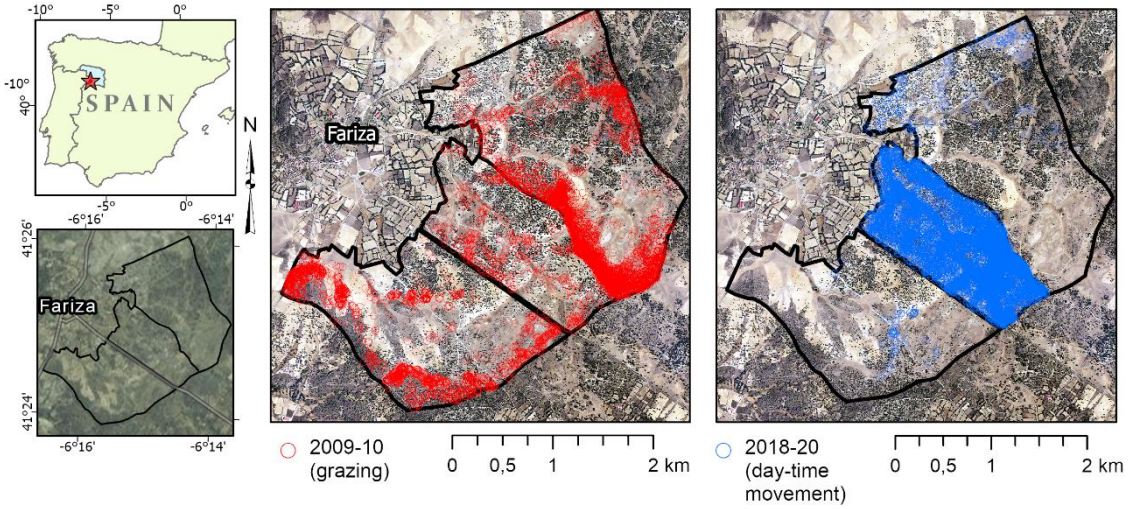

Figure 5.1. Location of the study area in Fariza, Spain.

5.2.2. Data and methods

a) Flock monitoring

This study involved two geolocation datasets derived from GPS collars on two sheep flocks that were collected 10 years apart. There were significant advances in geomatics in the intervening period, particularly in the geolocation devices and networks. However, it was assumed that the management system was the same for both flocks. Therefore, the second objective is to assess if the sheep's non-random grazing behavior may be detected by GPS devices, regardless of the technological level of those devices.

Both flocks were Churra breed sheep, characterized by having a medium size, a rustic metabolism, a meat/dairy aptitude, a white coat with black or peripheral brown coloring of the ear tips, around the eyes, nose, and distal parts of the limbs. Specifically, the ewes were the "sayaguesa" ecotype. Both flocks were maintained under a free grazing system.

The monitoring system consisted of a GPS sensor, a data storage unit, a GPRS SIM card, a long-life battery, and an antenna for receiving the satellite signal (most of the elements of the device were inside a hard plastic case with a hermetic seal, which protected them against shock and moisture). The first monitoring period took place between 2009 and 2010 (hereafter, 09-10 period) and the second period between 2018 and 2020 (hereafter, 18-20 period). Although the flocks differed in size, the management

operations were the same for both flocks. The specifics of each monitoring period are described below.

I. 09-10 monitoring period

The flock contained 614 reproductively mature animals (600 breeding females and 14 males), and GPS collars were placed on two healthy, randomly selected adult female ewes. Each time the battery was changed (every 15 recording days approximately), the GPS collar was placed on another two randomly selected female sheep; therefore, the data were not biased by the behavior of a single individual. A total of 12 ewes were monitored throughout this period. The GPS collars were prototypes developed by CONAN-GPS (GMV Innovating Solutions S.L., Valladolid, Spain). Geolocation data were collected every 5 min and daily sent to a Machine to Machine (M2M) platform via a GPRS connection.

The distance, time, and speed between consecutive GPS records were calculated at daily interval. The animal activity was defined based on the animal's speed. To do so, simultaneous to the data collection by the GPS devices, the flock's behavior was observed directly. These direct observations were taken after placement of the GPS device for each of the 12 monitored ewes. Specifically, these measurements were taken every 15 minutes along eight hours per day during the first two days of their monitoring. The observations were compared with the GPS locations and trajectories to classify the data set based on the animal's speed between two consecutive locations. Thus, the main activity of the flock was identified, distinguishing between resting, grazing or moving, specifically, speed< 0.043 m/s = “resting”, 0.043 m/s to 0.4 m/s = “grazing”, and > 0.4 m/s = “moving” (Sánchez-García, 2010). These activities have been defined similarly for cattle (Mora-Delgado et al., 2016; Venter et al., 2019), albeit the speed ranges are not the same since they are different species. Note that “grazing” is the target class of the study as it is the only one that implies the act of consuming grass.

II. 18-20 monitoring period

The flock had 650 reproductively mature animals (645 breeding females and 5 males), and the GPS devices that recorded geolocations were GPS DMS-CattleSat 1.4 with a UBX-R3 receiver chip (Domodis, Cordovilla, Spain). As in the previous

monitoring period, two GPS collars were placed on two healthy randomly selected adult female ewes, which were moved from one individual to another each time the battery had to be replaced (every 90 recording days approximately). A total of 18 ewes were monitored throughout this period. Data transmission was similar to that in 09-10 and was web-accessible. The number of data was higher than in 09-10 because the time series was continuous, even though the data recording interval was longer (every 30 min). Then, the same speed clustering as done in 09-10 was not possible.

Nevertheless, the speed between two consecutive locations was used to create a dichotomous analysis of the animal's movement, i.e., "rest" (if speed = 0 m/s) and "movement" (if speed > 0 m/s). In addition, based on sunrise and sunset times in each month, data were categorized as "day-time" or "night-time". This distinction can provide important information about the timing of active grazing by the animals, their spatial distribution in the study area, and the location of the sheepfolds used by the farmers to shelter the sheep at night. In short, the data were assigned to four groups: (1) day-time movement, (2) night-time movement, (3) day-time rest, and (4) night-time rest. Of those, the only day-time movement was associated with grazing.

b) Airborne data

I. LiDAR data

LiDAR data provide several vegetation and terrain observations at a fine spatial scale. The airborne LiDAR dataset was provided by the Agriculture Technological Institute of Castile and León in 2010 (ITACyL), available at http://ftp.itacyl.es/cartografia/02_Altimetria/023_LIDAR/. The point cloud (Figure 5.2a) had a point density of one point per 2 m^2 and an accuracy of 15-20 cm for Z and 10-15 cm for XY. Before extracting any derived product, a workflow of refinement and editing was performed on the *.las* files, including removing overlapped and outlier points, deleting duplicates, identifying noisy points, and reclassifying. This was performed in ArcGIS Pro 2.4 and the LAStools LiDAR processing toolbox (https://rapidlasso.com).

After refinement, the LiDAR point cloud (Figure 5.2a) was rasterized into the digital terrain model (DTM) (Figure 5.2b, top) and the digital surface model (DSM) (Figure 5.2b, bottom). To match the original point density, the spatial resolution of the

two raster files was set to 2 m. In both cases, elevation was interpolated; however, for the DTM, the points classified as ground data were selected, whereas, for the DSM, a filter of the first return signal was applied. It was shown that using the first return of the signal may lead to an underestimation of the crown height because the probability that a small footprint laser pulse intercepts the apex of a conic crown is low (Lim et al., 2003). In the study area, however, the trees (mostly *Quercus ilex*) have a rounded, typically plain crown, which is not affected by this problem.

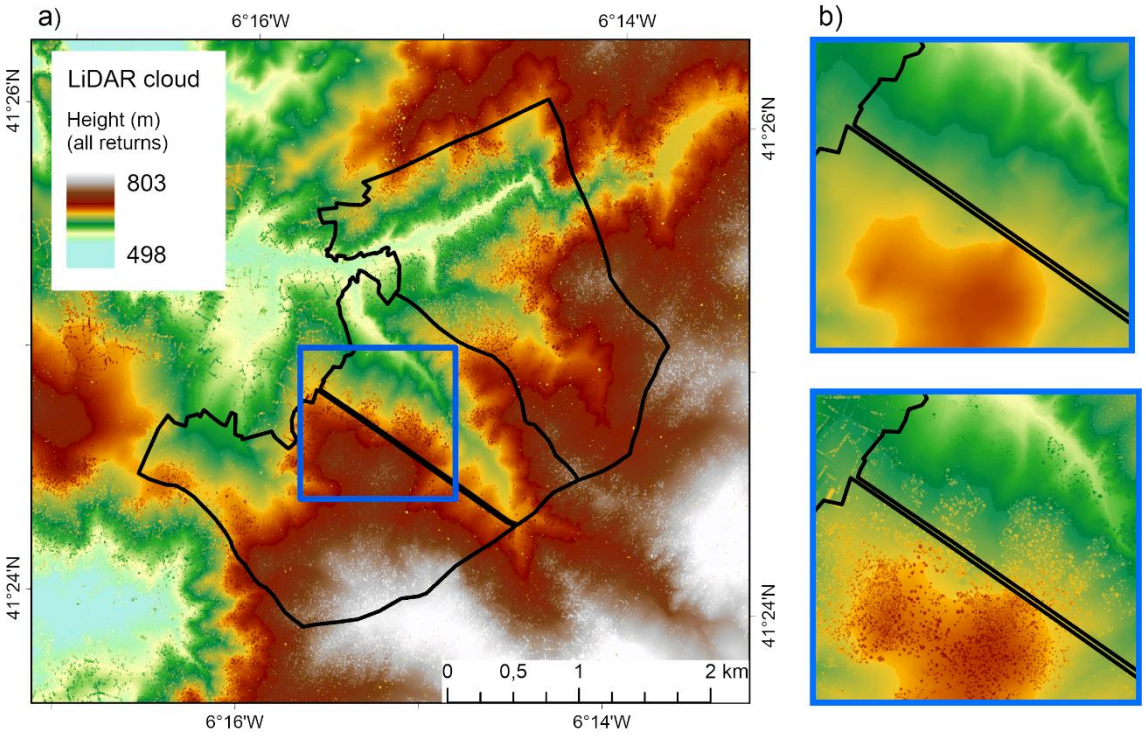

Figure 5.2. (a) LiDAR data with a point cloud density representation and the locations of the study area, and (b) details of the raster's DTM (top) and DSM (bottom) of the study area.

Based on the DTM, several terrain features were evaluated, including watershed slope, aspect, flow direction, and accumulation. A preliminary assessment identified slope and aspect as key attributes. In addition, the canopy height model (CHM) was calculated by subtracting the DTM from the DSM. Therefore, the elevation, slope, CHM, and aspect of the whole study area were extracted and analyzed at each location of the monitored sheep.

II. Aerial photographs and classification map

Four orthophotos from the ITACyL at 25-cm spatial resolution were mosaicked to cover the study area, including three RGB bands and one NIR.

To investigate the LU/LC in the study area, a supervised classification was tested by the ArcGIS Pro 2.4 schema of pixel-based classification and the support vector machine algorithm (Priya et al., 2012; Saini & Ghosh, 2018). The training dataset consisted in 100 ground-truth points randomly selected in the orthophotos, in which their LU/LC was estimated from the VNIR images. To reinforce the classification, the normalized difference vegetation index (NDVI) between red and NIR bands was calculated and used as a reference map in the process. The proposed legend identified the most common grazing scenarios, i.e., trees and/or shrublands, rainfed crop areas, grasslands and pasture, roads and tracks, and rocky-asphalt patches. The accuracy of the map produced was evaluated by a confusion matrix, a tool that allows a comparison of the real class and the class that resulted from the process within a range of known areas. Each column of the matrix indicates the number of predictions of each class, and each row indicates the instances in the real class. The tool calculates errors of omission and commission, the index of agreement (or kappa concordance), and an overall precision between the classified map and the reference data. For that purpose, a dataset of other 100 ground-truth points, previously selected in the orthophotos, was used as reference. Then, statistics were extracted from the expected *vs.* observed values, a typical schema of the accuracy assessment used in classifications (Foody, 2002; Lillesand et al., 2015). Similarly to the other LiDAR-derived maps, each GPS position was overlaid on the resulting LU/LC map, and each class was extracted for each record.

c) Analysis of spatial distribution by spatial statistics

Several spatial statistics were suggested as an objective way to identify both the empirical relationships between factors that influence grazing and the spatial patterns of the flock based on the GPS locations. Only the temporal continuity of the 18-20 data allowed that analysis.

A first analysis evaluated the directional distribution of the GPS point cloud. Standard deviation ellipses were used to quantify the spatial characteristics of the geographical features such as central tendency, dispersion, and directional trends.

Given the large number of records available, it is likely that locations might have been concentrated in some areas. Specifically, we evaluated the clustering patterns based on their statistical significance: from "hot" to "cold" spots (HS and CS, respectively). In addition, the Kernel density spatial interpolation provided indications of the possible locations of the HS. The ArcGIS Pro spatial statistics tool calculates a magnitude per unit area from the points of the geolocations based on a kernel function (Silverman, 1986), which includes the point density around each raster output cell.

d) Statistical analysis

The influence of several biotic and abiotic factors was studied over the two databases, i.e., aspect, slope, CHM, and LU/LC map. Histograms and statistics (observed and expected frequencies together with the Chi-square analysis) indicated the conditions preferred by sheep for grazing. Unfortunately, neither LIDAR data nor infrared orthophotos of the study area were available for 2018-2020. Therefore, the LU/LC map and the CHM could not be created for this period. Nevertheless, the topographical factors of the terrain (slope and aspect) are not supposed to differ between the two periods; therefore, the same maps were used for both periods.

To discard any correlations between the topographic features extracted from the LIDAR dataset, the spatial correlation (Pearson's linear correlation coefficient, R) between the slope maps, the aspect, and the CHM were calculated. The correlations between slope and aspect (0.02), aspect and CHM (-0.02), and CHM and slope (-0.04) were not statistically significant. Thus, they may be considered independent features.

All variables of interest (aspect, slope, CHM, and LU/LC) were expressed as codified values; therefore, the Chi-square test was used to evaluate the independence between two categorical variables. Here, the objective was to obtain an absolute value of dependence between the terrain variables or expected frequencies (N_E) and the sheep locations or observed frequencies (N_O) with no influence by the terrain itself; e.g., if a certain slope predominates the terrain, it is likely that that slope will occur more

frequently among the sheep locations. To avoid that problem, the N_E in the Chi-square tests were not equally distributed; indeed, they were adjusted to the percentage occupied by each class variable. Therefore, the N_E were different and duly adjusted to the terrain distribution of the variables.

5.3. Results

5.3.1. 09-10 monitoring period

The records were collected over 87 days: 63 days from February to December 2009 (scattered days of February, April, July, October, and December) and 24 days from January 2010. GPS devices recorded 12,652 locations, out of which 5,391 (42.61%) positions corresponded to resting activity, 3,021 (33.51%) to moving and 4,240 (23.88%) to grazing.

a) Effect of vegetation height

To classify the various vegetation strata in the study area, the classification of the food and agriculture organization of the United Nations (FAO, 2004) was followed. Accordingly, the herbaceous layer was considered the vegetation cover that did not exceed 0.5 m in height, the shrub layer was the vegetation between 0.5 and 3 m, and the tree layer was the vegetation cover that was > 3 m high (Figure 5.3).

In the CHM map, the area occupied by each class (N_E) was 81.2% herbaceous, 10.0% trees, and 8.8% shrub (Table 5.1). Sheep locations at the CHM map indicated that ewes tended to graze in areas that were distant to the highest vegetation strata. The N_O indicated that grazing occurred mainly on the herbaceous layer (71.6% of locations). Only 18.2% of the locations occurred under trees, and 10.2% occurred on scrublands. The remnants revealed that there were clear differences between N_E and N_O, and their statistical significance was confirmed ($p<0.05$) by the Chi-Square test value (χ^2).

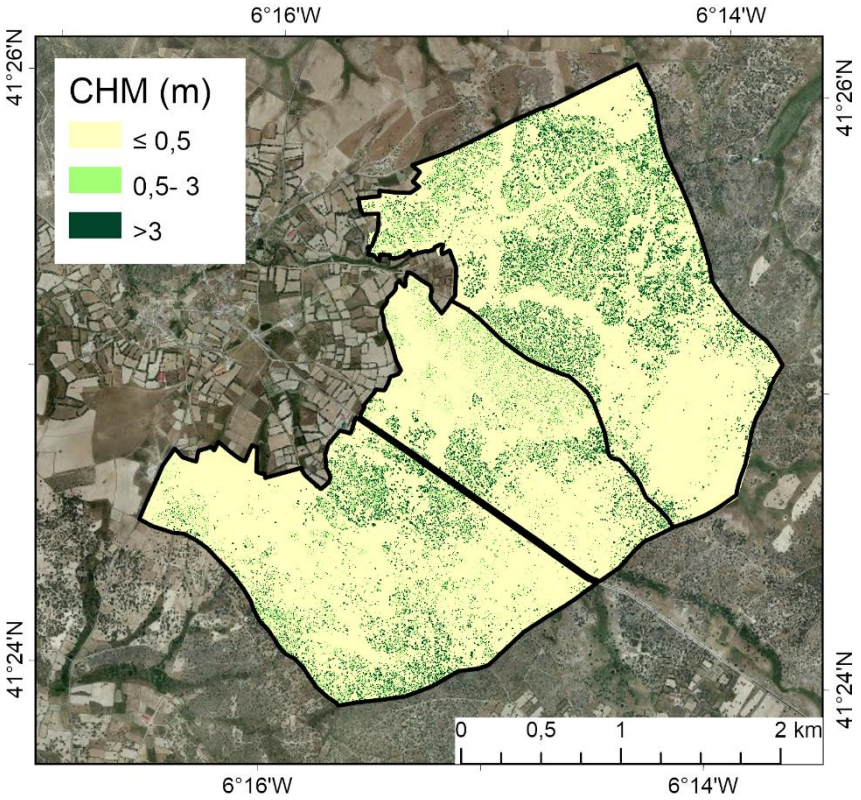

Figure 5.3. Map of CHM derived from the subtraction of the DSM from the DTM of the study area.

Table 5.1. Expected and observed frequencies in CHM (09-10 monitoring period).

	VARIABLE	N_O	N_E	R	χ^2	p
	Herbaceous layer	3,036 (71.6%)	3,444 (81.2%)	- 408 (- 9.6%)		
CHM	Shrub layer	434 (10.2%)	374 (8.8%)	+ 60 (+ 1.4%)	344.936	0.000
	Tree layer	770 (18.2%)	422 (10.0%)	+ 348 (+ 8.2%)		

* Statistically significant differences p <0.05

* N_O: observed frequencies (sheep locations distribution); N_E: expected frequencies (terrain distribution); R: remainder; χ^2: Chi-square value

b) Effect of aspect

The aspect map (Figure 5.4) depicts the four main compass directions taken into account. Northern areas range from 292.5º to 67.5º, eastern areas from 67.5º to 112.5º, southern areas from 112.0º to 202.5º, and western areas from 202.5º to 292.5º, whose N_E are shown in Table 5.2. The distribution of locations differed significantly ($p<0.05$) among aspects. Remarkably, 64.6% of the observations (N_O) are located on north-facing areas, followed by west-facing areas with 19.6%, then south-facing areas with 8.6%, and finally east-facing areas with 7.2% (Table 5.2).

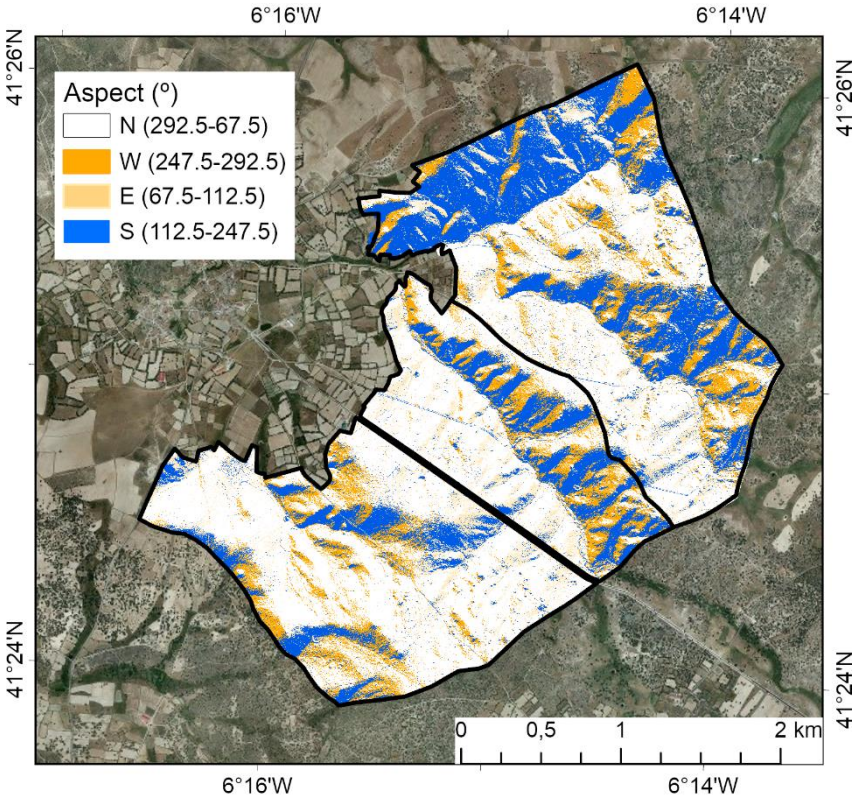

Figure 5.4. Map of aspect within the study area.

Table 5.2. Expected and observed frequencies of aspect (09-10 monitoring period).

VARIABLE		N_O	N_E	R	χ^2	p
Aspect	North	2,738 (64.6%)	1,548 (36.5%)	+ 1,190 (+ 28.1%)	1466.822	0.000
	East	304 (7.2%)	726 (17.1%)	- 422 (- 9.9%)		
	South	365 (8.6%)	689 (16.2%)	- 324 (- 7.6%)		
	West	833 (19.6%)	1,277 (30.2%)	- 444 (- 20.6%)		

* Statistically significant differences p <0.05

* N_O: observed frequencies (sheep locations distribution); N_E: expected frequencies (terrain distribution); R: remainder; χ^2: Chi-square value

c) Effect of slope

Except for some isolated escarpments and small gullies along the main river, the slope of the study area was very gentle (Figure 5.5). Specifically, most of the slopes spanned between 2%-6% (Table 5.3). Most (77.5%) of the sheep locations were on slopes that were <6%.

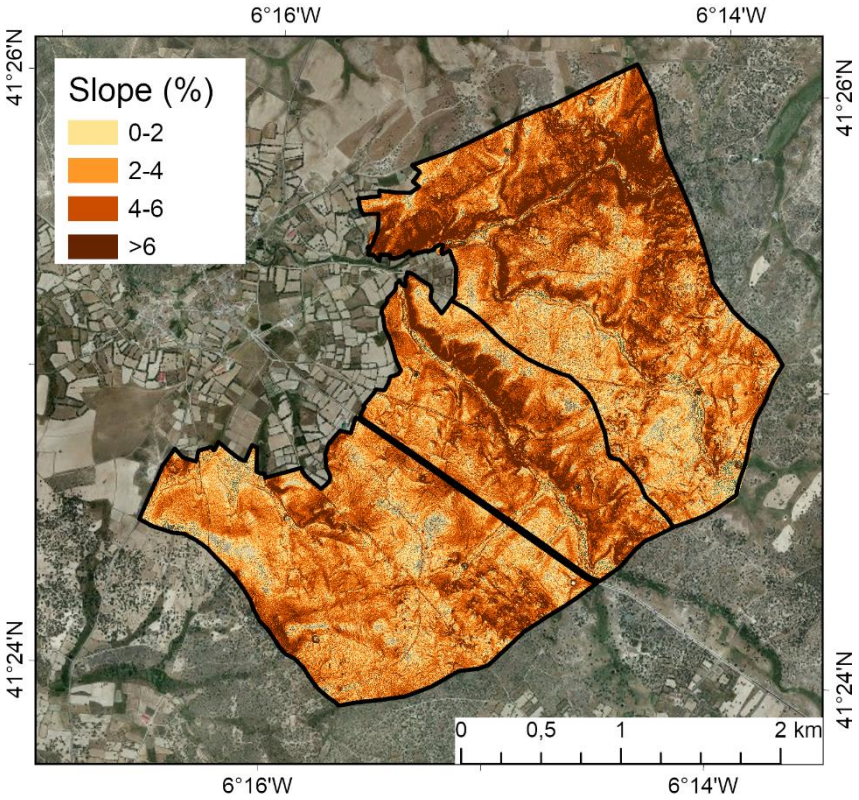

Figure 5.5. Map of slope within the study area.

The ewes' geolocations (N_O) slopes had a normal distribution, with an average of 4.76%, and quartiles Q_1=2.57%, Q_2=3.79%, and Q_3=5.69%. The highest number of records was in the range 2-4%, followed by the range 4-6% and the range >6%. Ewes preferred gentle slopes for grazing (particularly between 2% and 4%), although they were not the most common slope in the study area (Table 5.3).

Table 5.3. Expected and observed frequencies of slope (09-10 monitoring period).

VARIABLE		N_O	N_E	R	χ^2	p
Slope	0-2	580 (13.7%)	364 (8.6%)	+ 216 (+ 5.1%)	498.515	0.000
	2-4	1,688 (39.8%)	1,229 (29.0%)	+ 459 (+ 10.8%)		
	4-6	1,019 (24.0%)	1,190 (28.1%)	- 171 (- 4.1%)		
	>6	953 (22.5%)	1,457 (34.3%)	- 504 (- 11.8%)		

* Statistically significant differences p <0.05

* N_O: observed frequencies (sheep locations distribution); N_E: expected frequencies (terrain distribution); R: remainder; χ^2: Chi-square value

d) Effect of LU/LC

The LU/LC map (Figure 5.6) had a kappa concordance index of 0.76 and an average accuracy of 84%. Given that a kappa index of 1 indicates the closest concordance and that the minimum level of interpretation accuracy in the identification of LU/LC categories based on a remote sensor should be at least 85% (Anderson et al., 1976), the results of the LU/LC map were considered acceptable.

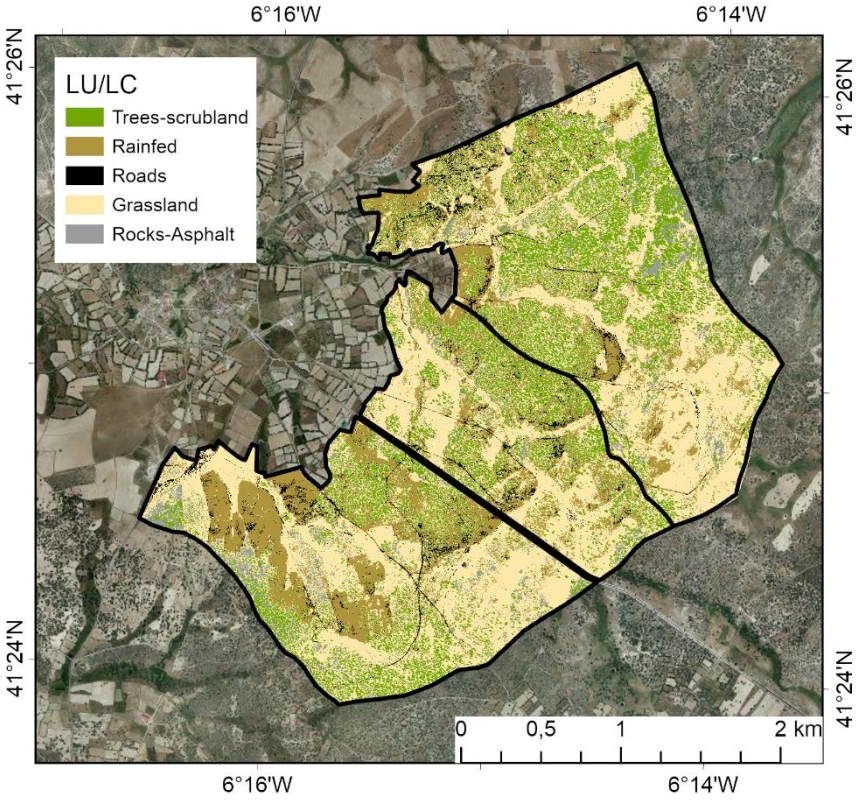

Figure 5.6. Map of LU/LC within the study area.

Grasslands, followed by trees and shrub layers, were the most common LU/LC (Table 5.4). Grazing sheep made the most use of grasslands and tree and shrub strata to a lesser extent (Table 5.4).

Table 5.4. Expected and observed frequencies of LU/LC (09-10 monitoring period).

VARIABLE		N_O	N_E	R	χ^2	p
LU/LC	Trees and/or shrub layer	1,124 (26.5%)	864 (20.4%)	+ 260 (+ 6.1%)	160.700	0.000
	Rainfed land	566 (13.4%)	806 (19.0%)	- 240 (- 5.6%)		
	Roads and tracks	125 (2.9%)	133 (3.1%)	- 8 (- 0.2%)		
	Grasslands	2,178 (51.4%)	2,136 (50.4%)	+ 42 (+ 1.0%)		
	Rocks and asphalt	247 (5.8%)	301 (7.1%)	- 54 (- 1.3%)		

* Statistically significant differences p <0.05

* N_O: observed frequencies (sheep locations distribution); N_E: expected frequencies (terrain distribution); R: remainder; χ^2: Chi-square value

5.3.2. 18-20 monitoring period

The locations of ewes in the 18-20 flock were recorded from 1 Jan 2018 to 14 Apr 2020 (N = 18,044 records). Of those records, 42.3% indicated day-time movement, 14.6% indicated night-time movement, 9.9% indicated day-time rest, and 33.2% indicated night-time rest. Although the number records differed between flocks in each period, the frequencies of slope and aspect of the terrain (N_E) were the same because the terrain's topography remained unaltered.

a) Effect of aspect

As in the 09-10 flock, ewes in 18-20 showed a significant ($p<0.05$) preference for north-facing areas (Table 5.5).

Table 5.5. Expected and observed frequencies of aspect (18-20 monitoring period).

VARIABLE		N_O	N_E	R	χ^2	p
Aspect	North	4,274 (56.0%)	2,788 (36.5%)	+ 1,486 (+ 19.5%)	1,757.358	0.000
	East	320 (4.2%)	1,307 (17.1%)	- 987 (- 12.9%)		
	South	718 (9.4%)	1,240 (16.2%)	- 522 (- 6.8%)		
	West	2,324 (30.4%)	2,301 (30.2%)	+ 23 (+ 0.2%)		

* Statistically significant differences p <0.05

* N_O: observed frequencies (sheep locations distribution); N_E: expected frequencies (terrain distribution); R: remainder; χ^2: Chi-square value

b) Effect of slope

Similar to the 09-10 period, 64.9% of the locations occurred in areas with a slope < 6%. This value is slightly smaller than its counterpart from the other monitoring period but confirms that the sheep show a preference for gentle slopes. The slopes of the geolocations had a normal distribution, an average of 5.6%, and quartiles Q_1=3.26%, Q_2=4.89%, and Q_3=6.97% (Table 5.6).

Table 5.6. Expected and observed frequencies of slope (18-20 monitoring period).

VARIABLE		N_O	N_E	R	χ^2	p
Slope	0-2	713 (9.3%)	655 (8.6%)	+ 58 (+ 0.7%)	21.662	0.000
	2-4	2,040 (26.8%)	2,214 (29.0%)	- 174 (- 2.2%)		
	4-6	2,201 (28.8%)	2,143 (28.1%)	+ 58 (+ 0.7%)		
	>6	2,682 (35.1%)	2,624 (34.3%)	+ 58 (+ 0.7%)		

* Statistically significant differences p <0.05

* N_O: observed frequencies (sheep locations distribution); N_E: expected frequencies (terrain distribution); R: remainder; χ^2: Chi-square value

En base a la posibilidad que ofrece la Universidad de Salamanca, la presente tesis doctoral se presenta como un compendio de artículos científicos, habiendo participado el doctorando Javier Plaza Martín activamente en todos ellos y siendo el autor principal de al menos tres de los mismos.

c) Analysis of spatial distribution

For the 18-20 flock, the standard deviation ellipse (Figure 5.7, left) encompassed about 68% of the geolocations. It indicated a faster change in the southwest-northeast direction and a more gradual change in the northwest-southeast direction.

The Kernel density analysis indicated HS presence in the study area (Figure 5.7, center). In particular, a very high point density occurred at the southeast end of the center of the communal pastures. Of the 7,636 geolocations, 43.0% were located in HS. To study the causes of the formation of this HS, that area was isolated (Figure 5.7, right), and the slope and aspect factors were studied within it. Within the HS, the most common slope was >6% (Table 5.7). Among the geolocations (n = 3,285) in the HS, however, the highest proportion has slopes of 2-4% (Table 5.7). In the HS (N_E in Table 5.7), west-facing areas were the most common (49%); however, the ewes preferred north-facing areas (55.8%).

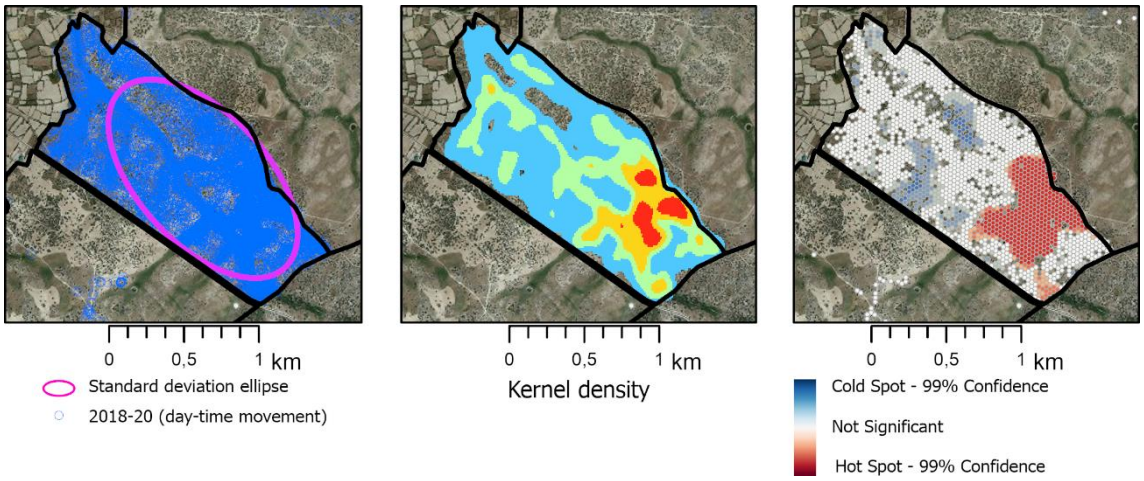

Figure 5.7. Standard deviation ellipse (left), Kernel density (center), and hot spots (right) for the geolocation of sheep in the 2018-20 monitoring period.

Table 5.7. Expected and observed frequencies of aspect and slope within the HS (18-20 monitoring period).

VARIABLE		N_O	N_E	R	χ^2	p
Slope	0-2	322 (9.8%)	240 (7.3%)	+ 82 (+ 2.5%)	414.913	0.000
	2-4	1194 (36.3%)	779 (23.7%)	+ 415 (+ 12.6%)		
	4-6	942 (28.7%)	979 (29.8%)	- 37 (- 1.1%)		
	>6	827 (25.2%)	1287 (39.2%)	- 460 (- 14.0%)		
Aspect	North	1834 (55.8%)	1074 (32.7%)	+ 760 (+ 23.1%)	799.290	0.000
	East	89 (2.7%)	144 (4.4%)	- 55 (- 1.7%)		
	South	304 (9.2%)	457 (13.9%)	- 153 (- 4.7%)		
	West	1058 (32.3%)	1610 (49.0%)	- 552 (- 16.7%)		

* Statistically significant differences p <0.05

* N_O: observed frequencies (sheep locations distribution); N_E: expected frequencies (terrain distribution); R: remainder; χ^2: Chi-square value; HS: Hot Spot

5.4. Discussion

5.4.1. Selection of the dominant factors influencing grazing

Biotic and abiotic factors affect the spatial and temporal patterns of livestock behavior and land use (Schoenbaum et al., 2017). The geodata afforded several mapping products, which described the main factors that appeared to be drivers of the grazing

locations in this study, i.e., aspect and slope, CHM (vegetation height), and the LU/LC map. Therefore, other factors did not show a clear pattern and were discarded. For example, a preliminary analysis of the grazing locations indicated no clear relationship with water bodies (mainly small creeks and pools). Direct observations in the 09-10 monitoring period indicated that, in general, ewes did not exhibit an active search for water sources. Therefore, the "water" factor was excluded. In addition, no artificial boundaries (except the main road) existed in the study area; thus, there were no limits to the flock movement.

5.4.2. Effect of vegetation height

Sheep always graze close to ground level, and studies have found an inverse relationship between sheep grazing preferences and vegetation cover height (Schieltz et al., 2017). Even though the trees and shrubs in the "dehesa" provide shelter from the heat and other adverse weather conditions, ewes demonstrated a preference for other areas to feed. Glimp & Swanson (1994) demonstrated that sheep are reluctant to go into areas with dense vegetation and vegetation higher than their line of sight. Furthermore, studies have shown that pastures that grow under mature tree canopies have a lower nutritional value (Percival & Knowles, 1983).

5.4.3. Effect of LU/LC

The strong predilection of sheep for grasslands, which are areas where the herbaceous layer predominates, supports the results from the CHM model, which indicated the preference of the ewes for pastures and grasslands for grazing. However, those preferences might be contradicted by the long-held common belief that sheep eat all types of vegetation (and on any slope) if food is in short supply. At those times, their diet can consist of 80% leaves from shrubs and woody vegetation above one m in height (Fernández-Carmona et al., 2017). Our study has shown that if sheep choose where to graze, they will always choose grasslands and pastures and the shrub layer to a lesser extent. In a study of the feeding habits of sheep and goats in Portugal (M. Castro & Fernández-Núñez, 2016), goats had significantly more tree and shrub species than sheep, and the sheep diet was 84% herbaceous plant species.

5.4.4. Effect of aspect

Probably, the apparent preference for north-facing lands is because, at the latitude of the study area, the conditions in these particular areas are the best for the growth of pastures with the best nutritional characteristics and highest density. Some authors (Nadal-Romero et al., 2014) have suggested that south-facing slopes tend to have less vegetation than do north-facing slopes because the former are subjected to greater water stress. North-facing areas in Mediterranean climates have higher humidity and, consequently, pastures have higher vigor and greenness. In addition, because north- and south-facing slopes differ in solar radiation and wind and rain patterns (mainly, from the northwest in winter), the former are cooler and wetter and, therefore, more productive (Golodets & Boeken, 2006). Furthermore, the sheep chose north-facing areas because the pastures probably have the highest nutritional quality and the thermal comfort provided by that aspect (Garcia-Gonzalez et al., 1990).

5.4.5. Effect of slope

Sheep can graze on almost any slope, but if the terrain is steep and rugged, the animals spend more time and energy moving to find suitable areas for grazing, which leaves less time for foraging (Vallentine, 2001). Therefore, it seems reasonable that, if sheep had no physical limitations and could move around freely, they would likely choose flat or nearly flat areas for grazing. In addition, if the herbage is plentiful and freely available, sheep will graze mainly on the lower slopes but, if the herbage is less abundant, sheep will also graze the steeper slopes (López et al., 2003). Other biotic or abiotic factors (e.g., soil properties, the content of mineral elements, or the nutritional quality of the pasture), rather than slope per se might influence the apparent preference of sheep for gentle slopes for grazing (Ganskopp & Vavra, 1987).

Although the 18-20 flock did not show a marked preference for the 2-4% slopes as did the 09-10 flock, nearly 65% of the records were from slopes < 6%, reflecting the sheep's preference for gentle slopes. Apparently, sheep, where possible, select gentle slopes for grazing rather than steeper areas, where the grasses tend to be less nutritious and less palatable to the animals (Garcia-Gonzalez et al., 1990; Aldezabal et al., 1999).

5.4.6. Analysis of spatial distribution

The directional distribution mirrored the relief model, adapting its orientation to the contours. That is, when the sheep move and graze freely, they choose areas where they can move and graze more easily. In short, the analysis of the spatial patterns of the HS indicated that the flock had a clear preference for areas that had slopes between 2% and 4% and northern aspects, which was the same for the entire study area.

5.5. Conclusions

The large exodus of humans from rural to urban areas and the intensification of production systems diminished traditional grazing practices and, consequently, led to the loss of traditional knowledge about livestock behavior while grazing. Shepherds know that grazing animals' behavior is not random and depends on terrain and food factors. However, this insight acquired through patient and lengthy contact with the animals is about to get loss.

In this work, conducted in the community pastures in Fariza, Spain, it was shown that the spatial distribution of grazing Churra sheep was non-random because the animals seem to develop common behavioral patterns. Particularly, vegetation height, LU/LC class, and slope and aspect had the most effect on the location of sheep grazing. When grazing, ewes showed strong preferences for areas that had gentle, north-facing slopes, open spaces away from scrublands and trees, and herbaceous layers of grasses. That choice appeared deliberate because it was proven in two independent study periods of two flocks that were evaluated based on different statistical approaches. In short, sheep choose the grazing areas that offer the freshest and most nutritional quality food.

GPS devices for monitoring livestock coupled with remote sensing techniques, particularly LiDAR, have been suggested as very powerful tools to quantify the environmental characteristics and explain the spatial patterns of the livestock freely grazing within it. Beyond the animal's nature, those patterns are influenced by external abiotic (slope and aspect) and biotic (predominant vegetation, plant stratification, height of vegetation, and land use) factors. In this study, terrain characteristics, namely slope, aspect, vegetation height, and LU/LC maps, were retrieved from the LiDAR and imagery datasets. Geotechnologies are not intended to replace traditional pastoralism. Still, they

have become an additional resource in decision-making in extensive livestock farming. They support the traditional observations made by farmers and shepherds, therefore paving the way to new management forms of grazing spaces. This fact is beneficial given the decline of traditional practices, which are much more respectful with the rural areas but more difficult to maintain nowadays.

Capítulo 6. Conclusiones y líneas futuras de investigación

Capítulo 6. Conclusiones y líneas futuras de investigación

Esta tesis doctoral se ha focalizado en proponer nuevas estrategias metodológicas de ámbito geotecnológico que pudiesen contribuir de forma relevante y sostenible a tecnificar el sector agroganadero, para así hacer frente a la gran demanda actual y futura de productos del sector primario. En este capítulo se exponen integradamente las conclusiones que se han alcanzado a partir de las investigaciones realizadas para la elaboración de la tesis. Posteriormente, con los objetivos planteados cumplidos satisfactoriamente, se mencionan las potenciales líneas futuras de investigación que han ido surgiendo durante el desarrollo del trabajo planteado.

6.1. Conclusiones

Las geotecnologías han demostrado ser potentes herramientas alternativas al servicio de un sector agroganadero que, en la era en la que estamos inmersos, requiere una drástica modernización. Su complementariedad con los conocimientos tradicionales adquiere un carácter sinérgico, puesto que han contribuido a mejorar notablemente la gestión integrada (económica, medioambiental y desde el punto de vista del bienestar animal) de un amplio abanico de actividades desarrolladas en los actuales sistemas agropecuarios. En definitiva, las geotecnologías podrán contribuir a que agricultores y ganaderos vean aumentados sus rendimientos productivos, y por ende sus beneficios económicos, sin minorar la sostenibilidad medioambiental y el bienestar animal. Como valor añadido, el uso de estas tecnologías no solo ha permitido mejorar lo presente sino ahondar en lo futuro, posibilitando el aprendizaje de nuevos conocimientos agrícolas y ganaderos que, unidos a los tradicionales, conformarán los cimientos de los nuevos sistemas de manejo que harán frente a la creciente demanda alimentaria.

Mediante esta contribución científica se ha pretendido poner de manifiesto la idoneidad de una serie de procedimientos y herramientas, fundamentalmente del ámbito de la teledetección, en su aplicación en el sector agroganadero. Se han presentado tres aplicaciones de muy diversa índole, aunque podrían plantearse muchas más, ya que no sólo es un campo de investigación imparable en la actualidad, sino que prácticamente ya está operativo en muchos aspectos de la gestión agrícola y ganadera.

Se ha demostrado la gran utilidad de los sensores aerotransportados como fuente de información de los cultivos agrícolas. Estos dispositivos han permitido monitorizar los cultivos a lo largo de su ciclo de crecimiento, predecir diversos parámetros agronómicos en cualquier momento del ciclo y determinar el nivel de afectación de la cobertura vegetal provocado por una plaga. Toda esa información es de gran relevancia en el proceso de toma de decisiones del agricultor, quién podrá ajustar los insumos necesarios de una forma mucho más coste-efectiva y podrá tomar las medidas pertinentes para combatir dicha plaga y paliar los daños sufridos.

Particularmente, se demostró que los índices espectrales de vegetación VNIR derivados del procesamiento de imágenes multiespectrales aerotransportadas captadas con drones, podrían ofrecer una alternativa eficaz y asequible a los laboriosos muestreos de campo para el seguimiento de distintas asociaciones forrajeras. La combinación de esta metodología con un modelo estadístico predictivo (PLS) mostró una alta fiabilidad (> 50%) para predecir diversos parámetros agronómicos de los cultivos forrajeros en cualquier momento de su ciclo de crecimiento. En general, se detectó una fuerte relación de dependencia lineal entre las variables explicativas (estimaciones de campo) y las variables observadas (índices espectrales), con una notable capacidad de predicción.

Del mismo modo, empleando de nuevo simultáneamente drones e imágenes multiespectrales, se consiguió desarrollar con éxito una alternativa metodológica para evaluar con precisión el impacto del topillo campesino (*Microtus arvalis*) en un ambiente concreto de alfalfar, demostrando ser un procedimiento efectivo y fácilmente transferible. La combinación de estas técnicas con las mediciones de campo de la actividad de los topillos, como el número de huras activas, reveló las fluctuaciones reales de la población de topillos. Esta metodología podrá servir de ayuda tanto a los agricultores como a los organismos competentes en gestión de plagas, puesto que actualmente no disponen de medios y procedimientos para determinar con precisión el impacto de los topillos en sus campos de cultivo. En general, los cuatro procedimientos de clasificación multiespectral estudiados mostraron resultados y precisiones similares, si bien es cierto que el método de segmentación del NDVI resultó ser el que mostró la afectación real con mayor precisión y fiabilidad, con la ventaja añadida de una mayor sencillez computacional y de cálculo. No obstante, en todos los casos, se encontró una relación significativa entre la

actividad de los topillos (medida en términos de número de huras situadas en colonias activas) y el daño observado en la cobertura vegetal de alfalfa.

Respecto a la rama ganadera, se ha demostrado que los dispositivos GPS utilizados para la monitorización de los rebaños, junto con técnicas de teledetección, como los datos LiDAR y las ortofotografías del espectro VNIR, se han postulado como herramientas muy potentes, tanto para cuantificar las características del entorno como para explicar los patrones de distribución espacial de las ovejas en libre pastoreo. Más allá de la naturaleza del animal, esos patrones de conducta están influidos por factores abióticos (pendiente y su orientación) y bióticos (vegetación predominante, estratificación vegetal, altura de la vegetación y uso del suelo). En concreto, en la investigación desarrollada, se encontró que la distribución espacial de los dos rebaños de ovejas churras estudiados no se basaba en la arbitrariedad, sino que los animales desarrollaron patrones habituales de comportamiento durante el pastoreo. Estos animales mostraron claras preferencias por áreas abiertas sin exceso de matorral y arbolado que dificultase su visibilidad, con pendientes suaves orientadas al norte y en las que, además, predominase el estrato herbáceo formado por especies pratenses. En definitiva, las ovejas eligieron deliberadamente zonas de pastoreo que ofreciese los pastos más frescos y con mayor calidad nutricional, junto con mayor facilidad de movimiento.

Como corolario final, aplicable a todas las investigaciones realizadas en esta tesis doctoral, es necesario señalar que las geotecnologías no pretenden desbancar o sustituir los conocimientos agroganaderos tradicionales, puesto que son la base para poder interpretar la información y los resultados obtenidos por estos procedimientos más vanguardistas. Más bien todo lo contrario, deben ser tomadas como herramientas complementarias a dichos conocimientos, es decir, como un recurso adicional para fundamentar el proceso de toma de decisiones en aquellos sistemas agropecuarios sostenibles con el medio natural, como es el caso de la agricultura y la ganadería extensiva. Deben servir de apoyo a las observaciones tradicionales realizadas por agricultores y ganaderos, abriendo así un camino hacia nuevas formas de gestión de los espacios de cultivo y pastoreo, lo que redundará en beneficios económicos, sociales y medioambientales para el conjunto de la población mundial.

6.2. Líneas futuras de investigación

Las aportaciones metodológicas presentadas en esta tesis doctoral son tan solo una mera representación de la vasta aplicabilidad de las geotecnologías en la agricultura y en la ganadería. La conceptualización de esta tesis y el planteamiento de sus objetivos han permitido desarrollar investigaciones de las que nacieron a su vez muchos interrogantes, abriendo la puerta a vías de trabajo futuras:

- En el caso de las asociaciones forrajeras, un aspecto muy provechoso consistiría en explotar aún más la fuerte relación de dependencia encontrada entre las mediciones de campo de parámetros agronómicos y los índices espectrales de vegetación. Es posible que dicha relación pueda dar lugar a predicciones fiables de otros parámetros de gran relevancia como el contenido en clorofila, altura o el rendimiento productivo potencial. Estas tres variables no fueron incluidas en el trabajo inicial; las dos primeras porque se observaron a escala de especie y no de asociación; y la tercera porque se ha considerado que merece una investigación independiente, dada su complejidad e interés. Actualmente, se están realizando algunas estimaciones preliminares respecto a este último, mediante las que se ha podido determinar que las mayores correlaciones entre mediciones de campo e índices espectrales, y, por tanto, el mayor poder predictivo del modelo estadístico, tiene lugar en la fecha del 2 de mayo de 2020. En dicho momento, las correlaciones espaciales de los índices con el mapa de cosecha real mostraron altos valores absolutos y alto nivel de significación, especialmente en el peso húmedo y en la cantidad de agua expresada en peso. En otras palabras: los índices espectrales tomados en esa fecha significativa pueden proporcionar una estimación de la futura cosecha. Esta caracterización y modelización predictiva está aplicada a cultivos forrajeros, sin embargo, la metodología seguida podría extrapolarse para todos aquellos cultivos cuyas producciones se basen en la cantidad de biomasa vegetal.
- Cabe también la posibilidad de utilizar estos índices de vegetación para calcular los coeficientes de cultivo necesarios, por ejemplo, para el cálculo

del balance hídrico de los cultivos. Este balance permite establecer la ratio consumo de agua/producción, consiguiendo evaluar qué asociación, con menor consumo, produce igual o más biomasa. Además, los coeficientes de cultivo apenas han sido considerados para asociaciones vegetales, ya que se tabulan para especies concretas.

- Dada la novedad inherente al procedimiento de utilización de sistemas remotos para la observación y cuantificación de impactos del topillo campesino, durante la investigación se plantearon varias líneas futuras de trabajo. En una de ellas, se propone abordar la detección y conteo de huras de topillo de manera automatizada en una superficie conocida. Las metodologías que se plantean para la consecución de este fin se basan bien en el uso de distintos algoritmos de clasificación multiespectral orientada a objetos o bien en el reconocimiento de patrones espaciales mediante técnicas encuadradas en el campo del llamado *Deep Learning*. No obstante, es necesario tener un gran control geométrico de las tomas y adquirir imágenes a una altísima resolución espacial (por debajo del cm), lo que es un reto para los drones convencionales y los actuales sistemas de geolocalización. Conseguir este objetivo significaría poder estimar la abundancia poblacional de topillo en una zona y momento concreto. Las actuales incursiones científicas en esta línea se plantean para animales e indicios de mayor envergadura, y sería de gran novedad explorar su aplicabilidad para el caso del topillo. Estos resultados podrían llegar a ser de vital importancia para tomar las acciones preventivas pertinentes para minimizar los daños, más aún en caso de que los datos sean indicativos de una probable explosión demográfica en un futuro cercano.
- El gran potencial encontrado en los datos LiDAR el en ámbito agroganadero sugirió futuras cuestiones de interés. Actualmente, existen en el mercado dispositivos LiDAR con una gran densidad de puntos y de alta precisión que pueden ser portados por un dron. Esta posibilidad dio lugar un planteamiento alternativo para la detección de huras de topillo campesino mencionada en el punto anterior. La hipótesis que se plantea es que quizá la acumulación de tierra en la boca de las huras forme un micro

relieve que podría ser más fácilmente detectable por el dispositivo LiDAR, en lugar de tratar de contabilizar las huras mediante un reconocimiento de patrones espaciales basado en la reflectividad. Puede que también sea posible utilizar ese dispositivo LiDAR para calcular con una alta precisión la altura de los cultivos forrajeros y estimar así el rendimiento productivo potencial en un momento del ciclo de crecimiento dado.

- En vista del potencial de las geolocalizaciones registradas por dispositivos GPS para el estudio del comportamiento de los pequeños rumiantes en sistemas de libre pastoreo, se ha propuesto profundizar más al respecto. Se ha decidido partir de la hipótesis de que dichos patrones de comportamiento no solamente son deliberados y están exentos de arbitrariedad, sino que vienen regidos por un modelo de ritmos circadianos inherentes a la propia naturaleza de los animales. Se considera que dicha modelización circadiana puede extraerse de la actividad registrada por los mismos dispositivos GPS, utilizando su información temporal. Este es un aspecto en el que se está trabajando a día de hoy.

Referencias

Referencias

Abdel-Rahman, E. M., Mutanga, O., Odindi, J., Adam, E., Odindo, A., & Ismail, R. (2014). A comparison of partial least squares (PLS) and sparse PLS regressions for predicting yield of Swiss chard grown under different irrigation water sources using hyperspectral data. *Computers and Electronics in Agriculture*, *106*, 11–19. https://doi.org/10.1016/j.compag.2014.05.001

Abdelkader, M. M. M., Puchkov, M., & Loktionova, E. (2019). Applying a digital method for measuring leaf area index of tomato plants. *Proceedings of the International Scientific and Practical Conference "Digital Agriculture - Development Strategy" ({ISPC} 2019)*, 5–8. https://doi.org/10.2991/ispc-19.2019.2

Abdi, H. (2010). Partial least squares regression and projection on latent structure regression (PLS Regression). *WIREs Computational Statistics*, *2*(1), 97–106. https://doi.org/10.1002/wics.51

Abràmoff, M. D., Magalhães, P. J., & Ram, S. J. (2004). Image processing with ImageJ. *Biophotonics International*, *11*(7), 36–42.

Adams, A., Jumpah, E. T., & Caesar, L. D. (2021). The nexuses between technology adoption and socioeconomic changes among farmers. *Technological Forecasting and Social Change*, *173*, 121133. https://doi.org/10.1016/J.TECHFORE.2021.121133

Addink, E. A., De Jong, S. M., Davis, S. A., Dubyanskiy, V., Burdelov, L. A., & Leirs, H. (2010). The use of high-resolution remote sensing for plague surveillance in Kazakhstan. *Remote Sensing of Environment*, *114*, 674–681. https://doi.org/10.1016/j.rse.2009.11.015

Agencia Estatal de Meteorología (AEMET). (2021). *Informe mensual climatológico. Enero 2021*. http://www.aemet.es/es/serviciosclimaticos/vigilancia_clima/resumenes

Aldezabal, A., Garin, I., & Garcia-González, R. (1999). Activity rhythms and the influence of some environmental variables on summer ungulate behaviour in ordesa-

monte perdido national park. *Pirineos*, *145*(153–154), 145–156. https://doi.org/10.3989/pirineos.1999.v153-154.110

Alves, W. dos S., Martins, A. P., Pôssa, É. M., Borges de Moura, D. M., Morais, W. A., Ferreira, R. S., & Silva dos Santos, L. N. (2021). Geotechnologies applied in the analysis of land use and land cover (LULC) transition in a hydrographic basin in the Brazilian Cerrado. *Remote Sensing Applications: Society and Environment*, *22*, 100495. https://doi.org/10.1016/J.RSASE.2021.100495

Anderson, J. R., Hardy, E. E., Roach, J. T., & Witmer, R. E. (1976). *A land use and land cover classification system for use with remote sensor data* (United States Government Print Offices (ed.); 1st Editio).

Arnold, G. W., & Dudzinski, M. L. (1978). *Ethology of free ranging domestic animals*. Elsevier Scientific Publishers.

Baccini, A., Goetz, S. J., Walker, W. S., Laporte, N. T., Sun, M., Sulla-Menashe, D., Hackler, J., Beck, P. S. A., Dubayah, R., Friedl, M. A., Samanta, S., & Houghton, R. A. (2012). Estimated carbon dioxide emissions from tropical deforestation improved by carbon-density maps. *Nature Climate Change*, *2*(3), 182–185. https://doi.org/10.1038/nclimate1354

Bacsa, C. M., Martorillas, R. M., Balicanta, L. P., & Tamondong, A. M. (2019). Correlation of UAV-based multispectral vegetation indices and leaf color chart observations for nitrogen concentration assesment on rice crops. *The International Archives of the Photogrammetry, Remote Sensing and Spatial Information Sciences*, *XLII-4-W19*, 31–38. https://doi.org/10.5194/isprs-archives-XLII-4-W19-31-2019

Bannari, A., Morin, D., Bonn, F., & Huete, A. R. (1995). A review of vegetation indices. *Remote Sensing Reviews*, *13*(1–2), 95–120. https://doi.org/10.1080/02757259509532298

Barbosa, B. D. S., Ferraz, G. a. S., Gonçalves, L. M., Marin, D. B., Maciel, D. T., Ferraz, P. F. P., & Rossi, G. (2019). RGB vegetation indices applied to grass monitoring: a qualitative analysis. *Agronomy Research*, *17*(2), 349–357. https://doi.org/10.15159/ar.19.119

Barnas, A. F., Darby, B. J., Vandeberg, G. S., Rockwell, R. F., & Ellis-Felege, S. N. (2019). A comparison of drone imagery and ground-based methods for estimating the extent of habitat destruction by lesser snow geese (Anser caerulescens caerulescens) in La Pérouse Bay. *PLOS ONE*, *14*(8), e0217049. https://doi.org/10.1371/JOURNAL.PONE.0217049

Barnsley, M. J., Lewis, P., O'Dwyer, S., Disney, M. I., Hobson, P., Cutter, M., & Lobb, D. (2000). On the potential of CHRIS/PROBA for estimating vegetation canopy properties from space. *Remote Sensing Reviews*, *19*(1–4), 171–189. https://doi.org/10.1080/02757250009532417

Becker-Reshef, I., Vermote, E., Lindeman, M., & Justice, C. (2010). A generalized regression-based model for forecasting winter wheat yields in Kansas and Ukraine using MODIS data. *Remote Sensing of Environment*, *114*(6), 1312–1323. https://doi.org/10.1016/j.rse.2010.01.010

Bendig, J., Yu, K., Aasen, H., Bolten, A., Bennertz, S., Broscheit, J., Gnyp, M. L., & Bareth, G. (2015). Combining UAV-based plant height from crop surface models, visible, and near infrared vegetation indices for biomass monitoring in barley. *International Journal of Applied Earth Observation and Geoinformation*, *39*, 79–87. https://doi.org/10.1016/j.jag.2015.02.012

Benz, U. C., Hofmann, P., Willhauck, G., Lingenfelder, I., & Heynen, M. (2004). Multi-resolution, object-oriented fuzzy analysis of remote sensing data for GIS-ready information. *ISPRS Journal of Photogrammetry and Remote Sensing*, *58*(3–4), 239–258. https://doi.org/10.1016/J.ISPRSJPRS.2003.10.002

Bertolozzi-Caredio, D., Garrido, A., Soriano, B., & Bardaji, I. (2021). Implications of alternative farm management patterns to promote resilience in extensive sheep farming. A Spanish case study. *Journal of Rural Studies*, *86*, 633–644. https://doi.org/10.1016/J.JRURSTUD.2021.08.007

Bolfe, É. L. (2019). Application of geotechnologies in the development of sustainable agriculture in Brazil. *International Journal of Advanced Engineering Research and Science*, *6*(12), 458–463. https://doi.org/10.22161/IJAERS.612.53

Booth, D. T., Cox, S. E., Fifield, C., Phillips, M., & Willlamson, N. (2005). Image

analysis compared with other methods for measuring ground cover. *Arid Land Research and Management*, *19*(2), 91–100. https://doi.org/10.1080/15324980590916486

Breiman, L. (2001). Random Forests. *Machine Learning*, *45*(1), 5–32. https://doi.org/10.1023/A:1010933404324

Breiman, L., Friedman, J. H., Olshen, R. A., & Stone, C. J. (2017). Classification and regression trees. In L. Breiman, J. H. Friedman, R. A. Olshen, & C. J. Stone (Eds.), *Classification and Regression Trees*. Routledge. https://doi.org/10.1201/9781315139470/CLASSIFICATION-REGRESSION-TREES-LEO-BREIMAN-JEROME-FRIEDMAN-RICHARD-OLSHEN-CHARLES-STONE

Calera, A., González-Piqueras, J., & Melia, J. (2004). Monitoring barley and corn growth from remote sensing data at field scale. *International Journal of Remote Sensing*, *25*(1), 97–109. https://doi.org/10.1080/0143116031000115319

Calera, A., Martínez, C., & Melia, J. (2001). A procedure for obtaining green plant cover: Relation to NDVI in a case study for barley. *International Journal of Remote Sensing*, *22*(17), 3357–3362. https://doi.org/10.1080/01431160010020100

Castro, M., & Fernández-Núñez, E. (2016). Seasonal grazing of goats and sheep on Mediterranean mountain rangelands of northeast Portugal. *Livestock Research for Rural Develpment*, *28*(5). http://www.lrrd.org/lrrd28/5/cast28091.html

Castro, W., Junior, J. M., Polidoro, C., Osco, L. P., Gonçalves, W., Rodrigues, L., Santos, M., Jank, L., Barrios, S., Valle, C., Simeão, R., Carromeu, C., Silveira, E., Jorge, L. A. de C., & Matsubara, E. (2020). Deep learning applied to phenotyping of biomass in forages with uav-based rgb imagery. In *Sensors* (Vol. 20, Issue 17, pp. 1–18). https://doi.org/10.3390/s20174802

Chandel, A. K., Khot, L. R., & Yu, L.-X. (2021). Alfalfa (Medicago sativa L.) crop vigor and yield characterization using high-resolution aerial multispectral and thermal infrared imaging technique. *Computers and Electronics in Agriculture*, *182*(3), 105999. https://doi.org/10.1016/j.compag.2021.105999

Chang, A., Jung, J., Maeda, M. M., & Landivar, J. (2017). Crop height monitoring with digital imagery from Unmanned Aerial System (UAS). *Computers and Electronics in Agriculture*, *141*, 232–237. https://doi.org/10.1016/j.compag.2017.07.008

Chen, Q., Vaglio Laurin, G., Battles, J. J., & Saah, D. (2012). Integration of airborne lidar and vegetation types derived from aerial photography for mapping aboveground live biomass. *Remote Sensing of Environment*, *121*, 108–117. https://doi.org/10.1016/j.rse.2012.01.021

Clark, D., Litherland, A., Mata, G., & Burling-Claridge, R. (2009). Pasture monitoring from space. *Proceedings of the South Island Dairy Event*, 108–123. http://side.org.nz/IM_Custom/ContentStore/Assets/7/74/58d8ae4353832551a174e54bd2c826f9/Satellite grass monitoring.pdf

Dammer, K. H., Intreß, J., Bzowska-Bakalarz, M., & Schirrmann, M. (2018). Identification of field mouse (Microtus spp.) infestation from UAV areal images in a winter wheat field. *Gesunde Pflanzen*, *70*(2), 57–64. https://doi.org/10.1007/s10343-018-0417-0

de Castro, A. I., Shi, Y., Maja, J. M., & Peña, J. M. (2021). UAVs for vegetation monitoring: overview and recent scientific contributions. *Remote Sensing*, *13*(11), 2139. https://doi.org/10.3390/RS13112139

Dronova, I., Gong, P., & Wang, L. (2011). Object-based analysis and change detection of major wetland cover types and their classification uncertainty during the low water period at Poyang Lake, China. *Remote Sensing of Environment*, *115*(12), 3220–3236. https://doi.org/10.1016/J.RSE.2011.07.006

Drucker, H., Burges, C. J. C., Kaufman, L., Smola, A., & Vapnik, V. (2003). Support vector regression machines. *Advances in Neural Information Processing Systems 9*, 155–161.

Du, L., Shi, S., Yang, J., Sun, J., & Gong, W. (2016). Using different regression methods to estimate leaf nitrogen content in rice by fusing hyperspectral LiDAR data and laser-induced chlorophyll fluorescence data. *Remote Sensing*, *8*(6), 526. https://doi.org/10.3390/rs8060526

Erler, A., Riebe, D., Beitz, T., Löhmannsröben, H.-G., & Gebbers, R. (2020). Soil nutrient detection for precision agriculture using handheld laser-induced breakdown spectroscopy (LIBS) and multivariate regression methods (PLSR, Lasso and GPR). *Sensors*, *20*(2), 418. https://doi.org/10.3390/s20020418

Escribano, A. J. (2019). The dehesa system for livestock production. Evolution, conservation issues and livestock planning for sustainability. In V. R. Squires & W. L. Bryden (Eds.), *Livestock: Production, Management Strategies and Challenges*. NOVA.

Escribano, Elghannam, A., & Mesias, F. J. (2020). Dairy sheep farms in semi-arid rangelands: A carbon footprint dilemma between intensification and land-based grazing. *Land Use Policy*, *95*, 104600. https://doi.org/10.1016/J.LANDUSEPOL.2020.104600

Eskandari, H., Ghanbari, A., & Javanmard, A. (2009). Intercropping of cereals and legumes for forage production. *Notulae Scientia Biologicae*, *1*(1), 07–13. https://doi.org/10.15835/nsb113479

Ezzy, H., Charter, M., Bonfante, A., & Brook, A. (2021). How the small object detection via machine learning and UAS-based remote-sensing imagery can support the achievement of SDG2: A case study of vole burrows. *Remote Sensing*, *13*(16), 3191. https://doi.org/10.3390/RS13163191

Fernández-Carmona, J., Blas Ferrer, E., Cervera Fras, C., Fernández Martínez, C., Jóver Cerdá, M., & Pascual Amorós, J. (2017). *Datos sobre conducta y bienestar de animales en granja [Data on farm animal behaviour and welfare]* (J. Fernández Carmona (ed.)). Polytechnic University of Valencia.

Fingas, M. F., & Brown, C. E. (1997). Review of oil spill remote sensing. *Spill Science & Technology Bulletin*, *4*(4), 199–208. https://doi.org/10.1016/S1353-2561(98)00023-1

Food and Agriculture Organization of the United Nations (FAO). (2004). *National forest inventory. Field manual. Template* (Forestry D). http://www.fao.org/3/a-ae578e.pdf

Foody, G. M. (2002). Status of land cover classification accuracy assessment. *Remote*

Sensing of Environment, *80*(1), 185–201. https://doi.org/10.1016/S0034-4257(01)00295-4

Fu, Z., Jiang, J., Gao, Y., Krienke, B., Wang, M., Zhong, K., Cao, Q., Tian, Y., Zhu, Y., Cao, W., & Liu, X. (2020). Wheat growth monitoring and yield estimation based on multi-rotor unmanned aerial vehicle. *Remote Sensing*, *12*(3), 508. https://doi.org/10.3390/rs12030508

Gamon, J. A., Field, C. B., Goulden, M. L., Griffin, K. L., Hartley, A. E., Joel, G., Peñuelas, J., & Valentini, R. (1995). Relationships between NDVI, canopy structure, and photosynthesis in three californian vegetation types. *Ecological Applications*, *5*(1), 28–41. https://doi.org/10.2307/1942049

Ganskopp, D. (2001). Manipulating cattle distribution with salt and water in large arid-land pastures: a GPS/GIS assessment. *Applied Animal Behaviour Science*, *73*(4), 251–262. https://doi.org/10.1016/S0168-1591(01)00148-4

Ganskopp, D., & Vavra, M. (1987). Slope use by cattle, feral horses, deer, and bighorn shee. *Northwest Science*, *61*(2), 74–81. https://www.researchgate.net/publication/279554402_Slope_use_by_cattle_feral_horses_deer_and_bighorn_sheep

García-Estévez, I., Quijada-Morín, N., Rivas-Gonzalo, J. C., Martínez-Fernández, J., Sánchez, N., Herrero-Jiménez, C. M., & Escribano-Bailón, M. T. (2017). Relationship between hyperspectral indices, agronomic parameters and phenolic composition of Vitis vinifera cv Tempranillo grapes: Hyperspectral indices, agronomic parameters and phenolic composition of V. vinifera. *Journal of the Science of Food and Agriculture*, *97*(12), 4066–4074. https://doi.org/10.1002/jsfa.8366

Garcia-Gonzalez, R., Hidalgo, R., & Montserrat, C. (1990). Patterns of livestock use in time and space in the summer ranges of the Western Pyrenees: a case study in the Aragon Valley. *Mountain Research & Development*, *10*(3), 241–255. https://doi.org/10.2307/3673604

Ghanbari-Bonjar, A., & Lee, H. C. (2003). Intercropped wheat (Triticum aestivum L.) and bean (Vicia faba L.) as a whole-crop forage: Effect of harvest time on forage

yield and quality. *Grass and Forage Science*, *58*(1), 28–36. https://doi.org/10.1046/j.1365-2494.2003.00348.x

Ghosh, A., Fassnacht, F. E., Joshi, P. K., & Kochb, B. (2014). A framework for mapping tree species combining hyperspectral and LiDAR data: Role of selected classifiers and sensor across three spatial scales. *International Journal of Applied Earth Observation and Geoinformation*, *26*, 49–63. https://doi.org/10.1016/j.jag.2013.05.017

Giraudoux, P., Villette, P., Quéré, J.-P., Damange, J.-P., & Delattre, P. (2019). Weather influences M. arvalis reproduction but not population dynamics in a 17-year time series. *Scientific Reports*, *9*(1), 1–11. https://doi.org/10.1038/s41598-019-50438-z

Glenn, E. P., Huete, A. R., Nagler, P. L., & Nelson, S. G. (2008). Relationship between remotely-sensed vegetation indices, canopy attributes and plant physiological processes: What vegetation indices can and cannot tell us about the landscape. *Sensors*, *8*(4), 2136–2160. https://doi.org/10.3390/S8042136

Glimp, H. A., & Swanson, S. (1994). Sheep grazing and riparian and watershed management. *Sheep Research Journal*, *Special Issue*, 65–71. http://d1cqrq366w3ike.cloudfront.net/http/DOCUMENT/SheepUSA/SGRJGrazing65-71Hudson1994.pdf

Golodets, C., & Boeken, B. (2006). Moderate sheep grazing in semiarid shrubland alters small-scale soil surface structure and patch properties. *Catena*, *65*(3), 285–291. https://doi.org/10.1016/j.catena.2005.12.005

Guan, J., & Nutter, F. W. (2003). Relationships between defoliation, leaf area index, canopy reflectance, and forage yield in the alfalfa-leaf spot pathosystem. *Computers and Electronics in Agriculture*, *37*(1–3), 97–112. https://doi.org/10.1016/S0168-1699(02)00113-8

Gutierrez, M., Escalante-Estrada, J. A., & Rodriguez-Gonzalez, M. T. (2005). Canopy reflectance, stomatal conductance, and yield of Phaseolus vulgaris L. and Phaseolus coccinues L. under saline field conditions. *International Journal of Agriculture and Biology*, *7*(3), 491–494.

Handcock, R. N., Swain, D. L., Bishop-Hurley, G. J., Patison, K. P., Wark, T., Valencia, P., Corke, P., & O'Neill, C. J. (2009). Monitoring animal behaviour and environmental interactions using wireless sensor networks, GPS collars and satellite remote sensing. *Sensors*, *9*(5), 3586–3603. https://doi.org/10.3390/s90503586

Harris, N. R., Johnson, D. E., George, M. R., & Mcdougald, N. K. (2002). The effect of topography, vegetation, and weather on cattle distribution at the San Joaquin experimental range, California. *Fifth Symposium on Oak Woodlands: Oaks in California's Challenging Landscape, 8515*, 53–63.

Hauggaard-Nielsen, H., & Jensen, E. S. (2001). Evaluating pea and barley cultivars for complementarity in intercropping at different levels of soil N availability. *Field Crops Research*, *72*(3), 185–196. https://doi.org/10.1016/S0378-4290(01)00176-9

Hearst, M. A., Dumais, S., Osman, E., Platt, J., & Schölkopf, B. (1998). Support vector machines. *IEEE Intelligent Systems and Their Applications*, *13*(4), 18–28. https://doi.org/10.1109/5254.708428

Helfer, G. A., Victória-Barbosa, J. L., Santos, R. dos, & da Costa, A. Ben. (2020). A computational model for soil fertility prediction in ubiquitous agriculture. *Computers and Electronics in Agriculture*, *175*, 105602. https://doi.org/10.1016/j.compag.2020.105602

Heroldová, M., Šipoš, J., Suchomel, J., & Zejda, J. (2021). Influence of crop type on common vole abundance in Central European agroecosystems. *Agriculture, Ecosystems & Environment*, *315*, 107443. https://doi.org/10.1016/J.AGEE.2021.107443

Heroldová, M., & Tkadlec, E. (2011). Harvesting behaviour of three central European rodents: Identifying the rodent pest in cereals. *Crop Protection*, *30*(1), 82–84. https://doi.org/10.1016/J.CROPRO.2010.09.002

Herrera, O. (2018). *Comportamiento en pastoreo del ganado bovino criollo Argentino y aberdeen angus ecotipo Riojano, en pastizales naturales del chaco árido [Grazing behavior of Argentine Criollo and Aberdeen Angus cattle of the Riojano ecotype, in natural pastures of the ar*. Universidad Nacional del Mar de Plata.

Hollinger, S. E. (1997). Field monitoring of crop photosynthesis and respiration. *Better Crops with Plant Food*, *81*(3), 23–24.

Hulbert, I. A. R., French, J., Hulbert, I. A. N. A. R., & Frencht, J. (2019). The accuracy of GPS for wildlife telemetry and habitat mapping. *British Ecological Society*, *38*(4), 869–878.

Hunt, E. R., Cavigelli, M., Daughtry, C. S. T., Mcmurtrey, J. E., & Walthall, C. L. (2005). Evaluation of digital photography from model aircraft for remote sensing of crop biomass and nitrogen status. *Precision Agriculture*, *6*(4), 359–378. https://doi.org/10.1007/s11119-005-2324-5

Hunt, E. R., Doraiswamy, P. C., McMurtrey, J. E., Daughtry, C. S. T., Perry, E. M., & Akhmedov, B. (2013). A visible band index for remote sensing leaf chlorophyll content at the Canopy scale. *International Journal of Applied Earth Observation and Geoinformation*, *21*(1), 103–112. https://doi.org/10.1016/j.jag.2012.07.020

Inoue, Y. (2020). Satellite- and drone-based remote sensing of crops and soils for smart farming – a review. *Soil Science and Plant Nutrition*, *66*(6), 798–810. https://doi.org/10.1080/00380768.2020.1738899

Jackson, R. D. (1983). Spectral indices in N-Space. *Remote Sensing of Environment*, *13*(5), 409–421. https://doi.org/10.1016/0034-4257(83)90010-X

Jackson, T. J., Chen, D., Cosh, M., Li, F., Anderson, M., Walthall, C., Doriaswamy, P., & Hunt, E. R. (2004). Vegetation water content mapping using Landsat data derived normalized difference water index for corn and soybeans. *Remote Sensing of Environment*, *92*(4), 475–482. https://doi.org/10.1016/j.rse.2003.10.021

Jacob, J., & Tkadlec, E. (2010). Rodent outbreaks in Europe: dynamics and damage. In G. R. Singleton, S. Belmain, P. R. Brown, & B. Hardy (Eds.), *Rodent Outbreaks-Ecology and Impacts* (pp. 207–223). International Rice Research Institute.

Jannoura, R., Brinkmann, K., Uteau, D., Bruns, C., & Joergensen, R. G. (2015). Monitoring of crop biomass using true colour aerial photographs taken from a remote controlled hexacopter. *Biosystems Engineering*, *129*, 341–351. https://doi.org/10.1016/j.biosystemseng.2014.11.007

Janoušek, J., Jambor, V., Marcoň, P., Dohnal, P., Synková, H., & Fiala, P. (2021). Using UAV-based photogrammetry to obtain correlation between the vegetation indices and chemical analysis of agricultural crops. *Remote Sensing*, *13*(10), 1878. https://doi.org/10.3390/rs13101878

Jareño, D., Viñuela, J., Luque-Larena, J. J., Arroyo, L., Arroyo, B., & Mougeot, F. (2014). A comparison of methods for estimating common vole (Microtus arvalis) abundance in agricultural habitats. *Ecological Indicators*, *36*, 111–119. https://doi.org/10.1016/J.ECOLIND.2013.07.019

Jareño, D., Viñuela, J., Luque-Larena, J. J., Arroyo, L., Arroyo, B., & Mougeot, F. (2015). Factors associated with the colonization of agricultural areas by common voles Microtus arvalis in NW Spain. *Biological Invasions*, *17*(8), 2315–2327. https://doi.org/10.1007/s10530-015-0877-4

Jiang, Z., Huete, A. R., Chen, J., Chen, Y., Li, J., Yan, G., & Zhang, X. (2006). Analysis of NDVI and scaled difference vegetation index retrievals of vegetation fraction. *Remote Sensing of Environment*, *101*(3), 366–378. https://doi.org/10.1016/j.rse.2006.01.003

Juanes, F. (2018). Visual and acoustic sensors for early detection of biological invasions: Current uses and future potential. *Journal for Nature Conservation*, *42*, 7–11. https://doi.org/10.1016/j.jnc.2018.01.003

Kawamura, K., Ikeura, H., Phongchanmaixay, S., & Khanthavong, P. (2018). Canopy hyperspectral sensing of paddy fields at the booting stage and PLS regression can assess grain yield. *Remote Sensing*, *10*(8), 1249. https://doi.org/10.3390/rs10081249

Khan, Z., Rahimi-Eichi, V., Haefele, S., Garnett, T., & Miklavcic, S. J. (2018). Estimation of vegetation indices for high-throughput phenotyping of wheat using aerial imaging. *Plant Methods*, *14*(1), 20. https://doi.org/10.1186/s13007-018-0287-6

Krishnan, A., Williams, L. J., McIntosh, A. R., & Abdi, H. (2011). Partial Least Squares (PLS) methods for neuroimaging: a tutorial and review. *NeuroImage*, *56*(2), 455–475. https://doi.org/10.1016/j.neuroimage.2010.07.034

Launchbaugh, K. L., & Howery, L. D. (2005). Understanding landscape use patterns of

livestock as a consequence of foraging behavior. *Rangeland Ecology and Management*, *58*(2), 99–108. https://doi.org/10.2111/03-146.1

Li, P., Zheng, J., Ni, Y., Wu, J., Wumaier, W., Aihemaijiang, A., & Nasongcaoketu, S. (2016). Estimating area of grassland rodent damage rangeland and rat wastelands based on remote sensing in Altun mountain, Xinjiang, China. *Xinjiang Agricultural Sciences*, *53*(7), 1346–1355. https://doi.org/10.6048/j.issn.1001-4330.2016.07.023

Li, R., Zhang, Z., Tang, W., Huang, Y., Coulter, J. A., & Nan, Z. (2020). Common vetch cultivars improve yield of oat row intercropping on the Qinghai-Tibetan plateau by optimizing photosynthetic performance. *European Journal of Agronomy*, *117*, 126088. https://doi.org/10.1016/j.eja.2020.126088

Li, X., Lee, W. S., Li, M., Ehsani, R., Mishra, A. R., Yang, C., & Mangan, R. L. (2012). Spectral difference analysis and airborne imaging classification for citrus greening infected trees. *Computers and Electronics in Agriculture*, *83*, 32–46. https://doi.org/10.1016/j.compag.2012.01.010

Lillesand, T., Kiefer, R. W., & Chipman, J. (2015). *Remote sensing and image interpretation* (7th Editio). Wiley.

Lim, K., Treitz, P., Wulder, M., St-Onge, B., & Flood, M. (2003). LiDAR remote sensing of forest structure. *Progress in Physical Geography: Earth and Environment*, *27*(1), 88–106. https://doi.org/10.1191/0309133303pp360ra

Liro, A. (1974). Renewal of burrows by the common vole as the indicator of its numbers. *Acta Theriologica*, *19*, 259–272. https://doi.org/10.4098/at.arch.74-19

López, I. F., Hodgson, J., Hedderley, D. I., Valentine, I., & Lambert, M. G. (2003). Selective defoliation by sheep according to slope and plant species in the hill country of New Zealand. *Grass and Forage Science*, *58*(4), 339–349. https://doi.org/10.1046/j.1365-2494.2003.00386.x

Luque-Larena, J. J., Mougeot, F., Roig, D. V., Lambin, X., Rodríguez-Pastor, R., Rodríguez-Valín, E., Anda, P., & Escudero, R. (2015). Tularemia outbreaks and common vole (Microtus arvalis) irruptive population dynamics in Northwestern Spain, 1997-2014. *Vector-Borne and Zoonotic Diseases*, *15*(9), 568–570.

https://doi.org/10.1089/vbz.2015.1770

Luque-Larena, J. J., Mougeot, F., Viñuela, J., Jareño, D., Arroyo, L., Lambin, X., & Arroyo, B. (2013). Recent large-scale range expansion and outbreaks of the common vole (Microtus Arvalis) in NW Spain. *Basic and Applied Ecology*, *14*(5), 432–441. https://doi.org/10.1016/j.baae.2013.04.006

Lussem, U., Bolten, A., Gnyp, M. L., Jasper, J., & Bareth, G. (2018). Evaluation of RGB-based vegetation indices from UAV imagery to estimate forage yield in grassland. *ISPRS - International Archives of the Photogrammetry, Remote Sensing and Spatial Information Sciences*, *XLII–3*, 1215–1219. https://doi.org/10.5194/isprs-archives-XLII-3-1215-2018

Ma, D., Maki, H., Neeno, S., Zhang, L., Wang, L., & Jin, J. (2020). Application of non-linear partial least squares analysis on prediction of biomass of maize plants using hyperspectral images. *Biosystems Engineering*, *200*, 40–54. https://doi.org/10.1016/j.biosystemseng.2020.09.002

Maresma, A., Chamberlain, L., Tagarakis, A., Kharel, T., Godwin, G., Czymmek, K. J., Shields, E., & Ketterings, Q. M. (2020). Accuracy of NDVI-derived corn yield predictions is impacted by time of sensing. *Computers and Electronics in Agriculture*, *169*, 105236. https://doi.org/10.1016/j.compag.2020.105236

Martin, T. N., Marchese, J. A., de Sousa, A. K., Curti, G. L., Fogolari, H., & Dos Santos, V. (2013). Using the Imagej software to estimate leaf area in bean crop. *Interciencia*, *38*(12), 843–848.

Martínez-Casanovas, J. A. (2021, November). *Digitalización y trabajo agrícola automatizado en la próxima década*. Canales Sectoriales. Interempresas. https://www.interempresas.net/Grandes-cultivos/Articulos/358524-Digitalizacion-y-trabajo-agricola-automatizado-en-la-proxima-decada.html

Montes, J. M., Technow, F., Dhillon, B. S., Mauch, F., & Melchinger, A. E. (2011). High-throughput non-destructive biomass determination during early plant development in maize under field conditions. *Field Crops Research*, *121*(2), 268–273. https://doi.org/10.1016/j.fcr.2010.12.017

Mora-Delgado, J., Nelson, N., Fauchille, A., & Utsumi, S. (2016). Application of GPS and GIS to study foraging behavior of dairy cattle. *Agronomía Costarricense*, *40*(1), 81–88. https://doi.org/10.15517/rac.v40i1.25336

Morley, C. G., Broadley, J., Hartley, R., Herries, D., MacMorran, D., & McLean, I. G. (2017). The potential of using Unmanned Aerial Vehicles (UAVs) for precision pest control of possums (Trichosurus vulpecula). *Rethinking Ecology*, *2*, 27. https://doi.org/10.3897/RETHINKINGECOLOGY.2.14821

Motohka, T., Nasahara, K. N., Oguma, H., & Tsuchida, S. (2010). Applicability of green-red vegetation index for remote sensing of vegetation phenology. *Remote Sensing*, *2*(10), 2369–2387. https://doi.org/10.3390/rs2102369

Mougeot, F., Lambin, X., Arroyo, B., & Luque-Larena, J. J. (2020). Body size and habitat use of the common weasel Mustela nivalis vulgaris in Mediterranean farmlands colonised by common voles Microtus arvalis. *Mammal Research*, *65*(1), 75–84. https://doi.org/10.1007/s13364-019-00465-y

Mulla, D. J. (2013). Twenty five years of remote sensing in precision agriculture: Key advances and remaining knowledge gaps. *Biosystems Engineering*, *114*(4), 358–371. https://doi.org/10.1016/j.biosystemseng.2012.08.009

Nadal-Romero, E., Petrlic, K., Verachtert, E., Bochet, E., & Poesen, J. (2014). Effects of slope angle and aspect on plant cover and species richness in a humid Mediterranean badland. *Earth Surface Processes and Landforms*, *39*(13), 1705–1716. https://doi.org/10.1002/esp.3549

Nadeem, M., Ansar, M., Anwar, A., & Hussain, A. (2010). Performance of Winter Cereal-Legumes Fodder Mixtures and Their Pure Stand At Different Growth Stages Under Rainfed Conditions of Pothowar. *Journal of Agricultural Research*, *48*(2), 181–192.

Nar, P., Amin, S. S., Banerjee, S., Garg, V., & Pardasani, A. (2020). Autonomous multifunctional quadcopter for real-time object tracking and seed bombing in a dynamic environment. In B. Subramanian, S. Chen, & K. Reddy (Eds.), *Emerging Technologies for Agriculture and Environment* (pp. 199–211). Springer, Singapore. https://doi.org/10.1007/978-981-13-7968-0_15

Nguyen, H. T., Kim, J. H., Nguyen, A. T., Nguyen, L. T., Shin, J. C., & Lee, B.-W. (2006). Using canopy reflectance and partial least squares regression to calculate within-field statistical variation in crop growth and nitrogen status of rice. *Precision Agriculture*, *7*(4), 249–264. https://doi.org/10.1007/s11119-006-9010-0

Orloff, S. B. (1996). Methods to assess alfalfa forage quality in the field. *Proceedings of the 27th National Alfalfa Symposium*, 183–193.

Osborne, S. L., Schepers, J. S., Francis, D. D., & Schlemmer, M. R. (2002). Use of spectral radiance to estimate in-season biomass and grain yield in nitrogen- and water-stressed corn. *Crop Science*, *42*(1), 165–171. https://doi.org/10.2135/cropsci2002.1650

Pádua, L., Vanko, J., Hruška, J., Adão, T., Sousa, J. J., Peres, E., & Morais, R. (2017). UAS, sensors, and data processing in agroforestry: a review towards practical applications. *International Journal of Remote Sensing*, *38*(8–10), 2349–2391. https://doi.org/10.1080/01431161.2017.1297548

Pandey, V., Kiker, G. A., Campbell, K. L., Williams, M. J., & Coleman, S. W. (2009). GPS monitoring of cattle location near water features in South Florida. *Applied Engineering in Agriculture*, *25*(4), 551–562. https://doi.org/10.13031/2013.27465

Pearson, K. (1901). LIII. On lines and planes of closest fit to systems of points in space. *The London, Edinburgh, and Dublin Philosophical Magazine and Journal of Science*, *2*(11), 559–572. https://doi.org/10.1080/14786440109462720

Pearson, K. (1904). XIII. On the theory of contingency and its relation to association and normal correlation. *Drapers' Company Research Memoirs. Biometric Series. Mathematical Contributions to the Theory of Evolution.*, *1*, 46. https://archive.org/details/cu31924003064833/page/n1/mode/2up?view=theater

Percival, N. S., & Knowles, R. L. (1983). Combinations of Pinus radiata and pastoral agriculture in New Zealand hill country. In D. B. Hannawey (Ed.), *Foothill for Food and Forest* (pp. 185–202). Oregon State University.

Pereira, L. S., Paredes, P., Melton, F., Johnson, L., Wang, T., López-Urrea, R., Cancela, J. J., & Allen, R. G. (2020). Prediction of crop coefficients from fraction of ground

cover and height. Background and validation using ground and remote sensing data. *Agricultural Water Management*, *241*, 106197. https://doi.org/10.1016/j.agwat.2020.106197

Phiri, D., & Morgenroth, J. (2017). Developments in Landsat land cover classification methods: A review. *Remote Sensing*, *9*(9), 967. https://doi.org/10.3390/RS9090967

Pilaš, I., Gašparović, M., Novkinić, A., & Klobučar, D. (2020). Mapping of the canopy openings in mixed beech–fir forest at Sentinel-2 subpixel level using UAV and machine learning approach. *Remote Sensing*, *12*(23), 3925. https://doi.org/10.3390/RS12233925

Plaza, J., Criado, M., Sánchez, N., Pérez-Sánchez, R., Palacios, C., & Charfolé, F. (2021). UAV Multispectral Imaging Potential to Monitor and Predict Agronomic Characteristics of Different Forage Associations. *Agronomy*, *11*(9), 1697. https://doi.org/10.3390/AGRONOMY11091697

Pons, X., & Solé-Sugrañes, L. (1994). A simple radiometric correction model to improve automatic mapping of vegetation from multispectral satellite data. *Remote Sensing of Environment*, *48*(2), 191–204. https://doi.org/10.1016/0034-4257(94)90141-4

Price, J. C. (1994). How unique are spectral signatures? *Remote Sensing of Environment*, *49*(3), 181–186. https://doi.org/10.1016/0034-4257(94)90013-2

Priya, C. A., Balasaravanan, T., & Thanamani, A. S. (2012). An efficient leaf recognition algorithm for plant classification using support vector machine. *International Conference on Pattern Recognition, Informatics and Medical Engineering, PRIME 2012*, 428–432. https://doi.org/10.1109/ICPRIME.2012.6208384

Puangbut, D., Jogloy, S., & Vorasoot, N. (2017). Association of photosynthetic traits with water use efficiency and SPAD chlorophyll meter reading of Jerusalem artichoke under drought conditions. *Agricultural Water Management*, *188*, 29–35. https://doi.org/10.1016/j.agwat.2017.04.001

Putfarken, D., Dengler, J., Lehmann, S., & Härdtle, W. (2008). Site use of grazing cattle and sheep in a large-scale pasture landscape: A GPS/GIS assessment. *Applied Animal Behaviour Science*, *111*(1–2), 54–67.

https://doi.org/10.1016/j.applanim.2007.05.012

Quirós-Rosado, E. M. (2009). *Clasificación de imágenes multiespectrales ASTER mediante funciones adaptativas* [Universidad de Extremadura]. https://dehesa.unex.es:8443/handle/10662/457

Robert Eadie, W., & Nelson, B. K. (1980). Mamíferos que constituyen plagas. In Natural Academy of Sciences (Ed.), *Control de plantas y animales. Problemas y control de plaga de vertebrados.* (pp. 99–125). Editorial Limusa.

Roberts, S. J. (1992). Effect of soil moisture on the transmission of pea bacterial blight (Pseudomonas syringae pv. pisi) from seed to seedling. *Plant Pathology*, *41*(2), 136–140. https://doi.org/10.1111/j.1365-3059.1992.tb02330.x

Rodríguez-Pastor, R., Luque-Larena, J. J., Lambin, X., & Mougeot, F. (2016). "Living on the edge": The role of field margins for common vole (Microtus arvalis) populations in recently colonised Mediterranean farmland. *Agriculture, Ecosystems and Environment*, *231*, 206–217. https://doi.org/10.1016/j.agee.2016.06.041

Rouse, J. W., Haas, R. H., Schell, J. A., Deering, D. W., & Harlan, J. C. (1974). Monitoring the vernal advancement and retrogradation (green wave effect) of natural vegetation. In NASA/GSFC (Ed.), *Final Report, Type III* (p. 371).

Saini, R., & Ghosh, S. K. (2018). Crop classification on single date Sentinel-2 imagery using random forest and suppor vector machine. *ISPRS - International Archives of the Photogrammetry, Remote Sensing and Spatial Information Sciences*, *XLII–5*(November), 683–688. https://doi.org/10.5194/isprs-archives-xlii-5-683-2018

Salama, H. S. A. (2020). Mixture cropping of berseem clover with cereals to improve forage yield and quality under irrigated conditions of the Mediterranean basin. *Annals of Agricultural Sciences*, *65*(2), 159–167. https://doi.org/10.1016/j.aoas.2020.09.001

Sánchez-García, M. (2010). *Estudio del comportamiento en pastoreo de ovejas churras en producción ecológica extensiva mediante dispositivo GPS-GPRS [Study of the grazing behavior of Churra-breed sheep in extensive organic production using a GPS-GPRS device]*. University of Salamanca.

Sánchez, N., Alonso-Arroyo, A., Martínez-Fernández, J., Piles, M., González-Zamora, Á., Camps, A., & Vall-llosera, M. (2015). On the synergy of airborne GNSS-R and Landsat 8 for soil moisture estimation. *Remote Sensing*, *7*(8), 9954–9974. https://doi.org/10.3390/rs70809954

Sánchez, N., Martínez-Fernández, J., González-Piqueras, J., González-Dugo, M. P., Baroncini-Turrichia, G., Torres, E., Calera, A., & Pérez-Gutiérrez, C. (2012). Water balance at plot scale for soil moisture estimation using vegetation parameters. *Agricultural and Forest Meteorology*, *166–167*, 1–9. https://doi.org/10.1016/j.agrformet.2012.07.005

Schieltz, J. M., Okanga, S., Allan, B. F., & Rubenstein, D. I. (2017). GPS tracking cattle as a monitoring tool for conservation and management. *African Journal of Range and Forage Science*, *34*(3), 173–177. https://doi.org/10.2989/10220119.2017.1387175

Schoenbaum, I., Kigel, J., Ungar, E. D., Dolev, A., & Henkin, Z. (2017). Spatial and temporal activity of cattle grazing in Mediterranean oak woodland. *Applied Animal Behaviour Science*, *187*, 45–53. https://doi.org/10.1016/j.applanim.2016.11.015

Schowengerdt, R. A. (2007). The nature of remote sensing. In *Remote Sensing: Models and Methods for Image Processing* (3rd ed., pp. 1–34). Academic Press.

Senft, R. L., Coughenour, M. B., Bailey, D. W., Rittenhouse, L. R., Sala, O. E., & Swift, D. M. (1987). Large herbivore foraging and ecological hierarchies. *BioScience*, *37*(11), 789–799. https://doi.org/10.2307/1310545

Shafiee, S., Lied, L. M., Burud, I., Dieseth, J. A., Alsheikh, M., & Lillemo, M. (2021). Sequential forward selection and support vector regression in comparison to LASSO regression for spring wheat yield prediction based on UAV imagery. *Computers and Electronics in Agriculture*, *183*, 106036. https://doi.org/10.1016/j.compag.2021.106036

Shi, Y., Wang, T., Skidmore, A. K., & Heurich, M. (2020). Improving LiDAR-based tree species mapping in Central European mixed forests using multi-temporal digital aerial colour-infrared photographs. *International Journal of Applied Earth Observation and Geoinformation*, *84*, 1–10.

https://doi.org/10.1016/j.jag.2019.101970

Sillero, N., & Gonçalves-Seco, L. (2014). Spatial structure analysis of a reptile community with airborne LiDAR data. *International Journal of Geographical Information Science*, *28*(8), 1709–1722. https://doi.org/10.1080/13658816.2014.902062

Silverman, B. W. (1986). *Estimación de densidad para las estadísticas y el análisis de datos [Density estimation for statistics and data analysis]*. (Chapman & Hall (eds.)).

Sripada, R. P., Heiniger, R. W., White, J. G., & Meijer, A. D. (2006). Aerial color infrared photography for determining early in-season nitrogen requirements in corn. *Agronomy Journal*, *98*(4), 968–977. https://doi.org/https://doi.org/10.2134/agronj2005.0200

Staniak, M., Ksiak, J., & Bojarszczuk, J. (2014). Mixtures of legumes with cereals as a source of feed for animals. In V. Pilipavicius (Ed.), *Organic Agriculture Towards Sustainability* (pp. 123–145). InTech. https://doi.org/10.5772/58358

Su, Y., Guo, Q., Fry, D. L., Collins, B. M., Kelly, M., Flanagan, J. P., & Battles, J. J. (2016). A vegetation mapping strategy for conifer forests by combining airborne LiDAR data and aerial imagery. *Canadian Journal of Remote Sensing*, *42*(1), 1–15. https://doi.org/10.1080/07038992.2016.1131114

Sumesh, K. C., Ninsawat, S., & Somard, J. (2021). Integration of RGB-based vegetation index, crop surface model and object-based image analysis approach for sugarcane yield estimation using unmanned aerial vehicle. *Computers and Electronics in Agriculture*, *180*, 105903. https://doi.org/10.1016/j.compag.2020.105903

Sun, D., Zheng, J. H., Ma, T., Chen, J. J., & Li, X. (2018). The analysis of burrows recognition accuracy in Xinjiang's pasture area based on UAV visible images with different spatial resolution. *International Archives of the Photogrammetry, Remote Sensing and Spatial Information Sciences - ISPRS Archives*, *42*(3), 1575–1579. https://doi.org/10.5194/isprs-archives-XLII-3-1575-2018

Teillet, P. M. (2007). Image correction for radiometric effects in remote sensing. *International Journal of Remote Sensing*, *7*(12), 1637–1651.

https://doi.org/10.1080/01431168608948958

Terraube, J., Arroyo, B., Madders, M., & Mougeot, F. (2011). Diet specialisation and foraging efficiency under fluctuating vole abundance: a comparison between generalist and specialist avian predators. *Oikos*, *120*(2), 234–244. https://doi.org/10.1111/J.1600-0706.2010.18554.X

Thomlinson, J. R., Bolstad, P. V., & Cohen, W. B. (1999). Coordinating methodologies for scaling landcover classifications from site-specific to global: Steps toward validating global map products. *Remote Sensing of Environment*, *70*(1), 16–28. https://doi.org/10.1016/S0034-4257(99)00055-3

Tou, J. T., & González, R. C. (1974). *Pattern recognition principles*. Addison-Wesley Publishing Company.

Truszkowski, J. (1982). The impact of the common vole on the vegetation of agroecosystems. *Acta Theriologica*, *27*(23), 305–345.

Tucker, C. J. (1979). Red and photographic infrared linear combinations for monitoring vegetation. *Remote Sensing of Environment*, *8*(2), 127–150. https://doi.org/10.1016/0034-4257(79)90013-0

Tukey, J. W. (1949). Comparing individual means in the analysis of variance. *Biometrics*, *5*(2), 99–114. https://doi.org/10.2307/3001913

Turner, L. W., Anderson, M., & Larson, B. T. (2001). Global positioning systems (GPS) and grazing behavior in cattle. In R. R. Stowell, R. Bucklin, & R. W. Bottcher (Eds.), *Livestock Environment VI: Proceedings of the 6th International Symposium. ASABE* (pp. 640–650).

Turner, L. W., Udal, M. C., Larson, B. T., & Shearer, S. A. (2000). Monitoring cattle behavior and pasture use with GPS and GIS. *Canadian Journal of Animal Science*, *80*(3), 405–413. https://doi.org/10.4141/A99-093

Undersander, D., Grau, C., Cosgrove, D., Doll, J., & Martin, N. (2011). Alfalfa stand assessment: Is this stand good enough to keep? *University of Wisconsin - Cooperative Extension*, 3–6.

Valcarce-Diñeiro, R., Lopez-Sanchez, J. M., Sánchez, N., Arias-Pérez, B., & Martínez-Fernández, J. (2018). Influence of incidence angle in the correlation of C-band polarimetric parameters with biophysical variables of rainfed crops. *Canadian Journal of Remote Sensing*, *44*(6), 643–659. https://doi.org/10.1080/07038992.2019.1579051

Valerio, F., Ferreira, E., Godinho, S., Pita, R., Mira, A., Fernandes, N., & Santos, S. M. (2020). Predicting microhabitat suitability for an endangered small mammal using Sentinel-2 data. *Remote Sensing*, *12*(3), 1–18. https://doi.org/10.3390/rs12030562

Vallentine, J. F. (2001). *Grazing management*. Academic Press.

Van Horne, B., Schooley, R. L., Knick, S. T., Olson, G. S., & Burnham, K. P. (1997). Use of burrow entrances to indicate densities of townsend's ground squirrels. *The Journal of Wildlife Management*, *61*(1), 92. https://doi.org/10.2307/3802418

Venter, Z. S., Hawkins, H. J., & Cramer, M. D. (2019). Cattle don't care: Animal behaviour is similar regardless of grazing management in grasslands. *Agriculture, Ecosystems and Environment*, *272*, 175–187. https://doi.org/10.1016/j.agee.2018.11.023

Verger, A., Vigneau, N., Chéron, C., Gilliot, J. M., Comar, A., & Baret, F. (2014). Green area index from an unmanned aerial system over wheat and rapeseed crops. *Remote Sensing of Environment*, *152*, 654–664. https://doi.org/10.1016/j.rse.2014.06.006

Wahab, I., Hall, O., & Jirström, M. (2018). Remote sensing of yields: Application of UAV imagery-derived NDVI for estimating maize vigor and yields in complex farming systems in sub-Saharan Africa. *Drones*, *2*(3), 28. https://doi.org/10.3390/DRONES2030028

Walter, V. (2004). Object-based classification of remote sensing data for change detection. *ISPRS Journal of Photogrammetry and Remote Sensing*, *58*(3–4), 225–238. https://doi.org/10.1016/J.ISPRSJPRS.2003.09.007

Weih, R. C., & Riggan, N. D. (2010). Object-based classification vs. pixel-based classification: Comparitive importance of multi-resolution imagery. *The International Archives of the Photogrammetry, Remote Sensing and Spatial*

Information Sciences, *XXXVIII*, 1–6.

Wiegand, C. L., Richardson, A. J., Escobar, D. E., & Gerbermann, A. H. (1991). Vegetation indices in crop assessments. *Remote Sensing of Environment*, *35*, 105–119. https://doi.org/10.1016/0034-4257(91)90004-P

Willey, R. W. (1979). *Intercropping : its importance and research needs. Part 1, competition and yield advantages* (Vol. 32 no). Field crop abstract.

Wilschut, L. I., Heesterbeek, J. A. P., Begon, M., de Jong, S. M., Ageyev, V., Laudisoit, A., & Addink, E. A. (2018). Detecting plague-host abundance from space: Using a spectral vegetation index to identify occupancy of great gerbil burrows. *International Journal of Applied Earth Observation and Geoinformation*, *64*, 249–255. https://doi.org/10.1016/j.jag.2017.09.013

Witmer, G. W. (2005). Wildlife population monitoring: some practical considerations. *Wildlife Research*, *32*(3), 259–263. https://doi.org/10.1071/WR04003

Wold, H. (1982). Soft modelling: The basic design and some extensions. In H. Wold & K. G. Jöreskog (Eds.), *Systems Under Indirect Observation: Causality-Structure-Prediction. Part {II}*. (pp. 1–54). North-Holland Publishing Company. /paper/Soft-modelling%3A-The-Basic-Design-and-Some-Wold/c8b4365e181ca55ec5891b07b56a9f5ffeab531f

Wold, S., Sjöström, M., & Eriksson, L. (2001). PLS-regression: a basic tool of chemometrics. *Chemometrics and Intelligent Laboratory Systems*, *58*(2), 109–130. https://doi.org/10.1016/S0169-7439(01)00155-1

Xu, Z., Zhao, Y., Li, B., Zhang, M., & Wang, Y. (2014). Assessing Yangtze vole damage in Dongting Lake region of outbreak year based on MODIS imagery. *Shengtai Xuebao/ Acta Ecologica Sinica*, *34*(23), 7101–7109. https://doi.org/10.5846/stxb201303050348

Yan, G., Mas, J. F., Maathuis, B. H. P., Xiangmin, Z., & Van Dijk, P. M. (2006). Comparison of pixel-based and object-oriented image classification approaches—a case study in a coal fire area, Wuda, Inner Mongolia, China. *International Journal of Remote Sensing*, *27*(18), 4039–4055.

https://doi.org/10.1080/01431160600702632

Yandún-Narváez, F. J., Salvo del Pedregal, J., Prieto, P. A., Torres-Torriti, M., & Auat Cheein, F. A. (2016). LiDAR and thermal images fusion for ground-based 3D characterisation of fruit trees. *Biosystems Engineering*, *151*, 479–494. https://doi.org/10.1016/j.biosystemseng.2016.10.012

Yao, X., Huang, Y., Shang, G., Zhou, C., Cheng, T., Tian, Y., Cao, W., & Zhu, Y. (2015). Evaluation of six algorithms to monitor wheat leaf nitrogen concentration. *Remote Sensing*, *7*(11), 14939–14966. https://doi.org/10.3390/rs71114939

Yuan, Y., & Hu, X. (2016). Random forest and objected-based classification for forest pest extraction from uav aerial imagery. *International Archives of the Photogrammetry, Remote Sensing and Spatial Information Sciences - ISPRS Archives*, *XLI-B1*, 1093–1098. https://doi.org/10.5194/isprsarchives-XLI-B1-1093-2016

Zanardo, F. H., Rodrigues, R. A. F., Silva, H. R., Marques, A. P., & Faria, G. A. (2016). Geotechnology application for data acquisition for agricultural and environmental management of the municipality of vitória Brazil-sp. *Engenharia Agricola*, *36*(4), 684–695. https://doi.org/10.1590/1809-4430-ENG.AGRIC.V36N4P684-695/2016

Zerrouki, N., & Bouchaffra, D. (2014). Pixel-based or object-based: Which approach is more appropriate for remote sensing image classification? *IEEE International Conference on Systems, Man and Cybernetics*, *2014-Janua*(January), 864–869. https://doi.org/10.1109/SMC.2014.6974020

Zhang, C., Xie, Z., & Selch, D. (2013). Fusing lidar and digital aerial photography for object-based forest mapping in the Florida Everglades. *GIScience and Remote Sensing*, *50*(5), 562–573. https://doi.org/10.1080/15481603.2013.836807

Zhang, L., & Milanova, M. (2013). An effective multi-feature fusion object-based classification method on ArcGIS platform using very high-resolution remote sensing image. *International Journal of Advanced Research in Computer Science and Software Engineering*, *3*(11), 10–23.

Zhang, X., Han, L., Han, L., & Zhu, L. (2020). How well do deep learning-based methods

for land cover classification and object detection perform on high resolution remote sensing imagery? *Remote Sensing*, *12*(3), 417. https://doi.org/10.3390/RS12030417

Zhang, Z., & Wang, B. (2017). Applications of unmanned aerial vehicles remote sensing technology in landscape ecology. *Acta Ecologica Sinica*, *37*(12), 4029–4036. https://doi.org/10.5846/stxb201702270318

Zhou, X., Zheng, H. B., Xu, X. Q., He, J. Y., Ge, X. K., Yao, X., Cheng, T., Zhu, Y., Cao, W. X., & Tian, Y. C. (2017). Predicting grain yield in rice using multi-temporal vegetation indices from UAV-based multispectral and digital imagery. *ISPRS Journal of Photogrammetry and Remote Sensing*, *130*, 246–255. https://doi.org/10.1016/j.isprsjprs.2017.05.003

Zhou, Z., Morel, J., Parsons, D., Kucheryavskiy, S. V, & Gustavsson, A.-M. (2019). Estimation of yield and quality of legume and grass mixtures using partial least squares and support vector machine analysis of spectral data. *Computers and Electronics in Agriculture*, *162*, 246–253. https://doi.org/10.1016/j.compag.2019.03.038